Another Hit On The Wall
Confined Wave Impacts on Hydraulic Structures

de Almeida Sousa, E.

DOI
10.4233/uuid:1c1796bd-9a12-4c82-b717-561acdeafea0

Publication date
2023

Document Version
Final published version

Citation (APA)
de Almeida Sousa, E. (2023). *Another Hit On The Wall: Confined Wave Impacts on Hydraulic Structures*. [Dissertation (TU Delft), Delft University of Technology]. https://doi.org/10.4233/uuid:1c1796bd-9a12-4c82-b717-561acdeafea0

Another Hit On The Wall

Confined wave impacts on hydraulic structures

ANOTHER HIT ON THE WALL

CONFINED WAVE IMPACTS ON HYDRAULIC STRUCTURES

Dissertation

for the purpose of obtaining the degree of doctor
at Delft University of Technology,
by the authority of the Rector Magnificus Prof. dr. ir. T.H.J.J. van der Hagen,
chair of the Board for Doctorates,
to be defended publicly on
Monday 15 May 2023 at 17:30 o'clock

by

Ermano DE ALMEIDA SOUSA

Master of Science in Civil Engineering,
Delft University of Technology, The Netherlands,
born in Nova Friburgo, Brazil.

This dissertation has been approved by the promotors.

Composition of the doctoral committee:

Rector Magnificus,	chairperson
Prof. dr. ir. S.N. Jonkman,	Delft University of Technology, promotor
Dr. ir. B. Hofland,	Delft University of Technology, promotor
Dr. ir. A. Antonini,	Delft University of Technology, copromotor

Independent members:

Prof. dr. ir. M.R.A. van Gent	Delft University of Technology
Prof. dr. ir. P. Troch	Ghent University, Belgium
Prof. dr.-ing. habil. N. Goseberg	TU Braunschweig, Germany
Ir. W. Kortlever	Rijkswaterstaat, The Netherlands
Prof. dr. ir. W.S.J. Uijttewaal	Delft University of Technology, reserve member

Keywords: confined wave impacts, hydraulic structures, overhangs, slamming loads, impulsive loads, pressure-impulse, physical modelling

Printed by: Ipskamp Printing

Front & Back: E. de Almeida Sousa

ISBN 978-94-6384-436-9

An electronic version of this dissertation is available at
http://repository.tudelft.nl/.

Education does not transform the World.
Education changes people.
People transform the World.

Paulo Freire

Contents

SUMMARY

Hydraulic structures are crucial for navigation, water management and flood protection in low-lying coastal and delta regions. Their importance is expected to continue growing in the coming years, based on two main factors. Firstly, because of the consequences of climate change (i.e. sea level rise, variations in water discharges, variations incoming wave fields, increase in the frequency and intensity of extreme events, etc.). Secondly, because of the continuous development and urbanization of coastal and delta regions, with an increase in the value of assets located in those areas combined with more strict safety requirements. Those two factors will lead to the construction of a series of new hydraulic structures around the world. In addition, existing hydraulic structures will be renovated after reaching the end of the envisaged design lifetime, and/or due to the previously described modification of load conditions and/or safety standards.

Wave loads play a significant role in the stability of these hydraulic structures and a knowledge gap was identified regarding the characterization of confined wave impacts acting on vertical hydraulic structures with overhangs. For this type of wave impact, no validated load prediction method or design approach was previously available. This research addresses this knowledge gap, providing an experimentally calibrated load prediction model and a design approach for characterizing confined wave impact loads. This research focuses on primarily vertical concrete and steel hydraulic structures subjected to confined wave impacts generated by non-breaking incident wave fields.

The first part of this research (Chapter 2) validates the pressure-impulse theory based on laboratory tests on vertical hydraulic structures with overhangs. To this end, two existing analytical pressure-impulse theory models for confined wave impacts and air influence were combined. The loads on the structure are described in the validated model by the pressure-impulse (i.e. integral of impulsive pressures during a wave impact). This study highlights the suitability of the pressure-impulse theory to describe confined wave impact loads. This validated theory contributes to the design of this type of structure, providing a first tool for pressure- and force-impulse estimations. This work also introduced a method to obtain the pressure- and force-impulses from laboratory measurements, using one single set of constant criteria. Furthermore, this study also shows that the force-impulse is a less variable magnitude compared with the force peaks. This reduced variability reinforces the advantages of considering pressure- and force-impulses in the design of hydraulic structures subjected to impulsive wave impact loads.

The second part of this research (Chapter 3) studies the air entrapment characteristics and the description of the wave surface impact velocity in confined wave impacts. This study highlights the complex wave hydrodynamics before and during the wave impacts, influenced by the incident wave conditions and the structural characteristics. With respect to impact velocity, this study shows that the wave surface impact velocity described by the linear wave theory with full reflection is suitable to be used for load estimations. With respect to air entrapment, this study shows a large variation in air entrapment for the different test conditions. Nevertheless, a constant range of dimensionless entrapped air area for both the shorter and the longer overhangs is observed ($0.005 < \alpha = A_A/W^2 < 0.035$). The variability in entrapped air characteristics leads to significant effects on the loading acting on the structure, as observed by the variability in pressure measurements. Furthermore, longer impact durations measured during the laboratory tests were found to be closely related to larger entrapped air dimensions.

The third part of this research (Chapter 4) extends the knowledge on confined wave impacts acting on overhang configurations, including loading prediction expressions for preliminary design. This is based on the analysis of extensive laboratory experiments carried out in the wave flume. These laboratory experiments included a total of 146 wave flume tests with variations in hydraulic loading conditions (regular/irregular waves and varying freeboards) and changes in the structure geometry (overhang length, lateral constriction and loading reducing ventilation gaps). Based on the results of these laboratory experiments, the Parameter Gamma (Γ, representing the effective air entrapment characteristics) was introduced and related to the Parameter Beta (β, representing the effective bounce-back factor). Based on those two parameters, the confined wave impact pressure- and force-impulses acting on a given hydraulic structure with an overhang could then be estimated. Furthermore, the tests showed that a lateral constriction amplifies the wave impact loads at the constriction edge, while the ventilation gaps were found to be effective in reducing confined wave impact impulses.

The fourth part of this research (Chapter 5) summarizes all previous contributions and presents the most important considerations and recommendations for the design of hydraulic structures subjected to confined wave impacts. Most importantly, it addresses the use of the validated load prediction expressions for preliminary design estimations. To this end, a design application example is presented to illustrate the use of the load prediction model for a realistic coastal hydraulic structure configuration. Design adaptations and considerations for reducing confined wave impact loads are also presented. Furthermore, this research highlights the importance of considering the effect of air entrapment (and also air entrainment) in confined wave impacts. This is crucial to describe accurately the impulsive loads acting on the structure, but also to correctly scale peak pressures and forces from laboratory experiments to prototype scales. This research also highlights previous conclusions that the Froude scaling rules can be used to accurately scale wave impact pressure- and force-impulses. But Froude scaling rules should not be used for scaling wave impact pressure and force peaks between model and prototype. Lastly, this research also discusses the importance and advantages of combining experimental, numerical and analytical methods and techniques for describing and quantifying wave impacts in both research and design practice.

In conclusion, this research addressed knowledge gaps for the design of hydraulic structures subjected to confined wave impacts. To this end, the experimentally calibrated load prediction tool and the discussed design approach can be used in combination with structural models. This would allow us to reduce the uncertainties and increase the reliability in the design of hydraulic structures subjected to such impulsive loads. This is particularly relevant for relatively thin structures (i.e. flood gates) which may experience a significant dynamic behaviour under these loads. Future studies on wave impacts should focus on three areas. Firstly, extending the range of wave impact types and structural configurations considered (e.g. combined wave impacts and 3D configurations). Secondly, extending the range of research tools and experiments (e.g. large scale tests, vacuum flumes and numerical models with compressible air). Thirdly, extending the coupling of load and response models applied to design. The aim of these future studies is to contribute to revised and modernized techniques, tools and guidelines for the design and renovation of hydraulic structures subjected to wave impacts.

Samenvatting

Waterbouwkundige constructies zijn van cruciaal belang voor de scheepvaart, het waterbeheer en de bescherming tegen overstromingen in laaggelegen kust- en deltagebieden. Naar verwachting zal dit belang de komende jaren blijven toenemen, voornamelijk vanwege twee factoren. Ten eerste vanwege de gevolgen van de klimaatverandering (d.w.z. zeespiegelstijging, variaties in waterafvoer, variaties in inkomende golfvelden, toename van de frequentie en intensiteit van extreme gebeurtenissen, enz.). Ten tweede, vanwege de voortdurende ontwikkeling en verstedelijking van kust- en deltagebieden, met een stijging van de economische waarde van deze gebieden in combinatie met strengere veiligheidseisen. Deze twee factoren zullen leiden tot de bouw van een reeks nieuwe waterbouwkundige constructies over de hele wereld. Bovendien zullen bestaande waterbouwkundige constructies worden gerenoveerd na het verstrijken van de geplande levensduur en/of als gevolg van de eerder beschreven wijziging van de belastingen en/of veiligheidsnormen.

Golfbelastingen spelen vaak een belangrijke rol in de stabiliteit van deze verschillend waterbouwkundige constructies. Er is een kennisleemte vastgesteld met betrekking tot de karakterisering van ingesloten golfklappen op verticale waterbouwkundige constructies met overhangende onderdelen. Voor dit type golfklap was nog geen gevalideerd belastingsmodel of ontwerpbenadering beschikbaar. Dit onderzoek voorziet hierin door het leveren van een experimenteel gekalibreerd belastingsmodel en een ontwerpbenadering voor het karakteriseren van belastingen bij ingesloten golfklappen. Dit onderzoek richt zich voornamelijk op verticale betonnen en stalen waterbouwkundige constructies die worden blootgesteld aan ingesloten golfklappen als gevolg van niet-brekende inkomende golfvelden.

Het eerste deel van dit onderzoek (hoofdstuk 2) valideert de drukstoottheorie op basis van laboratoriumproeven op verticale waterbouwkundige constructies met een overhang. Daartoe werden twee bestaande analytische drukstootmodellen voor ingesloten golfklappen en voor luchtinvloed gecombineerd. De belasting op de constructie wordt in het gevalideerde model beschreven door de drukstoot (d.w.z. de tijdsintegraal van de druk tijdens een golfklap). Deze studie benadrukt de geschiktheid van de drukstoottheorie voor de beschrijving van belastingen bij inslag van golven. Deze gevalideerde theorie draagt bij aan het ontwerp van dit soort constructies en biedt een eerste instrument voor het voorspellen van de druk- en krachtstoot als gevolg van golfklappen. Dit werk introduceerde ook een methode om de druk- en krachtstoten te verkrijgen uit laboratoriummetingen, met behulp van één enkele combinatie van constante criteria. Deze studie bevestigt verder dat de stoot in praktijk een minder variabele grootheid is dan de

krachtpiek. Deze verminderde variabiliteit versterkt de voordelen van het in aanmerking nemen van druk- en krachtstoten bij het ontwerp van waterbouwkundige constructies die worden blootgesteld aan impulsieve golfklapbelastingen.

In het tweede deel van dit onderzoek (hoofdstuk 3) worden de kenmerken van de luchtinsluiting en de beschrijving van de inslagsnelheid van het golfoppervlak bij ingesloten golfklap bestudeerd. Deze studie belicht de complexe hydrodynamica van de golf vóór en tijdens de golfklap, die wordt beïnvloed door de omstandigheden van de invallende golf en de constructieve kenmerken. Wat de inslagsnelheid betreft, toont deze studie aan dat de inslagsnelheid van het golfoppervlak volgens de lineaire golftheorie met volledige reflectie geschikt is voor het voorspellen van de belasting. Wat de luchtinsluiting betreft, blijkt uit deze studie een grote variatie in luchtinsluiting voor de verschillende testomstandigheden. Desondanks wordt voor zowel de kortere als de langere overhangen een constant bereik van het dimensieloze ingesloten luchtoppervlak waargenomen ($0.005 < \alpha = A_A/W^2 < 0.035$). De variabiliteit in de eigenschappen van de ingesloten lucht heeft een aanzienlijk effect op de belasting op de constructie, zoals blijkt uit de variabiliteit in de drukmetingen. Bovendien bleek een langere klapduur, gemeten tijdens de laboratoriumproeven, nauw samen te hangen met grotere afmetingen van de ingesloten lucht.

Het derde deel van dit onderzoek (hoofdstuk 4) breidt de kennis uit over de effecten van ingesloten golven op overhangende configuraties, inclusief het voorspellen van de belasting voor het voorlopige ontwerp. Dit is gebaseerd op de analyse van een uitgebreide reeks laboratoriumexperimenten in een golfgoot. Deze labexperimenten omvatten in totaal 146 golfproeven met variaties in de hydraulische belastingsomstandigheden (regelmatige en onregelmatige golven en variërende vrijboorden) en veranderingen in de geometrie van de constructie (overhanglengte, zijdelingse vernauwing en belastingsverminderende ventilatieopeningen). Op basis van de resultaten van deze laboratoriumexperimenten is de parameter Γ, die de effectieve luchtinsluitingskenmerken weergeeft, geïntroduceerd en gerelateerd aan de parameter β, die de effectieve terugstuiterfactor weergeeft. Op basis van deze twee parameters kunnen de druk- en krachtstoten van de ingesloten golfklap op een bepaalde hydraulische constructie met een overhang worden geschat. Voorts bleek uit de proeven dat een zijdelingse vernauwing de golfklapbelasting aan de rand van de vernauwing versterkt, terwijl de ventilatieopeningen effectief bleken te zijn bij het verminderen van ingesloten golfklapstoten.

Het vierde deel van dit onderzoek (hoofdstuk 5) vat alle eerdere bijdragen samen en presenteert de belangrijkste overwegingen en aanbevelingen voor het ontwerp van waterbouwkundige constructies die worden blootgesteld aan ingesloten golfklappen. Het belangrijkste is het gebruik van de gevalideerde relaties om golfbelastingen te voorspellen ten behoeve van voorlopige ontwerpen. Daartoe wordt een praktisch voorbeeld gepresenteerd om de toepassing van het belastingsmodel op een realistische configuratie van een hydraulische kustconstructie te illustreren. Ook worden ontwerpaanpassingen en overwegingen ter vermindering van de golfklapbelasting gepresenteerd. Verder wordt in dit onderzoek gewezen op het belang van het in beschouwing nemen van het effect van luchtinsluiting tussen constructie en golfoppervlak (alsmede het effect van gedispergeerde luchtbellen) bij ingesloten golfklappen. Dit is van cruciaal belang om de stootbelastingen op de constructie nauwkeurig te beschrijven, maar ook om de piekdrukken en -krachten van laboratoriumexperimenten correct te kunnen schalen naar prototypeschalen. Dit onderzoek onderstreept ook eerdere conclusies dat de Froude-schaling kan worden toegepast om druk- en krachtstoten van golfklappen nauwkeurig te schalen. Daarentegen mag Froude-schaling niet worden gebruikt voor het schalen van golfklapdruk- en krachtpieken tussen model en prototype . Tenslotte bespreekt dit onderzoek ook het belang en de voordelen van het combineren van experimentele, numerieke en analytische methoden en technieken voor het beschrijven en kwantificeren van golfklappen in zowel onderzoek als de ontwerppraktijk.

Concluderend kan worden gesteld dat dit onderzoek enkele kennisleemten voor het ontwerp van waterbouwkundige constructies onderhevig aan ingesloten golfklapbelastingen heeft aangepakt. Het experimenteel gekalibreerde belastingsmodel en de besproken ontwerpbenadering kunnen daartoe worden gebruikt in combinatie met constructieve modellen. Dit maakt het mogelijk om onzekerheden te reduceren en de betrouwbaarheid te vergroten bij het ontwerp van waterbouwkundige constructies die aan dergelijke impulsieve belastingen worden blootgesteld. Dit is met name van belang voor relatief slanke constructies (bijv. stormschuiven), die onder deze belastingen een aanzienlijk dynamisch gedrag kunnen vertonen. Toekomstig onderzoek naar golfklappen dient zich te richten op drie gebieden. Ten eerste, uitbreiding van het scala van golfklaptypes en constructieve configuraties (bijvoorbeeld gecombineerde golfklappen en 3D-configuraties). Ten tweede, uitbreiding van het scala van onderzoeksinstrumenten en experimenten (b.v. grootschalige proeven, vacuümgoten en numerieke modellen met samendrukbare lucht). Ten derde, uitbreiding van de koppeling van belasting- en responsmodellen ten behoeve van het ontwerp. Het doel van deze toekomstige studies is bij te dragen aan herziene en gemoderniseerde technieken, instrumenten en richtlijnen voor het ontwerp en de renovatie van waterbouwkundige constructies die onderhevig zijn aan golfklappen.

1

Introduction

1

1.1. BACKGROUND

LOW-LYING coastal and delta regions have presented advantageous conditions for the establishment of settlements and human activities throughout the centuries. The favourable conditions of such regions for agriculture and trade have then justified the significant proportion of the world population which has settled down in coastal and delta areas (Small and Cohen, 2004). According to United Nations (UN, 2017), 40% of the world's population lives within 100km of the coastline. As societies have developed, the urbanization and human activities in the coastal and delta areas have continued to increase, accompanied by significant modifications of the natural characteristics of these regions, with two main objectives. First, to enhance the development of trade activities, through the construction of harbours/ports and stabilization of navigation inlets and channels. Second, to enhance and protect the development of urban areas, through land reclamation and flood/erosion protection. This research addresses this second type of intervention. More precisely, this research focuses on hydraulic structures with the purpose of flood protection that are subjected to wave loads.

For those flood protection interventions in coastal and delta areas, several types of hydraulic structures have been designed and built throughout history, with increasing dimensions and complexity. In the Netherlands, marshes started to be drained and transformed into agricultural land more than 1000 years ago (Slomp, 2012). Later, the formation of the first Dutch water boards in the 13^{th} Century represented a fundamental innovation. They addressed, with a collective approach, various flood control measures, such as the construction and maintenance of dikes (Jonkman et al., 2018; Slomp, 2012). The large number of reclamation projects and dike construction during the period between the 15^{th} and 18^{th} centuries were also affected by frequent and large scale flood disasters. This led to the creation of Rijkswaterstaat (now part of the Dutch Ministry of Infrastructure and Water Management) in 1798, establishing a national approach towards water management and flood defences, overcoming the existing fragmentation of the various institutions involved.

At the beginning of the 20^{th} Century, several significant large scale flooding events, such as the Zuiderzee flood in 1916, lead to large scale interventions, such as the execution of the Zuiderzee project (including the Afsluitdijk, which was completed in 1932) (Jonkman et al., 2018). After World War II, the flood disaster of 1953 caused large economic and human losses in the South West of The Netherlands, and lead to a complete change in the flood management policy in The Netherlands. This implied the formal adoption of scientific methods towards flood protection, which were already being used during the Zuiderzee project. The Delta Committee established after 1953 led then to large changes in the flood risk policy and the shortening of the Dutch coastline through several dams and barriers in the South West of the country (Slomp, 2012).

Following such important changes, The Netherlands has been successful with its flood management for the last 60 years (Slomp, 2012). Existing design guidelines and methods have then been responsible for the successful implementation of a large number of hydraulic structures in the last decades. Nevertheless, the guidelines used during the last decades were based on the use of design events with the required exceedance probability (or return period) for a given flood protection area. In the case of The Netherlands, recent standards introduced in January 2017 are fully based on the consideration of flood risk. This requires the evaluation of the failure probabilities of all the elements of a flood defence system, and the adaptation of design guidelines of flood defences to probabilistic design methods (Eurotop, 2018).

Thus, it becomes vital to design flood defence systems with precise and sufficiently low failure probabilities. Hydraulic structures represent an important element of flood defence systems, and this research will focus exclusively on these types of structures. Those structures, often including movable gates, are crucial at locations where water and/or vessels have to be "let in" or "let out". Examples are the sluices in the Afsluitdijk, the locks in IJmuiden and the Eastern Scheldt Storm Surge Barrier. The design and assessment of such hydraulic structures should be addressed with increasingly reliable methods able to ensure the required low failure probability under extreme events, in an economically, technologically and environmentally efficient manner. This research aims to contribute to the design methods of hydraulic structures, with a focus on the wave impact loading conditions.

1.2. HYDRAULIC STRUCTURES

The importance of flood defence systems in The Netherlands can be observed in Figure 1.1. As shown in Figure 1.1a, 60% of The Netherlands is flood-prone, being more than 26% of the country situated below sea level (Slomp, 2012). As already mentioned above, the occurrence of disastrous flood events in the past such as in 1953 (see Figure 1.1b) have triggered the continuous development of new flood defence systems and strategies. Flood defence systems in The Netherlands include various types of features and structures. As previously described, this thesis focuses exclusively on hydraulic structures, which will be further described hereafter.

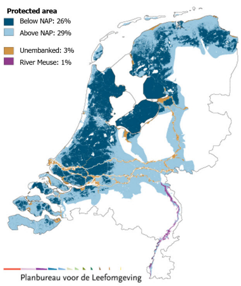

(a) Flood-prone areas of The Netherlands (ref: PBL).

(b) 1953 flood Zuid Beveland (ref: USAID).

Figure 1.1: Importance of flood defences in The Netherlands

A hydraulic structure is defined, following Molenaar et al. (2018), as any civil feature that is intended to divert, restrict, stop or otherwise manage the natural flow of water, or facilitate shipping. Examples of hydraulic structures are lock gates, sluice gates, dewatering sluices, flood gates, storm surge barriers, breakwaters (vertical caisson or rock/concrete units), jetties, groynes, piers, sea walls, quay walls, dolphins, closure dams, reservoir dams, bridge piers, soil retaining structures, tunnels (submerged and floating), pumping stations and docks, among others.

This research focuses on hydraulic structures defined as follows: primarily vertical hydraulic structures (i.e. vertical orientation of the front face of the structure which supports the main hydraulic loading), located in coastal and delta areas, consisting mainly of concrete and/or steel elements, with the aim of modifying water levels, currents and wave propagation to ensure safety against flooding and contribute to the social, economical and environmental development. Examples of the main hydraulic structures considered in this research are: lock gates, sluice gates, dewatering sluices, flood gates and storm surge barriers. Figure 1.2 presents a summary of vertical hydraulic structures relevant to this research where confined wave impacts may take place. Examples are found in The Netherlands, such as the flood gates complex in the Afsluitdijk at Den Oever (Figure 1.2a) and the Eastern Scheldt Storm Surge Barrier (Figure 1.2b). Nevertheless, other examples of such hydraulic structures can be found in the United States (Figure 1.2c), Japan (Figure 1.2d), United Kingdom (Figure 1.2e) or France (Figure 1.2f).

(a) Afsluitdijk, NL (MPower)

(b) Eastern Scheldt, NL (Shutterstock)

(c) Lake Borge, US (USACE)

(d) Fudai, JP (Junichiro Niwa)

(e) Cardiff Bay, UK (Cardiff Harbour Authority)

(f) Bourgneuf Bay, FR (Bureau Etudes Structures)

Figure 1.2: Hydraulic structures relevant for this research and susceptible to confined wave impacts.

A significant recent development in The Netherlands is the renovation of the Afsluitdijk, a project which started in 2018 and will lead to the complete refurbishment of all parts of the structure, which dates back to 1932. The Afsluitdijk is a 32 km long structure that has been successfully ensuring flood safety around the old Zuiderzee (currently freshwater lakes IJsselmeer and Markermeer), but it no longer meets the current safety standards. An important part of the project is the renovation of the existing flood gates complexes, the construction of new flood gates complexes and the construction of new pumping stations, see Figure 1.3. The design and re-design of those hydraulic structures represent an important demand for contributions to the design of such structures. Thus, it is an important source of motivation for this research. Nevertheless, the geometry of the Afsluitdijk flood gates complexes (e.g. featuring longer overhangs than considered in this study), is not directly investigated in this research. Also, the contributions and conclusions from this research aim for being general and applicable in any other location, as shown in Figure 1.2. Such possible applications are the various flood defence interventions that may be carried out in the coming decades worldwide. Climate change and sea level rise scenarios will affect the wave loads acting on such hydraulic structures and may increase the occurrence and intensity of confined wave impact.

Figure 1.3: New Afsluitdijk flood gates complex in Den Oever (ref: Levvel).

1.3. WAVE LOADS

In the design of hydraulic structures, the full range of load scenarios and their combinations should be considered. A comprehensive list of the loads that should be taken into account in the design of hydraulic structures is presented in Molenaar and Voorendt (2017). These loads would include, among others, weight, wind, water, ice, temperature and seismic forces. This present study focuses on the hydraulic loadings, where hydrostatic and hydrodynamic loading conditions can be distinguished.

Firstly, hydrostatic loads are determined by the position of the still water level(s) on the structure, where the total force can be calculated as the integral of the hydrostatic pressures acting on the inner or outer surface(s) of the structure. The variation of the hydrostatic loading acting on the structure is given by the still water level variations caused mainly by astronomical tides, meteorological surges, precipitation or river discharge. Secondly, hydrodynamic loading on hydraulic structures can be caused by two different processes: flow and waves. Flow loads are present where currents take place through and along the structure, caused by mechanisms such as river discharge, tides, storm overflow, levelling of navigation locks, estuarine or oceanic circulation and other processes leading to water level differences and water exchange between two locations. Wave loads are present where water surface waves, mainly wind-generated gravity-restored waves, propagated along the water surface encounter a given hydraulic structure.

This study addresses the hydrodynamic wave loads. Such wave loading conditions can be divided into two types. Firstly quasi-static loading conditions, caused by reflecting non-breaking waves (see Figure 1.4a). Second, impulsive loading conditions, caused by violent wave impacts on the structure due to wave breaking or due to the structural configuration (see Figure 1.4b). The method from Goda (Goda, 2010) is widely used to estimate non-breaking and breaking (with impulsive coefficients by Takahashi et al. (1994)) wave pressures on vertical structures. Nevertheless, these methods were developed for caisson breakwaters and are not entirely suited for hydraulic structures (Meinen et al., 2020; Tuin et al., 2022). Furthermore, Kortenhaus and Oumeraci (1998) presents a classification of wave loading, defining four types of loading as follows: quasi-standing, slightly breaking, impact loads and broken waves. This research focuses on the impulsive loading (impact loads), which can lead to very high pressure and forces acting on the structure for a very short duration (e.g. 10-100 ms) (Kolkman and Jongeling, 1996).

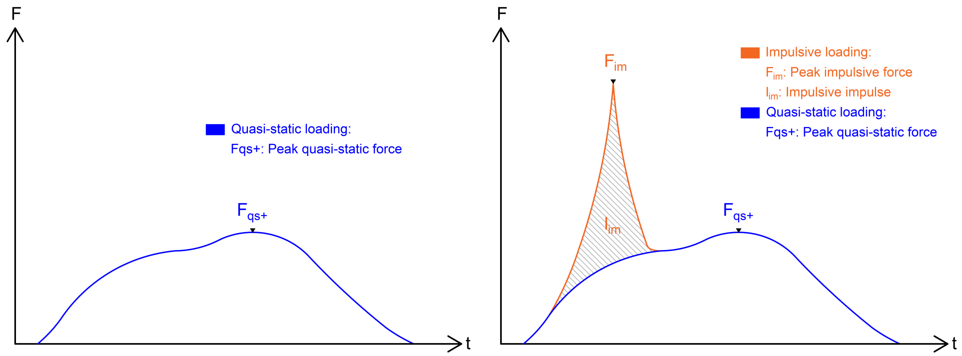

(a) Quasi-static wave loading (b) Impulsive wave loading

Figure 1.4: Illustration of quasi-static and impulsive wave loading over time.

In hydraulic structures, three types of wave impacts can take place, as shown in Figure 1.5. Those three types are: breaking waves acting on a vertical wall, overtopping waves acting on a crest wall and non-breaking waves acting on a vertical wall with a horizontal overhang. This study focuses on this third type of confined wave impact (i.e. standing wave impacts on vertical structures with overhangs). This is justified because of the importance of this wave impact type for the design, safety assessment and renovation of various hydraulic structure types, as shown in Figure 1.2. Also, because of the limited number of design methods and guidelines for this type of impact condition, in contrast to the other wave impact types. Breaking wave impacts have been more widely studied in the past (Bagnold, 1939; Goda, 2010; Cuomo et al., 2010b; Hofland et al., 2010), and overtopping wave impacts have also been addressed recently (Altomare et al., 2014; Chen et al., 2015, 2016; van Doorslaer et al., 2017; Suzuki et al., 2022). Figure 1.6 shows the main design parameters of a typical hydraulic structure with an overhang.

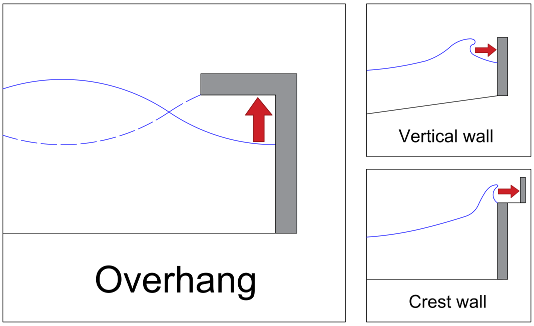

Figure 1.5: Types of wave impacts in hydraulic structures.

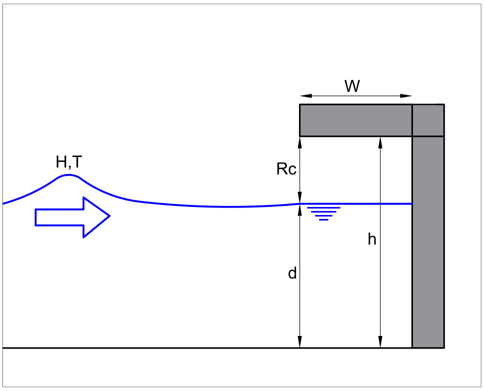

Figure 1.6: Overhang configuration main parameters: incident wave height H [m]; incident wave period T [s]; still water depth at the overhang d [m]; overhang height h [m]; overhang width W [m]; freeboard Rc [m].

1.4. PROBLEM DEFINITION

Four important knowledge gaps were identified in academic literature and design tools for hydraulic structures with overhangs subjected to confined wave impacts. These limitations are described hereafter and were addressed in this research in four parts.

- **Validation of pressure-impulse theory**. The pressure-impulse theory applied to wave impacts was introduced by Cooker and Peregrine (1990, 1995), showing its potential to be used for wave impact load estimations. Nevertheless, the theory was only partially confirmed by measurements (Wood et al. (2000); Bredmose et al. (2009)), which mainly treated breaking wave impacts. However, this low correspondence was considered to be caused by the complex kinematics within a breaking wave that is not fully captured by the assumed constant impact velocity. The confined wave impacts in the research in hand are characterized by more uniform impact velocities, but a validation of the theory with this overhang configuration has not been addressed in the past. Such validation would also address a significant knowledge gap in the description of confined wave impact loads acting on vertical hydraulic structures with overhangs, to be used in the design practice.

- **Wave surface impact velocity and air entrapment**. For describing the confined wave impacts loads on vertical hydraulic structures with overhangs, the details of the air entrapment and the impact velocity are two key aspects. Existing literature addressed the effect of air in breaking waves (Peregrine and Thais, 1996; Wood et al., 2000; Bredmose et al., 2009), but it did not address confined wave impact conditions. On the other hand, WL (1979b) concludes for confined wave impacts that air pockets have a decisive influence on the characteristics and magnitudes of wave impacts, but it did not describe general design criteria. Furthermore, several authors addressed the description of wave kinematics and loads at a vertical wall (Sainflou (1928); Miche (1944); Goda (1967)) but they did not address the description of the impact velocity of the wave surface against a horizontal boundary.

- **Varying incident wave fields and configurations**. Wave impact loads on vertical hydraulic structures with overhangs of different dimensions and subjected to diverse non-breaking incident waves were not studied in the past. For example, the pressure-impulse theory (Cooker and Peregrine, 1990, 1995; Wood and Peregrine, 1996) was developed for a schematized wave impact but was not related to realistic wave fields and structures. Furthermore, well-known equations for obtaining wave loads such as Goda (2010) do not present prediction methods for overhang configurations. Also, laboratory tests (i.e. Hofland (2015)) have been carried out in the past including non-standard overhang configurations (i.e. with ventilation gaps or lateral constrictions), but they did not describe general design criteria.

- **Design approach for confined wave impact loads**. As previously described in this chapter, there are currently no expressions available in the design practice for estimating confined wave impact loads on vertical hydraulic structures with overhangs. This is remarkable, given the large number of such structures that will be designed, built and renovated in the coming years at many locations worldwide.

The previously identified four areas of knowledge gaps were addressed in this research, as described in the research objectives in the section hereafter.

1.5. RESEARCH OBJECTIVES

This research aims to address the previously described limitations on the design of hydraulic structures with relatively short overhangs (i.e. structures with ratios h/W between 3 and 6 and with ratios L/W between 10 and 40) facing confined wave impacts, and is summarized in the following research objective. To realize this research objective, four research steps were taken as summarized below in four research questions.

"To develop a load prediction method and design considerations for vertical hydraulic structures with horizontal overhangs subjected to confined wave impacts".

1. How valid is the pressure-impulse theory for describing the confined wave impact loads on vertical hydraulic structures with relatively short overhangs?
2. How can we describe the wave impact velocity and quantify the air entrapment?
3. How can we extend the validation of the pressure-impulse theory to include varying incident wave fields (e.g. regular/irregular) and structural configurations?
4. How can we consider confined wave impacts in the design of hydraulic structures?

1.6. RESEARCH APPROACH

This section presents an overview of the four research steps that compose this dissertation, addressing the research objectives and questions described in the previous section. Figure 1.7 presents a visual outline of the chapters that compose this dissertation.

Validation of pressure-impulse theory (Chapter 2)
This work validates the pressure-impulse theory based on laboratory tests on vertical hydraulic structures with overhangs. This study highlights the suitability of the pressure-impulse theory to describe confined wave impact loads on overhang configurations. This validated theory represents a significant contribution to the design of this type of structure, providing a first tool for pressure- and force-impulse estimations.

Wave surface impact velocity and air entrapment (Chapter 3)
This work studies the air entrapment characteristics and the description of the wave surface impact velocity in confined wave impacts in overhang configurations. This study highlights the complex wave hydrodynamics before and during the wave impacts, influenced by the incident wave conditions and the structural characteristics.

Varying incident wave fields and configurations (Chapter 4)
This work extends the knowledge on confined wave impacts on overhang configurations, including loading prediction expressions for preliminary design. This was based on the analysis of laboratory experiments. These laboratory experiments included a total of 146 wave flume tests with variations in hydraulic loading conditions (regular/irregular waves and varying freeboards) and changes in the structure geometry (overhang length, lateral constriction and loading reducing ventilation gaps). Finally, this study presented loading prediction expressions built up by the pressure-impulse theory that were empirically calibrated using the acquired experimental data.

Design approach for confined wave impact loads (Chapter 5)
This work summarizes all the contributions from this research and the recommendations on how to apply them to design practice. Most importantly, it addresses the use of the validated load prediction expressions for preliminary design estimations. Furthermore, it highlights the importance of describing the air entrapment effect for the correct scaling of peak pressures and forces based on laboratory wave flume experiments.

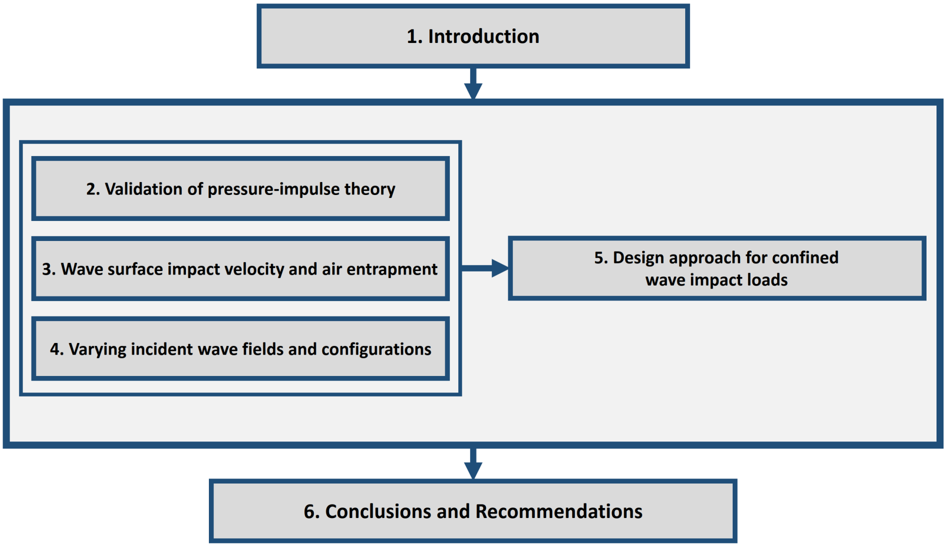

Figure 1.7: Dissertation outline

1.7. RESEARCH CONTEXT: DYNAHICS

This research was carried out within the DynaHicS (Dynamics of Hydraulic Structures) Project. Six partners were involved in this research: the Netherlands Organisation for Scientific Research (NWO), Delft University of Technology, Deltares, Rijkswaterstaat, Witteveen+Bos and PT Structural. Within DynaHicS, two PhD research projects took place. First, the Structural Dynamics research focused on the design response part was carried out by Orson Tieleman. Second, the Wave Impacts research focused on the design load part, and is the basis for this thesis. The laboratory measurements obtained in this research are published in the 4TU Repository (DOI: 10.4121/16989046).

2

VALIDATION OF PRESSURE-IMPULSE THEORY

This chapter has been published in "Validation of pressure-impulse theory for standing wave impact loading on vertical hydraulic structures with short overhangs" in Coastal Engineering (De Almeida & Hofland 2020a).

Coastal Engineering 159 (2020) 103702

Contents lists available at ScienceDirect

Coastal Engineering

journal homepage: http://www.elsevier.com/locate/coastaleng

Validation of pressure-impulse theory for standing wave impact loading on vertical hydraulic structures with short overhangs

Ermano de Almeida *, Bas Hofland

Department of Hydraulic Engineering, Faculty of Civil Engineering and Geosciences, Delft University of Technology, Stevinweg 1, 2628 CN, Delft, the Netherlands

ARTICLE INFO

Keywords:
Wave impacts
Impulsive loading
Hydraulic structures
Overhangs
Pressure-impulse
Physical modelling

ABSTRACT

The applicability of pressure-impulse theory is evaluated for predicting wave impact loading magnitudes for non-breaking standing wave impacts on vertical hydraulic structures with relatively short overhangs. To this end, tests were carried out on a schematized but realistic configuration with low steepness regular wave impacts on a straight overhang perpendicular to a vertical wall. This paper aims to fill the existing knowledge gap on this type of wave impact with reliable and simple expressions. Pressure-impulses and force-impulses are the wave impact loading magnitudes considered in this study, which are defined as the integral of the impulsive pressures/forces over time during a wave impact. These impulses can be used to determine the resulting stresses in a structure for sudden, impulsive loads. The proposed theoretical model is based on the pressure-impulse theory and validated with laboratory experiments. The laboratory tests are done with regular waves for relatively short overhangs, with ratios of wave length to overhang length between 12.1 and 43.6, and ratios of overhang height to overhang length of 3 and 6. Thus, the theory is verified for conditions where the wave impact takes place along the full length of the overhang. From the experimental results, a mean effective bounce-back factor $\beta = 1.17$ is obtained, accounting for the bounce-back effect of entrapped air and other secondary sources of discrepancies between theoretical and experimental results. The standard deviation of β for all the different tests is $\sigma_\beta = 0.11$. This method seems suitable for carrying out preliminary loading estimations, including the pressure-impulse profile at the wall and the total force-impulse at the wall. This study also shows that the force-impulse is a more stable magnitude compared with the force peaks, with about half the relative standard deviation. The impulses predicted by this model are recommended to be coupled with fluid-structure interaction models for analysing the response of the loaded structure.

1. Introduction

In the coming years and decades, various new hydraulic structures will be constructed around the world at coastal areas, delta regions, lakes or reservoirs. In addition, several of the existing hydraulic structures will be renovated after reaching the end of the envisaged design lifetime or due to increasing safety standards and/or loading conditions. Wave loads often play a key role in the design of these structures. This leads to a demand for extended knowledge on the design of hydraulic structures subjected to wave impacts. Three wave impact configurations can be distinguished in Fig. 1. Among these three types of wave impacts, this study addresses wave impacts on overhang configurations, caused by non-breaking reflecting waves.

Previous research has mainly focused on the study of wave impacts caused by breaking waves on vertical structures (Bagnold, 1939; Minikin, 1950; Goda, 1974; Takahashi et al., 1994; Oumeraci et al., 2001; Cuomo et al., 2010). In addition, vertical structures with overhangs have been studied but only subjected to breaking wave impacts (Kisacik et al., 2014). Wave impacts caused by overtopping waves have been also studied in the last years (Chen et al., 2015, 2016). The study from Dias and Ghidaglia (2018) presents recent developments of numerical and experimental models and tools for evaluating slamming magnitudes on ship hulls, natural gas tanks and offshore structures. In contrast, a significant knowledge gap exists on wave impacts caused by standing waves on vertical structures with overhangs, such as crest walls, lock gates, sluice gates, dewatering sluices, flood gates and storm surge barriers (De Almeida et al., 2019; Ramkema, 1978). The study presented hereafter addresses this knowledge gap on wave impacts caused by non-breaking standing waves on a vertical structure with a relatively small overhang and a flat bottom, considering the

* Corresponding author.
E-mail address: e.dealmeid@tudelft.nl (E. de Almeida).

https://doi.org/10.1016/j.coastaleng.2020.103702
Received 10 December 2019; Received in revised form 23 March 2020; Accepted 30 March 2020
Available online 9 April 2020

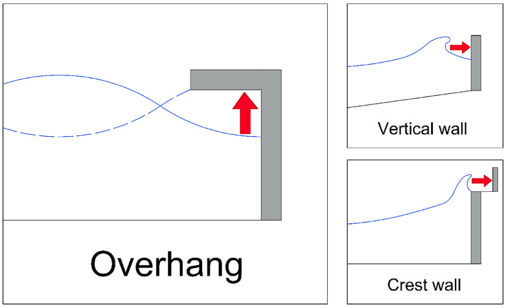

Fig. 1. Main wave impact configurations. Left: Overhang, subjected to non-breaking reflecting wave impacts. Top right: Vertical wall, subjected to breaking waves impacts. Bottom right: Crest wall, subjected to overtopping wave impacts.

pressure-impulse theory and experimental test results.

Fig. 2 shows a cross-section of a flood gate system in the Afsluitdijk in The Netherlands, which is currently undertaking major renovations after more than 80 years of service and additional structures are being built. Such flood gates remain open during low tides in order to allow the water to flow from the lake to the sea. During high tides and storms, these flood gates remain closed in order to avoid the flooding of the hinterland. As it can be observed both from the sea side and from the lake side, overhangs (shown in dark grey) are present in front/back of the gates (shown in red). In such structures, the vertically upwards moving standing wave surface at the vertical wall can produce violent global wave impacts when hitting the rigid horizontal lower overhang surface. Furthermore, wave impacts can take place also locally at the gate reinforcement beams with incident waves from the lake side. Thus, this structure represents an example of conditions where standing waves lead to violent global and local wave impacts, also as it was investigated in the design of the Eastern Scheldt Storm Surge Barrier (Ramkema, 1978). Nevertheless, as mentioned above, many other examples of hydraulic structures with overhangs can be found in coastal areas, delta regions, lakes and reservoirs (Ramkema, 1978; Castellino et al., 2018; Martinelli et al., 2018; Van der Meer et al., 2018). Similar impacts on overhang configurations also occur in nature, for instance on the fracture of cliffs and shore platforms (Herterich et al., 2018).

In Fig. 3 the main hydraulic and structural parameters to be considered in wave impacts on vertical structures with overhangs are shown. This paper focuses on relatively small overhangs, with ratios of wave length (L) to overhang length (W) in the range of $12.1 < L/W < 43.6$, and ratios of overhang height (h) to overhang length (W) of $h/W = 3$ and $h/W = 6$. This study focusses on the conditions with zero free-board ($d = h$) which leads to the expected maximum wave surface velocity impacting the overhang.

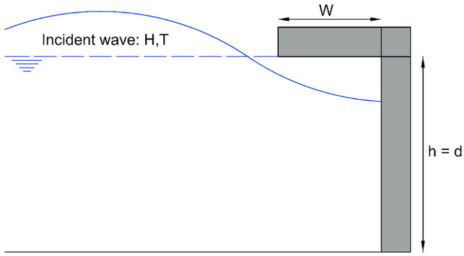

Fig. 3. H: incident wave height; T: incident wave period; d: still water depth; h: overhang height; W: overhang width.

1.1. Literature

Bagnold (1939) presented significant progress to the study of impulsive loading due to wave breaking, including two significant contributions. Firstly, on the study of the effect of air in wave impacts, observing the highest pressure magnitudes when the air cushion is small, but not zero. Secondly, with the observation that although maximum peak pressures present large variations, the area enclosed by the pressure-time curve (which can be defined as pressure-impulse, as shown in Equation (1) was remarkably constant.

$$P(x)_i = \int_{t_0}^{t_1} p(x,t)\cdot dt \tag{1}$$

where $P(x)_i$ [Pa·s] is the pressure-impulse from impact i at location x, $p(x,t)$ [Pa] is the pressure time-series during impact i at location x, t_0 [s] is start of impact i and t_1 [s] is end of impact i.

Extensive experimental tests were carried out in The Netherlands during the design of the Delta Works (1953–1997). For the Eastern Scheldt Storm Surge Barrier design, a large number of tests (Ramkema, 1978; WL, 1977; WL, 1978) studied wave loading on various configurations such as vertical wall and overhangs. Nevertheless, those studies were focused on the design optimization and did not address the definition of general design methods. Furthermore, according to WL, 1979 water can be considered incompressible for wave impact problems in civil engineering structures such as hydraulic structures. On the other hand, according to WL, 1979 the presence of air in wave impacts has a significant effect on aspects such as wave impact magnitudes, duration and variability, and the presence of pressure oscillations in the water body due to the compression and decompression of air pockets.

Also based on experimental results, Kisacik et al. (2014) defined formulas for vertical structures with long overhangs under wave breaking. Moreover, Renzi et al., 2018 studied wave slamming on oscillating water column converters based on wave tank tests. Hofland (2015) carried out experiments in order to study the wave loading on the flood gates of the Afsluitdijk, including the effect of the existing

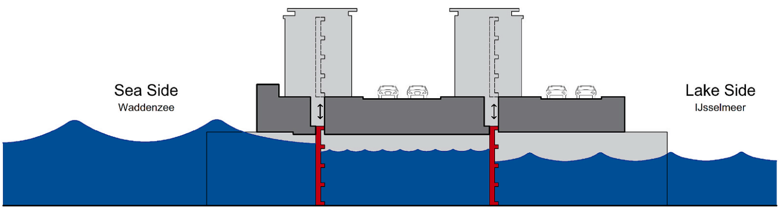

Fig. 2. Impression of an existing flood gate complex in the Afsluitdijk, closed during high water level at the sea side. Standing wave impacts can occur in this flood gate complex at the sea side due to extreme incident waves (global impact on the overhang), and/or at the lake side due to moderate incident waves (global impact on the overhang or local impact on gate reinforcements).

overhang and ventilation gaps. In those tests, a large variation of the measured extreme forces ($\sigma_F/\mu_F = 70\%$) was observed.

Cooker and Peregrine, 1990, 1995 introduced the pressure-impulse theory applied to wave impacts. This theory presents a theoretical model to estimate the wave impact pressure-impulses, based on the Navier-Stokes equation of motion. These two first contributions consider a vertical wall configuration with a horizontally moving body of water, representing a simplified breaking wave, impacting the vertical structure. Later on, Wood and Peregrine (1996) adapted the pressure-impulse theory to conditions where a vertically upward moving body of water impacts a horizontal rigid boundary above the vertical wall. This model is used in this study, as shown in Fig. 4. In addition, Peregrine and Thais, 1996, Wood et al., 2000 and Bredmose et al., 2009 address the effect of air in wave impacts, while Peregrine, 2003 combines all the contributions to the pressure-impulse theory up to that time. Most of the works on the pressure-impulse theory are analytical, with some validation in Wood et al., 2000and Bredmose et al., 2009. The theory is only partially confirmed by measurements in these studies which mainly treat breaking wave impacts. However, this low correspondence is considered to be caused by the very complicated kinematics within a breaking wave (Wood et al., 2000; Peregrine, 2003) that are not fully captured by the assumed constant impact velocity. In this present work, we address a configuration with a potentially much more uniform impact velocity.

For the design of hydraulic structures, Chen et al. (2019) introduce the use of pressure-impulses and force-impulses for the design of hydraulic structures, instead of the peak forces, and proposes a model for obtaining the wave impacts reaction forces. According to this method, the total reaction force of a wave impact is obtained from Equation (2).

$$F_{tot,r} = F_{qs+} + I_{im} \cdot \omega_n \cdot DLF_I \tag{2}$$

where $F_{tot,r}$ [N] is the total reaction force, F_{qs+} [N] is the quasi-static force, I_{im} [N·s] is the total impulsive force-impulse acting on the structure, ω_n [s^{-1}] is the angular natural frequency of the structure and DLF_I [-] is the dynamic load factor of the structure.

For impact durations smaller than one fourth of the longest natural period of the structure ($t_d < T_n/4$), the impact can be regarded as fully impulsive in a structural sense and the dynamic load factor from Equation (2) can be approximated to $DLF_I = 1$. This highlights the importance of considering the structural characteristics in the design of coastal and hydraulic structures under impulsive loads such as wave impacts. These structural characteristics define the response of the structure to impulsive loads, and in consequence the applicability of the impulse for the design or the need of considering the impulse in combination with the impact duration. Furthermore, Tieleman et al. (2019)

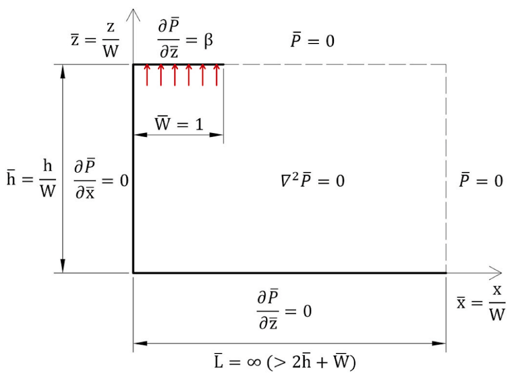

Fig. 4. Dimensionless pressure-impulse model for a vertical impact on a horizontal overhang (based on (Wood and Peregrine, 1996)).

developed a semi-analytical fluid-structure interaction model that can be used for wave impact loading, which result is the structural response of elastic structures due to such wave impacts.

1.2. Paper aims

From the previous sources, a conclusion can be drawn on the various possible advantages of using pressure-impulses and force-impulses for the design of vertical hydraulic structures with overhangs subjected to wave impacts. Those are mainly the observed lower variability (Bagnold, 1939), the availability of a theoretical model that is based on basic principles (Wood and Peregrine, 1996) and the proposed use in the design process (Chen et al., 2019).

Thus, the aim of this study is to validate the use of pressure-impulse theory for predicting wave load magnitudes (i.e. pressure-impulses and force-impulses) on vertical hydraulic structures with overhangs. The applied approach is the validation of the pressure-impulse theory based on laboratory experimental data on a setup that is realistic and strictly resemble the theoretical schematization. The scope of this study includes relatively short overhangs, regular non-breaking standing wave with limited wave steepness ($0.023 < s < 0.042$) and zero freeboard.

Section 2 describes the theoretical model based on the pressure-impulse theory. Section 3 presents the experimental tests carried out. The validation of the theoretical model is carried out in Section 4. Section 5 discusses its applicability and causes of error, while Section 6 summarizes the main conclusions of this study.

2. Theoretical model

This section describes the theoretical model for estimating standing wave impact loadings on vertical structures with overhangs, based on the pressure-impulse theory.

2.1. Pressure-impulse theory

The pressure-impulse concept in Equation (1) (integral of the impulsive pressures over time, during a wave impact) is considered in this theory. Bagnold and other authors (Bagnold, 1939; Richert, 1968), have observed that the pressure-impulse during wave impacts are significantly more constant than other magnitudes, such as pressure peaks.

The pressure-impulse theory is based on the Navier-Stokes equation of motion, for a large-scale motion such that the viscosity and surface tension terms are considered negligible. Considering that the wave impact occurs in such a small period of time, gravity and the non-linear convective terms can also be neglected. Gravity is neglected given that during those violent impacts accelerations are assumed to be much larger than gravity. The non-linear convective terms are neglected given that those violent impacts have a short duration such that the temporal derivative ($\partial \vec{u}/\partial t$) becomes very large compared to the spatial-derivative terms. Wood et al. (2000) state that this assumption is valid when the number ($t_d U/S$) is very small, where t_d is the impact duration, U is the impact velocity and S a length scale. In this paper we refer to this number as the Peregrine Number Λ considering the overhang length as the length scale, being $\Lambda = t_d U/W$. With the previous considerations, it is possible to approximate the equation of motion to Equation (3).

$$\frac{\partial \vec{u}}{\partial t} = -\frac{1}{\rho}\nabla p \tag{3}$$

where $\vec{u}$ [m/s] is the velocity vector, p [Pa] is the pressure and ρ [kg/m3] is the fluid density.

Combining Equations (1) and (3), and considering continuity for an incompressible fluid, we observe that the pressure-impulse satisfies the Laplace equation ($\nabla^2 P = 0$). Together with the boundary conditions shown in Fig. 4 (in dimensionless form), this equation can be solved in order to obtain the dimensionless pressure-impulse distribution in the desired domain and on the vertical wall.

In this paper, the pressure-impulse model is used in a dimensionless form. This is obtained considering the overhang length W (see Fig. 3) as the geometric scaling magnitude and making the impact area boundary condition also dimensionless (see Fig. 4). The geometric dimensions are made dimensionless as follows:

- The dimensionless overhang length $\overline{W}$ is equal to 1,
- the dimensionless overhang height $\overline{h}$ is equal to h/W, and
- the dimensionless axes are $\overline{x} = x/W$ and $\overline{z} = z/W$.

The impact area boundary condition is made dimensionless by the wave impact velocity (U) and the fluid density (ρ) as shown in Equation (4). The factor β was introduced by Wood et al. (2000) to describe the increase in impact pressure-impulse due to the bounce-back of entrapped air. An impact area fully covered by air would have $\beta = 2$ while an impact in vacuum would have a $\beta = 1$. In this paper β is used to account for all differences between theory and measurement, so we name it the effective bounce-back factor.

$$\frac{\partial \overline{P}}{\partial \overline{z}} = \beta \tag{4}$$

For the nondimensionalization and re-dimensionalisation of the results, the following conversion expressions are used for the pressure-impulse (P) obtained at any point in the fluid domain and for the total force-impulse (I) integrated over a given boundary such as the vertical structure below the overhang.

$$\overline{P} = \frac{P}{\rho U W} \tag{5}$$

$$\overline{I} = \frac{I}{\rho U W^2} \tag{6}$$

where ¯ represents dimensionless values, P [Pa·s] is the pressure-impulse obtained at any point in the fluid domain, I [N·s/m] is the total force-impulse integrated over a given boundary (e.g. vertical wall below overhang) for 1 m length, ρ [kg/m3] is the fluid density, U [m/s] is the impact velocity and W [m] is the overhang length and the scaling factor.

2.2. Theoretical solution

This section presents the solution for the pressure-impulse theory, taking into account the nondimensionalization described previously and considering the configuration as shown in Fig. 4. This solution is based on that of Wood and Peregrine (1996), using the semi-analytical method. This semi-analytical solution resolves the pressure-impulse theory using conformal maps. The three domain transformations used in this solution are shown hereafter.

- Conformal map: $w = u + iv = \cosh(\pi y/\overline{h})$, being $y = x + iz$ the original plane in Fig. 4.
- Translation and magnification: $c = f + ig = Mw + N$, being $M = 2/(\cosh(\pi/\overline{h}) - 1)$ and $N = M + 1$.
- Conformal map. $\zeta = \xi + i\lambda = \overline{h}\cosh^{-1}(c)/\pi$, being ζ the plane where the solution is obtained.

Following these three transformations, and solving by separation of variables, the semi-analytical expressions for calculating the pressure-impulse are shown in Equations (7) and (8). This method is solved in this study considering $n = 30$ summations, after which convergence in the results is obtained.

$$\overline{P}_{\overline{x},\overline{z}} = \beta \sum_{n=1}^{30} a e^{-\alpha_n \xi} \cos(\alpha_n \lambda) \tag{7}$$

$$a = \frac{2}{\alpha_n \overline{h}} \int_0^{\overline{h}} \frac{1}{M} \frac{\sin(\pi\lambda/\overline{h})\cos(\alpha_n \lambda)}{\sqrt{b^2 - 1}} d\lambda \tag{8}$$

where $\overline{P}^n_{\overline{x},\overline{z}}$ is the dimensionless pressure-impulse at location $(\overline{x},\overline{z})$, $\alpha_n = (n + 1/2)/\pi$, $b = (\cos(\pi\lambda/\overline{h}) - N)/M$ and the additional parameters should be used as previously defined in this paper. Note that the original variables names have been modified for consistency in this study. Note also two corrections made from expressions from Wood and Peregrine, 1996, which are assumed to be typos in Wood and Peregrine, 1996 given that the results are in full agreement. First, the original variable a_m is used as equal to a_n, while A_m is used as equal to A_n. Secondly, the expression for b is corrected with the addition of $/\overline{h}$ inside the cosine parenthesis.

This semi-analytical solution is compared with a numerical solution for the same problem using a second order central differences relaxation scheme as given in Hofland et al., 2019, and a very high agreement is observed. The deviation for the total force-impulse on the wall is 0.3% for the shorter overhang, and 0.9% for the longer overhang. Given the much higher efficiency of the semi-analytic solution, this is the method that is used in this study. According to these calculations, the total force-impact on the wall ($\overline{I} = I/\rho U W^2$) is equal to 1.62β for the shorter overhang and 1.30β for the longer overhang.

2.3. Dimensionless pressure-impulse estimation

This section presents the graphs and expressions in order to estimate the dimensionless pressure-impulse and force-impulse of a wave impact. It addresses both the dimensionless local pressure-impulses ($\overline{P} = P/\rho U W$) and the dimensionless total force-impulses acting at the vertical wall ($\overline{I} = I/\rho U W^2$).

Fig. 5a shows (for $\beta = 1$) the dimensionless pressure-impulse profile for various dimensionless overhang heights $\overline{h}$, with a normalized overhang height $\overline{z}/\overline{h}$. The fully analytical solution for an infinite depth presented by Wood and Peregrine, 1996 is also plotted for a depth of $\overline{h} = 10$. Fig. 5b presents (for $\beta = 1$) the maximum and minimum dimensionless local pressure-impulse $\overline{P}$ calculated at the top ($\overline{z} = \overline{h}$) and the bottom ($\overline{z} = 0$) of the vertical wall respectively. Equations (9) and (10) give fits of the semi-analytical solution for the maximum and minimum pressure-impulse as function of overhang height, and for other values of β.

Fig. 6 shows (for $\beta = 1$) the dimensionless force-impulse on the vertical wall below the overhang ($\overline{I}$) for different dimensionless overhang heights $\overline{h}$. It is not known to the authors that the pressure-impulse theory has been used for this estimation of the total force-impulse at the vertical wall before, as it is introduced here. This force-impulse can be estimated for any value of dimensionless overhang heights $\overline{h}$ and effective bounce-back factor β according to the fit presented in Equation (11).

2.4. Impact velocity prediction

The wave impact velocity is required for obtaining the dimensional pressure-impulse from theoretical estimations, or for obtaining the dimensionless pressure-impulse from experimental measurements. For

2

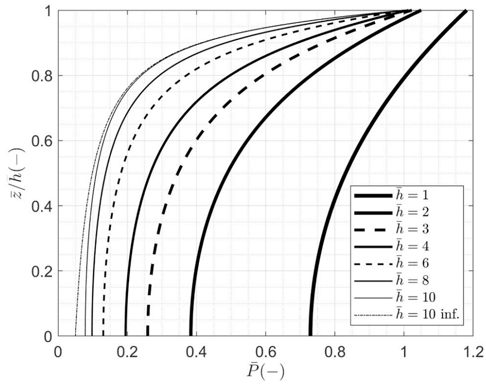

(a) Pressure-impulse profile at wall for $\beta = 1$.

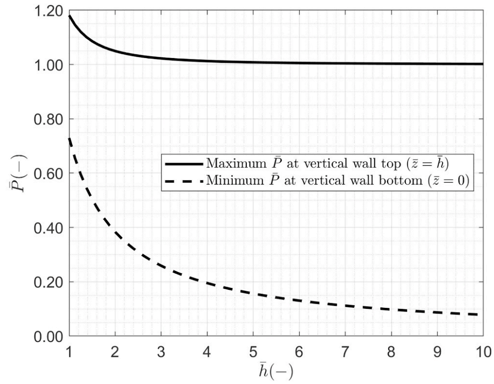

(b) Max and min pressure-impulse at wall for $\beta = 1$.

Fig. 5. Dimensionless pressure-impulse at wall ($\overline{P} = P/\rho UW$) for various $\overline{h}$ for $\beta = 1$.

$$\overline{P}_{max} = \beta\left(0.18\overline{h}^{-1.9} + 1\right) \text{ for } 1 \leq \overline{h} \leq 10 \tag{9}$$

$$\overline{P}_{min} = \beta\left(0.75\overline{h}^{-0.97}\right) \text{ for } 1 \leq \overline{h} \leq 10 \tag{10}$$

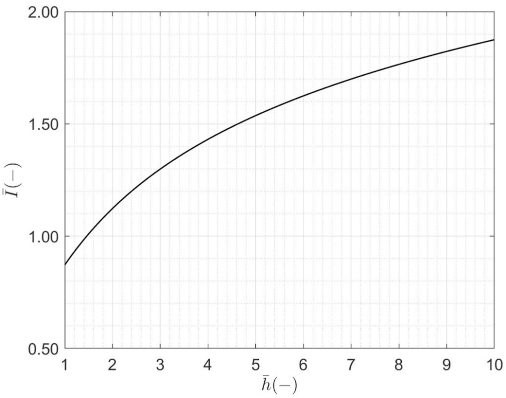

Fig. 6. Total dimensionless force-impulse at wall ($\overline{I} = I/\rho UW^2$) for $\beta = 1$.

$$\overline{I} = \beta\left(2\overline{h}^{0.18} - 1.14\right) \text{ for } 1 \leq \overline{h} \leq 10 \tag{11}$$

predicting this impact velocity, an expression based on linear wave theory is used in this study. This theory is considered suitable for the waves used in this study (Hedges, 1995) and it is a well known theory that can be implemented in a simple way in future design methodologies. According to this theory, a linear wave reflecting against a vertical wall can be described as in Equation (12).

$$\eta = (1 + cr)\frac{H_i}{2}\sin\omega t = A_w \sin\omega t \tag{12}$$

where η is the surface elevation at the wall, cr is the wave reflection coefficient at the wall, H_i is the incident wave height, ω is the angular wave frequency ($\omega = 2\pi/T$, where T is the incident wave period) and A_w is the total wave amplitude at the wall.

Combining Equation (12) (water surface position) with its derivative (water surface velocity), the water surface velocity $\dot{\eta}$ can also be expressed as function of the water surface position η ($\dot{\eta} = \omega\sqrt{A_w^2 - \eta^2}$). Furthermore, this study considers the reflection coefficient as $cr = 1$, since the incident wave is not influenced by the overhang during the period $T/2$ before the wave impact occurs. The impact velocity (U) can then be obtained from Equation (13), for the condition of zero freeboard ($d = h$) considered in this study.

$$U = \omega H_i \tag{13}$$

3. Laboratory experiments

This section describes the experimental tests carried out in this study, including the experimental facility, the main characteristics of the setup configuration, the instrumentation used, how the pressure-impulses and force-impulses are estimated and a first overview of the measured results.

3.1. Facility

The experimental data used in this paper was obtained from two test campaigns (2018 and 2019) carried out at the wave flume at the Hydraulic Engineering Laboratory at the Delft University of Technology. Fig. 7a shows an overview of the test area, illustrating the impact structure (vertical structure with an overhang) inside the wave flume and connected to instrumentation and acquisition systems. Fig. 7b shows in more detail the aluminium overhang surface supported by a 1500 kg concrete block during a wave impact. The use of this massive concrete block, solid aluminium profiles and 10 mm thick aluminium plates provided the stability and rigidity for the wave impact tests. The wave flume is 42 m long, 1 m high and 0.8 m wide. The wave generation equipment consists of a piston-type wave maker able to generate regular and irregular waves and is equipped with active reflection compensation (ARC) and second order wave steering.

Coastal Engineering 159 (2020) 103702

(a) Experimental test area.

(b) Overhang structure model setup.

Fig. 7. Overview of the experimental facility and model setup.

3.2. Experiment description

The test setup was built with an aluminium structure mounted on a concrete block inside the wave flume (see Fig. 7), with the vertical wall located at 23.3 m away from the wave generator paddle (30.8 m in the 2018 tests). The concrete block is 0.8 m wide, 0.8 m long and 1 m high and provides the stability for the structure subjected to wave impacts. The configurations considered in this study include a shorter overhang ($W = 0.1$ m) and a longer overhang ($W = 0.2$ m), as shown in the test setup illustration in Fig. 8. The regular incident waves considered in the tests are shown in Table 1. In total, 14 tests were carried out (seven for the shorter overhang and seven for the longer overhang): conditions A, B, C, D and E in 2019 and conditions A and F in 2018. For the two configurations and all incident wave conditions, the water level is located at the same height of the overhang ($d = h = 0.6$ m). These conditions are chosen because the vertically upwards moving wave surface is expected to have the maximum speed when impacting the overhang. This is expected to lead to the highest wave impact loading. For all the test conditions and configurations, 50 regular waves were considered, in order to obtain statistical information regarding the repeatability and variability of wave impact magnitudes for identical repeated incident wave conditions.

3.3. Instrumentation

An array of 3 wave gauges, with a sampling rate of 100 Hz, allowed to obtain the incident and reflected waves at 1.5 m away from the vertical wall, according to the method from Zelt and Skjelbreia (1992), see Fig. 8. All wave gauges were equipped with temperature compensation systems in order to ensure the accuracy of the water level measurements in all conditions during the tests.

Table 1
Experimental target wave conditions (see Appendix A - List of symbols).

Condition	H [m]	T [s]	L_0 [m]	s_0 [-]	h [m]	d [m]	Number of waves [-]
A	0.06	1.30	2.64	0.023	0.6	0.6	50
B	0.08	1.60	3.99	0.020	0.6	0.6	50
C	0.10	1.30	2.64	0.038	0.6	0.6	50
D	0.10	1.60	3.99	0.025	0.6	0.6	50
E	0.10	2.00	6.24	0.016	0.6	0.6	50
F	0.10	1.90	5.63	0.018	0.6	0.6	50

The results from 4 pressure sensors are analysed (6 in the 2018 tests). The pressure sensors used in the tests are Kulite HKM-375M-SG with 1 bar measurement range and sealed gauge. The sampling frequency was 20 kHz. The location of these pressure sensors is shown in Fig. 8. The pressure sensors PS2 and PS4 were only used in the 2018 tests. In all the analyses in this study, the used pressures/forces are the dynamic values, obtained once the hydrostatic pressures/forces (the pressures/forces measured before wave motion) are removed from the measurements.

Three Olympus Tough TG-5 cameras were used during the tests, with a frame rate of 59.94 fps and a resolution of 1920x1080. These camera recordings are synchronized with the pressure/wave measurements through LED light pulses recorded by the camera. In this study, only Camera 1 is used, which was located 0.5 m from the flume wall, and

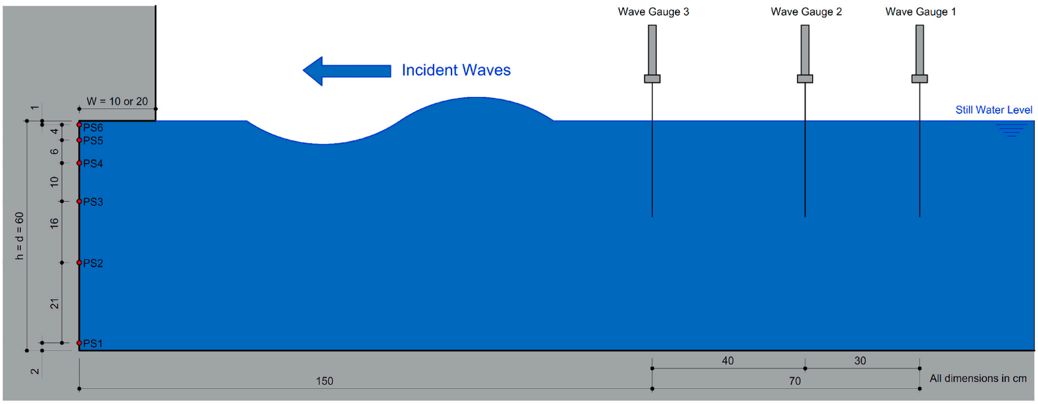

Fig. 8. Illustration of test setup and instrumentation. Note that all dimensions are in centimetres (cm).

slightly below the overhang height.

3.4. Experimental pressure-impulse calculation

This section describes the procedure used to estimate the pressure-impulses from the experimental results. Various methods were previously presented for obtaining the pressure-impulse (De Almeida et al., 2019; Cooker and Peregrine, 1990; Wood et al., 2000), but the large range of variations on the wave impact impulsive pressure signals leads to a lack of a unique method to objectively determine the pressure-impulse of different wave impacts. The method presented here addresses this issue as it follows a consistent procedure to objectively estimate pressure-impulses from the large range of different wave impact types observed in this study, with a constant criteria. This method is shown in Fig. 9 and described hereafter. The pressure-impulse is defined as the grey dashed area located between the impact start and the impact end. In this figure, the orange colours represent the impulsive part of the load while the blue ones represent the quasi-static part. The dashed blue line represents a low-pass filter applied to the impulsive time-series. In this method, the impact start is roughly defined when the pressure becomes larger than zero (i.e. hydrostatic pressure), and the impact end is roughly defined when the pressure becomes smaller than the quasi-static component.

This method is used for the analysis of the experimental results, as shown in the examples from Fig. 10. The measured impulsive pressure time-series was used after being filtered according to a low-pass third order Butterworth filter with a cut-off frequency of 100 Hz. This cut-off frequency was defined given that it allows to remove small higher frequency components but it is sufficiently large to not affect the pressure-impulse magnitude or the impact duration. Similarly, the quasi-static component was obtained after filtering the same measured pressure time-series with low-pass third order Butterworth filter with a cut-off frequency equal to two times the frequency of the incident waves. The impact start is obtained when the impulsive pressure time-series, black line, rises above 20% of the quasi-static peak, shown with the black dot. Further, the impact end is obtained when the impulsive pressure time-series, black line, approaches the quasi-static component, blue line, and their difference becomes smaller than 20% of the quasi-static peak, as shown with the magenta dot. For wave impacts with post-peak vibrations, the impact-end position is obtained after the pressure time-series, black line, is further filtered (with 25 Hz cut-off frequency), in order to limit the effect of post-impact vibrations on the estimation of the pressure-impulse and impact duration. Finally, the pressure-impulse is obtained as the integral of the area shown in green (see Fig. 10). This procedure is applied first at the uppermost location at the vertical wall (PS6, as shown in Fig. 8), which is the closest to the wave impact location and the one that shows the highest impulsive pressures. Thus, the impact duration measured at PS6 is used as the global impact duration for a given wave impact. For the other locations lower in the vertical wall (PS1 to PS5, see Fig. 8), an equivalent calculation is made based mainly on the impact durations defined at PS6. The impact start for PS1 to PS5 is equal to the impact start for PS6. Similarly, the impact end for PS1 to PS5 is equal to the impact end for PS6, but only if, and after, the difference between the impulsive pressure time-series and the quasi-static component is smaller than 20% of the peak impulsive pressure at that location, in order to capture accurately the complete pressure-impulse at those locations. The total force-impulse is then calculated by integrating the obtained pressure-impulse profile over the vertical wall height. For the validation of the theoretical model, the measured pressure-impulses are made dimensionless according to Equation (5) for $\overline{P}$ and Equation (6) for $\overline{I}$. In those equations, the wave impact velocity is obtained according to the linear wave theory expression shown in Equation (13).

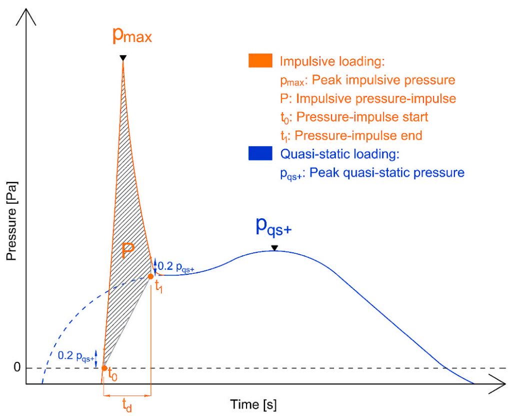

Fig. 9. Pressure-impulse calculation method.

3.5. Experimental results

This section presents a summary of the experimental results, with focus on the incident wave height characteristics, the pressure/forces measurements and the camera recordings. For decomposing the incident and reflected wave conditions, the method presented by Zelt and Skjelbreia (1992) was used. Table 2 summarizes the experimental results for the 14 tests, named according to the wave condition (see Table 1), the overhang dimension (S represents the shorter overhang with W = 0.1 m, while L represents the longer overhang with W = 0.2 m) and the year when the tests were carried out. It includes the mean incident wave height (H), the variability of the incident wave height (σ_H/μ_H), the mean wave period (T), the mean wave length (L), the mean steepness (s), the reflection coefficient (c_r) and the Ursell Number ($U_r = HL^2/d^3$) as a measure of the wave field non-linearities. According to Hedges, 1995 and considering the range of Ursell Number in all tests (1.6–9.0), and the ratios of H/L (0.02–0.04), d/L (0.14–0.25) and H/d (0.10–0.18), this wave field can be described theoretically by linear wave theories, as it is done in this study. Fig. 11 presents two examples of incident wave time-series, for condition A (smaller shorter waves, Fig. 11a) and for condition E (higher longer waves, Fig. 11b). For all test conditions, the incident wave for tests with overhangs presented reduced deviations when compared with additional tests carried out with a vertical wall without an overhang. The average deviation in incident wave height is 3.7% (3.0% for short overhangs and 4.5% for long overhangs), when comparing tests with and without overhangs exposed to the same wave generation signal. In the tests without overhangs, the measured total wave height at the vertical wall (H_{tot}) was compared with the assumed total wave height from the incident wave height ($H_{tot} = 2H_i$), leading to an average difference of 1.1%.

Table 2 includes also the mean impact durations (t_d), the calculated impact velocity (U) according to Equation (13) and the Peregrine Number ($\Lambda = t_d U/W$), similar to the one introduced by Wood et al., 2000 that describes the validity of the pressure-impulse theory. Given the small values of Λ ($\Lambda \ll 1$) it is plausible that the wave impacts considered in this study can be described theoretically by the pressure-impulse theory. Furthermore, Table 2 also includes for each test the mean dimensionless force-impulse ($\overline{I}$), the variability of the dimensionless force-impulse ($\sigma_{\overline{I}}/\mu_{\overline{I}}$) and the effective bounce-back factor (β).

Fig. 10 presents the six wave impact types observed during the tests. These figures display the pressure time-series for the pressure sensors at the highest position at the vertical wall (PS6), including the pressure peaks, impact start point, impact end point and the estimated impact-

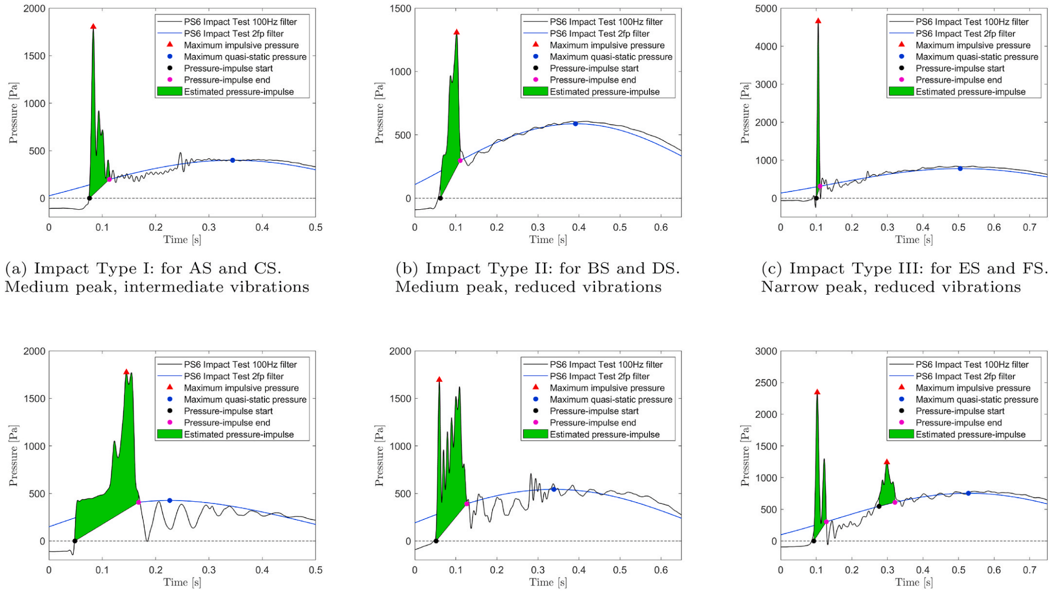

(a) Impact Type I: for AS and CS. Medium peak, intermediate vibrations

(b) Impact Type II: for BS and DS. Medium peak, reduced vibrations

(c) Impact Type III: for ES and FS. Narrow peak, reduced vibrations

(d) Impact Type IV: for AL and CL. Stepped peak, intermediate vibrations

(e) Impact Type V: for BL and DL. Wide peak, large vibrations

(f) Impact Type VI: for EL and FL. Double peak, intermediate vibrations

Fig. 10. Recorded pressure peaks for various wave impact types, at the highest location in the vertical wall (PS6), with coloured areas representing pressure-impulse (P). Note that axis scales differ.

Table 2
Summary of experimental results (see Appendix A - List of symbols).

Test	W [m]	H [m]	$\frac{\sigma_H}{\mu_H}$ [%]	T [s]	L [m]	s [-]	c_r [-]	U_r [-]	t_d [ms]	U [$\frac{m}{s}$]	Λ [-]	$\bar{I}$ [-]	$\frac{\sigma_{\bar{I}}}{\mu_{\bar{I}}}$ [%]	β [-]
AS19	0.1	0.061	2.3	1.30	2.42	0.025	0.84	1.7	37	0.294	0.11	1.68	4.6	1.04
BS19	0.1	0.084	1.8	1.60	3.27	0.026	0.93	4.1	52	0.328	0.17	1.78	4.3	1.10
CS19	0.1	0.103	3.7	1.31	2.43	0.042	0.81	2.8	36	0.497	0.18	2.19	6.2	1.35
DS19	0.1	0.104	2.4	1.60	3.27	0.032	0.94	5.2	42	0.409	0.17	2.00	6.2	1.23
ES19	0.1	0.101	0.4	2.00	4.36	0.023	0.92	8.9	10	0.318	0.03	1.68	7.5	1.03
AS18	0.1	0.059	1.4	1.30	2.42	0.024	0.85	1.6	40	0.283	0.11	1.76	4.8	1.08
FS18	0.1	0.099	1.1	1.90	4.09	0.024	0.99	7.7	14	0.329	0.05	1.88	5.8	1.15
AL19	0.2	0.060	1.3	1.30	2.42	0.025	0.67	1.6	110	0.288	0.16	1.43	3.3	1.10
BL19	0.2	0.085	3.1	1.60	3.27	0.026	0.78	4.2	69	0.335	0.11	1.55	3.7	1.19
CL19	0.2	0.100	2.0	1.30	2.43	0.041	0.63	2.7	101	0.483	0.24	1.76	3.5	1.36
DL19	0.2	0.108	3.5	1.60	3.27	0.033	0.74	5.4	57	0.426	0.12	1.62	7.0	1.25
EL19	0.2	0.103	0.6	2.00	4.36	0.024	0.82	9.0	37	0.323	0.06	1.67	9.1	1.29
AL18	0.2	0.059	1.2	1.30	2.42	0.024	0.69	1.6	116	0.286	0.17	1.38	3.4	1.06
FL18	0.2	0.105	1.7	1.90	4.09	0.026	0.82	8.1	54	0.347	0.09	1.46	10.4	1.12

related pressure-impulse. Impact Type I is observed in the tests AS and CS, characterized by one peak, an intermediate level of vibrations and an intermediate impact duration. Impact Type II is observed in the tests BS and DS, characterized by one peak, almost no vibrations and an intermediate impact duration. Impact Type III is observed in the tests ES and FS, characterized by one peak, a reduced level of vibrations and a very short impact duration. Impact Type IV is observed in the tests AL and CL, characterized by one stepped wide peak, an intermediate level of low-frequency vibrations and a very long impact duration. Impact Type V is observed in the tests BL and DL, characterized by one peak with a close secondary peak, large vibrations and a long impact duration. Impact Type VI is observed in the tests EL and FL, characterized by two peaks with an interval of 0.2 s ($\approx T/10$) between them, an intermediate level of vibrations and an intermediate impact duration. For wave impact Type VI, the impact duration (t_d) in Table 2 represents the duration of the first impact.

Fig. 12 illustrates the six wave impact types, with camera recordings at the moment when the water surface is seen to impact the overhang. Six different wave impact patterns are observed, with distinct wave shapes and air entrapments, both of which are considered to be related to each other. Thus, it can be expected that, although in different ways in each test, this entrapped air (but possibly also less extensive entrained air) plays a role in the measured wave impact loads on the structure. Furthermore, it was observed that a singular impact occurs for wave impact Type VI (conditions EL and FL), where the external part of the overhang is hit first (first peak in Fig. 10f), followed by a second impact on the left inner side of the overhang (second peak in Fig. 10f).

The experimental results show that in all the tests air is entrapped

2

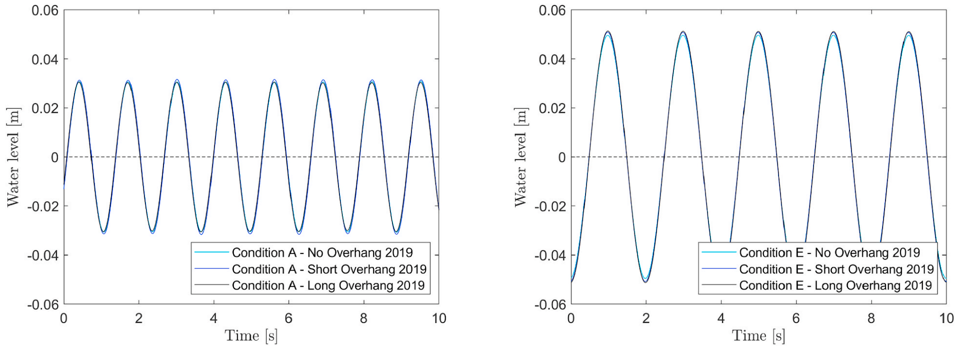

(a) Smaller shorter waves - Condition A.

(b) Higher longer waves - Condition E.

Fig. 11. Example of incident wave time series measured at 1.5 m from the vertical wall.

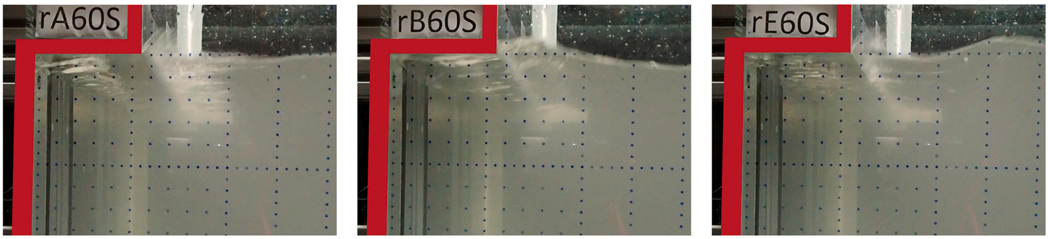

(a) Impact Type I: for AS and CS. Intermediate entrapped air, near the wall

(b) Impact Type II: for BS and DS. Intermediate entrapped air, distributed

(c) Impact Type III: for ES and FS. Reduced entrapped air, distributed

(d) Impact Type IV: for AL and CL. Extensive entrapped air, distributed

(e) Impact Type V: for BL and DL. Intermediate entrapped air, far from wall

(f) Impact Type VI: for EL and FL. Double peak, singular air pattern

Fig. 12. Impact types, from camera recordings at the moment when the water surface impacts the overhang. For wave impact Type VI, Fig. 12f displays the moment of the first impact, corresponding to the first pressure peak shown in Fig. 10f.

during the wave impact. In the tests with larger air entrapment, such as Impact Type IV, the impact duration was much longer. In the tests with smaller air entrapment, such as Impact Type III, the impact duration was much shorter, and the pressure peak was remarkably higher. Furthermore, a comparison between wave impact Type II (medium peak) and Type III (narrow high peak) is carried out, both of which have the same overhang length and relatively similar incident waves. This comparison (considering the examples shown in Fig. 10b and c) shows a very large difference in peak pressures (356%) while the difference in the pressure-impulse (P) is much smaller and negative (−6.47%). In summary, the experimental tests in this study indicate that an increased presence of air in wave impacts leads to a larger variability of wave impact magnitudes, a slight increase in the impulses, a large increase in the impact durations and a large decrease of the pressure/force peaks.

4. Validation of the theoretical model

This section addresses the validation of the theoretical model presented in Section 2, with the experimental results described in Section 3. The long waves considered in this study ($L \gg W$) are used to theoretically have a uniform impact velocity over the length of the overhang, in agreement with how it is considered in the pressure-impulse theory schematization (see Section 2). All the tests used in this study were carried out with regular waves and the following ranges of dimensionless ratios.

- d/H: between 5.6 and 10.2
- W/H: between 0.96 and 3.38
- L/W: between 12.1 and 43.6
- h/W: 3 and 6
- $\Lambda = t_d U/W$: between 0.05 and 0.24

4.1. Pressure-impulse profile $\overline{P}$

This section addresses the pressure-impulse profile at the vertical wall ($\overline{P}$) caused by a standing regular wave impact. Fig. 13 shows the theoretical formulae compared with the experimental results for all the tests carried out. In the graphs from Fig. 13, the solid line represents the dimensionless pressure-impulse profile on the vertical wall based on the pressure-impulse theory for $\beta = 1$. The black dots represent the dimensionless pressure-impulse measured from the laboratory tests, obtained as the mean of the 50 regular waves used in the analysis of each test. From these results, the dashed line represents the experimental pressure-impulse profile, obtained as a power fit from to the measured data. In addition, from the analysis of the 50 waves from each test, a 95% confidence band for the mean ($\delta = \pm 2.009\sigma\sqrt{1/50}$) and a 95% prediction interval for a separate observation ($\delta = \pm 2.009\sigma\sqrt{1+1/50}$) are shown, calculated according to the student-t distribution. In order to make the measured pressure-impulse dimensionless, the impact velocity according to Equation (13) is used, considering the measured incident wave data from Table 2.

According to the graphs in Fig. 13, the experimental results showed good agreement with the theoretical estimations. In all the cases, the shape of the vertical distribution is in agreement, with a general underestimation by pressure-impulse predictions with the theoretical no air effect ($\beta = 1$). The total force-impulse estimations of the 14 tests are summarized in the last three columns in Table 2. For each of the tests shown in Fig. 13, the total force-impulse ($\overline{I}$) is calculated as the integral of the power fit profile (dashed line in Fig. 13) over the overhang height. Table 2 includes the measured mean values of the total force-impulse at the vertical wall ($\overline{I}$), the mean variations of the measured force-impulses from the 50 waves in a test ($\sigma_{\overline{I}}/\mu_{\overline{I}}$) and the calculated experimental effective bounce-back factor (β) for each test. These experiential results showed that the averaged mean variability of the total force-impulses ($\langle\sigma_{\overline{I}}/\mu_{\overline{I}}\rangle_{mean} = \langle\sigma_I/\mu_I\rangle_{mean} = 5.7\%$) is smaller than that of the total force peaks ($\langle\sigma_F/\mu_F\rangle_{mean} = 11.4\%$).

4.2. Total force-impulse at wall $\overline{I}$

In this section, the total force-impulse at the vertical wall $\overline{I}$ caused by a standing regular wave impact is analysed. The validation of the theoretical model is made based on regular wave experimental data, which were analysed individually in the previous section. Fig. 14 shows the experimental results (see Table 2) compared with the theoretical formulae.

These results show the suitability of the theoretical model based on the pressure-impulse theory for preliminary estimations of wave impact loading on vertical structures with overhangs. Fig. 14 (and also Table 2) shows that the measured force-impulses from the experimental tests are always higher than the theoretical estimations without the influence of air ($\beta = 1$). The experimental data in this study presents a mean value of $\beta = 1.17$ with a standard deviation of $\sigma_\beta = 0.11$, showing a relatively reduced deviation ($\sigma_\beta/\beta = 9.4\%$). Fig. 14 also shows the theoretical formulae with maximum bounce-back air effect ($\beta = 2$) according to pressure-impulse theory (Wood et al., 2000). According to this, the impact surface extension fully covered by an air bubble leads to a double pressure-impulse magnitude. Thus, the measured impulses above the no-air ($\beta = 1$) theoretical solution are in agreement with the camera recording from Fig. 12 where in all the tests a portion of impact surface below the overhang was covered by an air bubble with varying dimensions. It is remarkable that the impacts in test ES (Fig. 10c) lead to an impulse very close to the no-air theoretical solution ($\beta = 1$) while in Fig. 12c it can be seen that indeed only a small portion of air is entrapped at the moment of impact.

Fig. 15 combines all the pressure-impulse ($\overline{P}$) results from shorter overhang (Fig. 15a) and longer overhangs (Fig. 15b). The measured pressure-impulses (black dots) are combined with a power fitting of these combined measured results (dashed line), the no-air model estimation with $\beta = 1$ and the experimentally calibrated model estimation with $\beta = 1.17$. The model estimation with $\beta = 1.17$ is able to predict accurately the total force-impact on the wall ($\overline{I}$) as shown previously, but it underestimates the pressure-impulse at the lower part of the wall, while overestimates the pressure-impulse at the upper part of the wall. Furthermore, and especially for longer overhangs, the variability on the pressure-impulse at the upper part of the wall is remarkably higher. These differences observed at the upper part of the wall are expected to be caused by highly dynamic processes that take place during the wave impacts, and deviate partially from the assumptions of the pressure-impulse theory.

For estimating force-impulses from a wave impact (I), the following steps could be followed. First, the dimensionless overhang height $\overline{h} = h/W$ should be obtained from a given structure geometry. Second, the dimensionless force-impulse $\overline{I}$ can be obtained from Equation (11), using $\beta = 1.17$. Third, the wave impact velocity can be obtained from linear wave theory (see Equation (13), for $d = h$ and 100% wave reflection). And fourth, the dimensional force-impulse I can be estimated according to Equation (5). More extensive validation data is recommended in order to use this theoretical model as a design tool, including broader incident wave conditions and structure configurations.

5. Discussion

This section discusses the potential causes for differences between theory and measurements, which possibly are the suitability of the impact velocity estimation based on linear wave theory (U), the impulsive character of the wave impact assumed by the pressure-impulse theory (Λ), the influence of the air and other wave impact processes on the pressure-impulses (β) and the uncertainty regarding the method for obtaining the pressure-impulse (summarized in Fig. 9).

According to the data presented in Table 2 and the criteria from Hedges, 1995, the incident wave field can be described by the linear wave theories as used in this study. Furthermore, the additional tests carried out without an overhang showed that the measured total wave height at the wall and the vertical velocities were in agreement with the linear wave theory (3.2% discrepancy). Thus, it is concluded that the linear wave theory is suitable for describing the wave field in this study, and in consequence is suitable for the estimations of the wave impact velocity U, as presented in Equation (5). Furthermore, the simplicity of its expressions makes it particularly suitable for being used for a design estimation. The influence of the overhang on the kinematics near the structure should be accounted for, but the impact follows half a wave period ($T/2$) without the influence of the overhang on the incident wave. It is thus considered that the assumption of a 100% reflection ($cr = 1$) considered in this study is also valid.

Considering the data presented in Table 2 and the criteria from Wood et al., 2000, all the wave impacts in this study can be described by the pressure-impulse theory. The limited obtained values of Λ ($\Lambda = 0.05$ to $0.24 < 1$) indicate that the assumptions made in the derivation of this theory (see Section 2) can be considered valid. The tests carried out in Wood et al., 2000 for breaking waves lead to values of Λ (considering the wave impact length as the length scale) between 0.14 and 0.40, which were also considered to be within the limits of the pressure-impulse theory validity. Nevertheless, it is also highlighted that

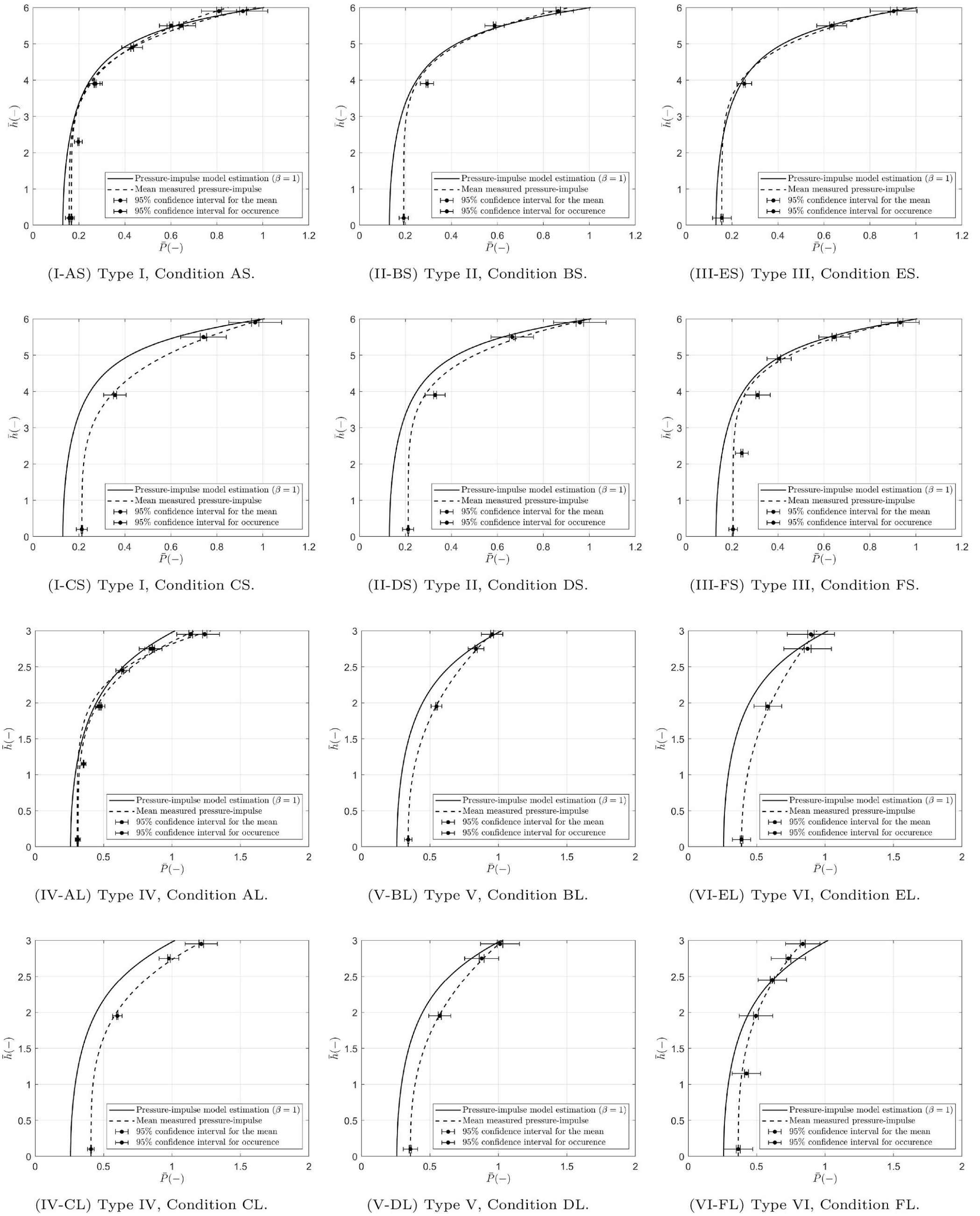

(I-AS) Type I, Condition AS.
(II-BS) Type II, Condition BS.
(III-ES) Type III, Condition ES.
(I-CS) Type I, Condition CS.
(II-DS) Type II, Condition DS.
(III-FS) Type III, Condition FS.
(IV-AL) Type IV, Condition AL.
(V-BL) Type V, Condition BL.
(VI-EL) Type VI, Condition EL.
(IV-CL) Type IV, Condition CL.
(V-DL) Type V, Condition DL.
(VI-FL) Type VI, Condition FL.

Fig. 13. Dimensionless pressure-impulse profile $\overline{P}$. Note that axis scales differ.

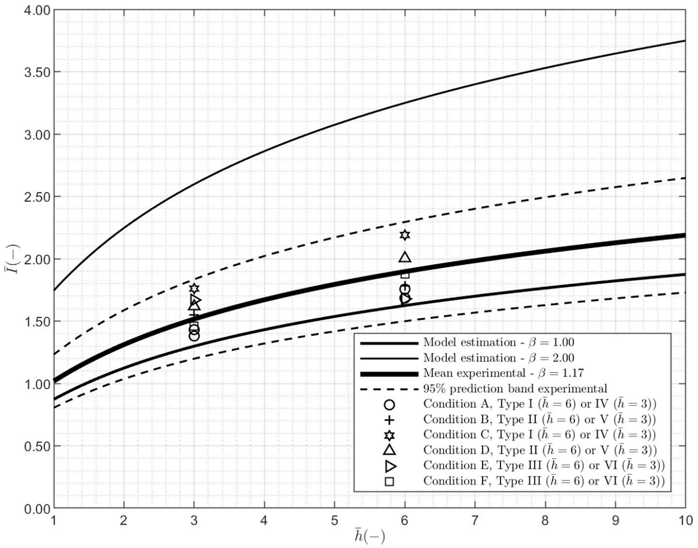

Fig. 14. Regular waves - Total dimensionless force-impulse at wall $\bar{I}$.

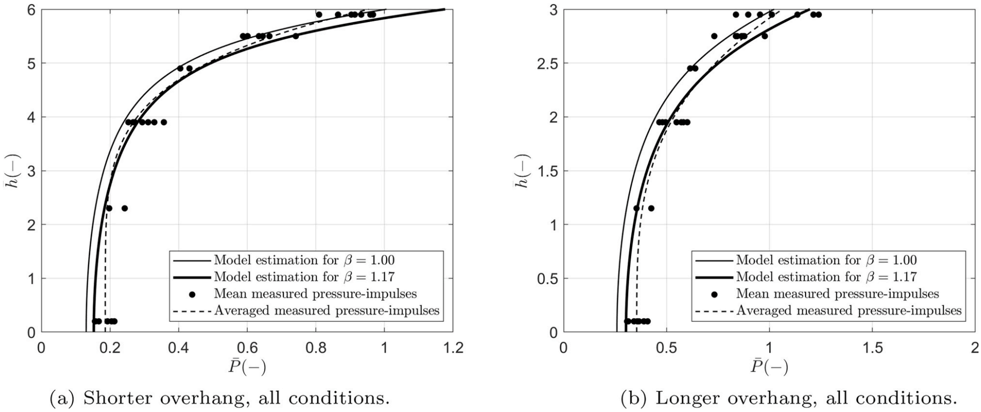

Fig. 15. Summary dimensionless pressure-impulse profile $\bar{P}$.

more violent impacts with lower Λ are expected to show better agreement with the theory. Thus, although the test CL present a higher value of Λ, it is considered that all the tests in this study fall within the range of validity for the pressure-impulse theory.

Taking into account the observations from Fig. 12, the presence of vibrations in the time series from Fig. 10, the variation in pressure peaks and the variations in impact duration, it is concluded that the results of this study are influenced by the distinct presence of air in the various tests. It is also highlighted how the measured pressure-impulse from tests with a reduced amount of entrapped air at the impact (ES), is very similar to the theoretical estimations for no-air conditions ($\beta = 1$). In general, it is observed that a large air entrapment seems to be the main common factor for tests where $\beta \gg 1$. Thus, the factor β accounts in this study mainly for the presence of air in the impacts and the consequent deviations from the theoretical results with no air presence.

This study presents a method for the estimation of the pressure-impulse from the pressure measurements. This method follows other proposals from (De Almeida et al., 2019; Cooker and Peregrine, 1990; Wood et al., 2000), which do not define a consistent procedure to estimate the pressure-impulse of different impulsive pressure signals from different wave impact types. The method used in this study addresses this issue and provides a consistent criteria to calculate pressure-impulses in all tests in this study, including all different impulsive pressure signals. Thus, this method allows to limit the variability of pressure-impulse estimations based on varying estimation criteria. Nevertheless, this method should be further evaluated in a wider range of impulsive pressure time series.

2

6. Conclusions

The use of the pressure-impulse theory for estimating wave impact load magnitudes caused by standing regular waves on vertical structures with relatively short overhangs is evaluated. The theory is compared to laboratory experimental data, and a simplified but realistic configuration with regular waves was used to this end. This addresses an existing knowledge gap on wave impact loading estimations on such structures, since such an experimental validation of the pressure-impulse theory is not known to the authors. The aim of this paper is thus to contribute to the assessment of new and renovated coastal hydraulic structures with overhangs. The experimental data used in this study included relatively short overhangs with respect to the overhang height ($3 < h/W < 6$), relatively short overhangs with respect to the wave length ($12.1 < L/W < 43.6$), low steepness regular waves ($0.023 < s < 0.042$) and non-breaking conditions ($5.6 < d/H < 10.2$).

A model for estimating the pressure-impulse field caused by standing wave impacts on structures with overhangs based on the pressure-impulse theory is used. This allows to determine the pressure-impulse profile at the vertical wall below the overhang (P), and the total force-impulse (I) acting in such a vertical wall. The theoretical estimations are validated with experimental data, from which an effective bounce-back factor of $\beta = 1.17$ is obtained ($\sigma_\beta = 0.11$), accounting mainly for the effect of the air in the wave impact. The assumptions considered in the pressure-impulse theory are verified in this study, as the measured values of the newly named Peregrine Number ($\Lambda = t_d U/W$) are sufficiently small ($\Lambda = 0.05$ to $0.24 < 1$). Furthermore, the wave impact velocity is estimated by linear wave theory ($U = \omega H_i$), for the condition of 100% reflection ($cr = 1$) and the zero freeboard used in this study. The use of a linear wave theory is supported, among others, by the reduced non-linearities of the incident waves as described by the Ursell Number ($1.6 < U_r < 9.0$) and the low steepness of the incident waves ($0.023 < s < 0.042$).

The analysis of the experimental data reinforces the previous observations that the pressure-impulses and force-impulses are more constant than pressure/force peaks. In this study the measured force-impulses are more stable ($\langle \sigma_{\bar{I}}/\mu_{\bar{I}} \rangle_{mean} = \langle \sigma_I/\mu_I \rangle_{mean} = 5.7\%$) compared with the force peaks ($\langle \sigma_F/\mu_F \rangle_{mean} = 11.4\%$), for tests consisting of 50 regular incident waves. Furthermore, a comparison between wave impact Type II (medium peak) and Type III (narrow high peak) is carried out, both of which have the same overhang length and relatively similar incident waves. This comparison shows a very large difference in peak pressures (356%) while the difference in the measured pressure-impulse (P) is much smaller and negative (−6.47%). This lower variability of pressure-impulses and force-impulses is regarded as a positive factor to recommend its use in the design of hydraulic structures. The theoretical model presented in this study can be used to this end, in order to estimate pressure-impulses and force-impulses from standing wave impacts on structures with relatively short overhangs. Nevertheless, more extensive validation of this method is recommended, accounting for a more extensive range of structure configurations and incident wave conditions.

Author Statement

E.d.A.: Conceptualization, Methodology, Validation, Investigation, Software, Writing-Review & Editing, Formal Analysis, Data Curation, Writing-Original Draft and Visualization.

B.H.: Conceptualization, Methodology, Validation, Investigation, Software, Writing-Review & Editing, Resources, Supervision, Funding Acquisition and Project Administration.

Declaration of competing interest

The authors declare that they have no known competing financial interests or personal relationships that could have appeared to influence the work reported in this paper.

Acknowledgements

This study is part of the DynaHicS (Dynamics of Hydraulic Structures) research programme, supported by NWO (Nederlandse Organisatie voor Wetenschappelijk Onderzoek) grant ALWTW.2016.041.

List of symbols

A_w	Total wave amplitude at wall [m]
c_r	Wave reflection coefficient [-]
d	Still water depth [m]
DLF_I	Structure dynamic load factor [-]
F	Force [N]
$F_{tot,r}$	Total reaction force [N]
F_{qs+}	Quasi-static force [N]
h	Overhang height [m]
$\bar{h}$	Dimensionless overhang height [-]
H	Wave height [m]
H_i	Incident wave height [m]
I	Force-impulse [N · s]
$\bar{I}$	Dimensionless force-impulse [-]
I_{im}	Total impulsive force-impulse [N · s]
L	Wave length [m]
L_0	Deep water wave length [m]
p	Pressure [Pa]
$p(x,t)$	Pressure time-series during impact i at location x [Pa]
P	Pressure-impulse [Pa · s]
$\bar{P}$	Dimensionless pressure-impulse [-]
$P(x)_i$	Pressure-impulse from impact i at location x [Pa · s]
s	Wave steepness [-]
s_0	Deep water wave steepness [-]
T	Wave period [s]

T_n	Structure natural period [s]
t_d	Wave impact duration [s]
t_0	Start of wave impact i [s]
t_1	End of wave impact i [s]
U	Impact velocity [m/s]
U_r	Ursell Number [-]
$\vec{u}$	Velocity vector [m/s]
x	Horizontal dimension [m]
$\overline{x}$	Dimensionless horizontal dimension [-]
W	Overhang length [m]
$\overline{W}$	Dimensionless overhang length [-]
z	Vertical dimension [m]
$\overline{z}$	Dimensionless vertical dimension [-]
β	Effective bounce-back effect [-]
η	Wave surface position [m]
$\dot{\eta}$	Wave surface velocity [m/s]
Λ	Peregrine Number [-]
μ_F	Mean force [N]
μ_H	Mean wave height [m]
$\mu_{\overline{I}}$	Mean dimensionless force-impulse [-]
σ_β	Standard deviation of effective bounce-back effect [-]
σ_F	Standard deviation of force [N]
σ_H	Standard deviation of wave height [m]
$\sigma_{\overline{I}}$	Standard deviation of dimensionless force-impulse [-]
ω	Angular wave frequency [s^{-1}]
ω_n	Angular structure natural frequency [s^{-1}]
ρ	Fluid density [kg/m^3]

References

Bagnold, R.A., 1939. Wave-pressure Research, vol. 12. The institution of Civil Engineers, pp. 202–226.
Bredmose, H., Peregrine, D., Bullock, G., 2009. Violent breaking wave impacts. part 2: modelling the effect of air. J. Fluid Mech. 641, 389–430.
Castellino, M., Sammarco, P., Romano, A., Martinelli, L., Ruol, P., Franco, L., Girolamo, P.D., 2018. Large impulsive forces on recurved parapets under non-breaking waves. a numerical study. Coast Eng. 136, 1–15.
Chen, X., Hofland, B., Altomare, C., Suzuki, T., Uijttewaal, W., 2015. Forces on a vertical wall on a dike crest due to overtopping flow. Coast Eng. 95, 94–104.
Chen, X., Hofland, B., Uijttewaal, W., 2016. Maximum overtopping forces on a dike-mounted wall with a shallow foreshore. Coast Eng. 116, 89–102.
Chen, X., Hofland, B., Molenaar, W., Capel, A., Gent, M.R.V., 2019. Use of impulses to determine the reaction force of a hydraulic structure with an overhang due to wave impact. Coast Eng. 147, 75–88.
Cooker, M.J., Peregrine, D.H., 1990. A model for breaking wave impact pressures. In: Proc. Coastal Engineering Conference 1990, Delft, The Netherlands.
Cooker, M.J., Peregrine, D.H., 1995. Pressure-impulse theory for liquid impact problems. J. Fluid Mech. 297, 193–214.
Cuomo, G., Allsop, W., Bruce, T., Pearson, J., 2010. Breaking wave loads at vertical seawalls and breakwaters. Coast Eng. 57 (4), 424–439.
De Almeida, E., Hofland, B., Jonkman, S., 2019. Wave impact pressure-impulse on vertical structures with overhangs. In: Proc. Coastal Structures Conference 2019, Hannover, Germany. Bundesanstalt für Wasserbau.
Dias, F., Ghidaglia, J.-M., 2018. Slamming: recent progress in the evaluation of impact pressures. Annu. Rev. Fluid Mech. 50 (1), 243–273.
Goda, Y., 1974. A new method of wave pressure calculation for the design of composite breakwater. In: Proc. Coastal Engineering Conference 1974, Copenhagen, Denmark.
Hedges, T., 1995. Regions of validity of analytical wave theories. In: Proc. ICE Water Maritime and Energy 1995, London, United Kingdom.
Herterich, J., Cox, R., Dias, F., 2018. How does wave impact generate large boulders? modelling hydraulic fracture of cliffs and shore platforms. Mar. Geol. 399, 34–46.
Hofland, B., 2015. Modeltesten Golfkrachten Spuisluizen Afsluitdijk, Meetrapport 1220263. Deltares, Delft, The Netherlands.
Hofland, B., Passos, M., De Almeida, E., 2019. Effect of venting holes to relieve wave impact pressures on flood gates with overhangs. In: Proc. Coastal Structures Conference 2019, Hannover, Germany. Bundesanstalt für Wasserbau.
Kisacik, D., Troch, P., Bogaert, P.V., Caspeele, R., 2014. Investigation of uplift impact forces on a vertical wall with an overhanging horizontal cantilever slab. Coast Eng. 90, 12–22.
Martinelli, L., Ruol, P., Volpato, M., Favaretto, C., Castellino, M., Girolamo, P.D., Franco, L., Romano, A., Sammarco, P., 2018. Experimental investigation on non-breaking wave forces and overtopping at the recurved parapets of vertical breakwaters. Coast Eng. 141, 52–67.
Minikin, R.R., 1950. Winds, Waves and Maritime Structures. Griffin, London, United Kingdom.
Oumeraci, H., Kortenhaus, A., Allsop, W., de Groot, M., Crouch, R., Vrijling, H., Voortman, H., 2001. Proverbs: Probabilistic Design Tools for Vertical Breakwaters. Balkema, Lisse.
Peregrine, D.H., 2003. Water-wave impact on walls. Annu. Rev. Fluid Mech. 35, 23–43.
Peregrine, D.H., Thais, L., 1996. The effect of entrained air in violent wave impacts. J. Fluid Mech. 325, 377–397.
Ramkema, C., 1978. A model law for wave impacts on coastal structures. In: Proc. Coastal Engineering Conference 1978, Hamburg, Germany.
Renzi, E., Wei, Y., Dias, F., 2018. The pressure impulse of wave slamming on an oscillating wave energy converter. J. Fluid Struct. 82, 258–271.
Richert, G., 1968. Experimental investigation of shock pressures against breakwaters. In: Proc. Coastal Engineering Conference 1968, London, United Kingdom.
Takahashi, S., Tanimoto, K., Shimosako, K., 1994. A proposal of impulsive pressure coefficient for design of composite breakwaters. In: Proc. International Conference of Hydro-Technical Engineering for Port and Harbour Construction 1994, Yokosuka, Japan.
Tieleman, O.C., Tsouvalas, A., Hofland, B., Jonkman, S.N., 2019. A three dimensional semi-analytical model for the prediction of gate vibrations. Mar. Struct. 65, 134–153.
Van der Meer, J.W., Allsop, N.W.H., Bruce, T., De Rouck, J., Kortenhaus, A., Pullen, T., Schüttrumpf, H., Troch, P., Zanuttigh, B., 2018. Eurotop, Manual on Wave Overtopping of Sea Defences and Related Structures. An Overtopping Manual Largely Based on European Research, but for Worldwide Application, second ed. www.overtopping-manual.com.
WL, 1977. Wave impacts on the gate in the Eastern Scheldt caisson (In Dutch: Golfklappen op de schuif in de oosterschelde-caisson, Verslag M 1335 deel I). WL Delft Hydraulics (presently Deltares), Delft, The Netherlands.
WL, 1979. A piston model with compressible water (In Dutch: Golfklappen: Een Zuigermodel Met Samendrukbaar Water, Verslag M 1335 Deel II). WL Delft Hydraulics (presently Deltares), Delft, The Netherlands.
WL, 1978. Wave impacts against concrete perforated gates (In Dutch: Golfklappen Tegen Betonnen Roosterschuiven, Verslag M 1381 Deel II). WL Delft Hydraulics (presently Deltares), Delft, The Netherlands.
WL, 1979. A literature review and scale effects in model studies (In Dutch: Golfklappen: een literatuuroverzicht en schaaleffekten in modelonderzoek, Verslag M 1335 deel III). WL Delft Hydraulics (presently Deltares), Delft, The Netherlands.
Wood, D.J., Peregrine, D.H., 1996. Wave impact beneath a horizontal surface. In: Proc. Coastal Engineering Conference 1996, Orland, United States.
Wood, D.J., Peregrine, D.H., Bruce, T., 2000. Study of wave impact against a wall with pressure-impulse theory. i: trapped air. J. Waterw. Port, Coast. Ocean Eng. 126 (4), 182–190.
Zelt, J., Skjelbreia, J., 1992. Estimating incident and reflected wave fields using an arbitrary number of wave gauges. In: Proc. Coastal Engineering Conference 1992, Venice, Italy.

3

Wave surface impact velocity and air entrapment

This chapter has been published in "Experimental observations on impact velocity and entrapped air for standing wave impacts on vertical hydraulic structures with overhangs" in the Journal of Marine Science and Engineering (De Almeida & Hofland 2020b).

Journal of
Marine Science and Engineering

MDPI

Article

Experimental Observations on Impact Velocity and Entrapped Air for Standing Wave Impacts on Vertical Hydraulic Structures with Overhangs

3

Ermano de Almeida * and Bas Hofland

Department of Hydraulic Engineering, Faculty of Civil Engineering and Geosciences, Delft University of Technology, Stevinweg 1, 2628 CN Delft, The Netherlands; B.Hofland@tudelft.nl
* Correspondence: E.deAlmeida@tudelft.nl

Received: 12 October 2020; Accepted: 27 October 2020; Published: 30 October 2020

check for updates

Abstract: This study focusses on increasing the understanding on vertical hydraulic structures with relatively short overhangs subjected to standing wave impacts. To this end, the impact velocity and the entrapped air are studied in detail, given their influence on the impulsive loading characteristics and consequently on the structural dynamic response. This study is based on regular wave laboratory experimental data obtained for relatively short overhangs with respect to the wave length and with respect to the overhang height. The laboratory tests illustrate the complex wave hydrodynamics before the wave impacts, influenced by the incident wave conditions and structural characteristics. Regarding the impact velocity, the experimental measurements with a wall wave gauge in the tests without overhangs show that the maximum upward velocities deviate from linear wave theory between +5.5% and +13.0%, while the zero-crossing upward velocities deviate from linear wave theory between +1.9% and +7.0%. The zero-crossing upward velocities estimated from third order wave theory deviate from the linear wave theory between +1.8% and +4.7%. In the tests with overhangs, the maximum upward velocity below the overhang estimated by camera recording measurements deviates from linear wave theory between −11.8% and +13.4%. It was also found that when considering the experimental impact velocity from camera recordings in the tests with overhangs, the mean effective bounce-back factor β deviates relatively little from when linear wave theory is used (≈1%), while the uncertainty described by the standard deviation increases significantly (≈35%). Regarding the entrapped air, it is shown that the interaction between incident wave parameters and structural configurations leads to a large variation in the entrapped air area, up to a factor of 5.7 for shorter overhangs and a factor of 9.5 for longer overhangs. This variability in entrapped air characteristics leads to significant effects on the loading on the structure, as observed by the variability on pressure measurements. The experimental results showed increasing impact durations and increasing effective bounce-back factor β in the tests with increasing entrapped air dimensions. This study highlights the importance of the details of the impact velocity and entrapped air for load estimations during the design of vertical hydraulic structures exposed to standing wave impacts. This is particularly important for thin structures such as steel gates which are susceptible to a dynamic behaviour under such impulsive loads.

Keywords: wave impacts; impulsive loading; overhangs; impact velocity; entrapped air

1. Introduction

During the next years and decades, a wide range of new vertical hydraulic structures will be designed and constructed worldwide. Furthermore, a number of existing vertical hydraulic structures will be renewed and modernised after the end of their original design lifetime, due to more strict safety requirements, due to increased environmental loads or due to a combination of these factors. Wave loads, and more precisely wave impacts, usually play an important role in the design of these hydraulic structures. Thus, extended knowledge on the design of vertical hydraulic structures exposed to wave impacts is needed. According to Reference [1], three different wave impact types can take place at hydraulic structures: caused by breaking waves on a vertical wall, caused by overtopping waves on a crest wall and caused by non-breaking waves on a vertical wall with a horizontal overhang. Among these three configurations, this study focusses on wave impacts on vertical hydraulic structures with horizontal overhangs, generated by non-breaking standing waves.

As described in Reference [1], previous studies focused on wave impacts generated by breaking waves acting on vertical walls [2–9]. Vertical walls with long overhangs were also studied but only exposed to breaking wave impacts [10], while References [11,12] addressed wave impacts on structures exposed to overtopping waves. Furthermore, wave impact loads acting on piers and bridge decks were studied in References [13–16]. Also, References [17–19] show recent numerical and experimental models and tools for assessing slamming loads on offshore structures, natural gas tanks and ship hulls. In opposition to this, an important knowledge gap existed until recently regarding wave impact loads generated by non-breaking standing waves on vertical structures with overhangs, which can be found in storm surge barriers, flood gates, sluice gates, dewatering sluices, lock gates and crest walls [20–23]. Nevertheless, this gets increasing attention, as recently addressed by Reference [1], with a validation of the pressure-impulse theory applied to wave impacts caused by non-breaking standing waves on vertical hydraulic structures with short overhangs. The present study has the aim to extend the existing knowledge on this particular type of wave impact by means of a more detailed analysis of additional measurements from the experiments presented in Reference [1], considering the impact velocity and the entrapped air.

1.1. Literature

Bagnold [2] is a fundamental reference on the study of impulsive loading caused by wave breaking, based on two important observations. Firstly, describing that although the maximum measured pressure peaks varied significantly from impact to impact, the pressure impulse (i.e., area enclosed by the pressure-time curve) was remarkably more constant. Secondly, observing that the highest measured pressure peaks took place when the air cushion is smaller but not zero. In addition, Bagnold [2] introduced the piston model for the effect of entrapped air cushions in wave impacts, which has been later used and extended, among others, in References [6,20].

During the design and construction of the Delta Works (1953–1997), a wide range of laboratory test campaigns took place in The Netherlands, in order to study the wave loads acting on these hydraulic structures. These tests examined structures such as the Eastern Scheldt Storm Surge Barrier, where wave loadings were studied considering various geometries which included vertical walls with overhangs [20,24,25]. However, these studies did not present general design guidelines, as they were focused on the design optimization of these singular structures. Based on these experimental tests, Reference [26] concludes that water can be considered incompressible for conditions such as wave impacts on hydraulic structures. Furthermore, Reference [27] concludes that air pockets have a decisive influence on the characteristics and magnitudes of wave impacts. More recently, Hofland [28] studied the sluice gates of the Afsluitdijk subjected to wave loads, by means of experimental tests that included the effect of the existing overhang (i.e., defence beam) and ventilation gaps.

The pressure-impulse theory applied to wave impacts was introduced by References [29,30]. This model is based on the Navier-Stokes equation of motion and allows to determine the pressure-impulse caused by a wave impact. These first two studies address a vertical wall with a horizontally-moving water volume (which describes a simplified breaking wave) impacting on the vertical wall. Furthermore, Wood and Peregrine [31] extended this theory to a different configuration, which addresses a vertically-upward-moving water volume (which describes a simplified reflecting wave) impacting on a horizontal surface. Later on, References [32–34] studied the presence of air in wave impact conditions, and Reference [35] summarized the pressure-impulse theory contributions. The majority of the studies on pressure-impulse theory are analytical with limited experimental validation in References [33,34]. These studies include mainly breaking waves experimental data and lead to only partial validation of the theory. This low agreement between theory and experiments is considered to be caused by the complicated kinematics observed in breaking waves, and which may not be correctly described by a uniform impact velocity. The experimental validation presented in Reference [1], considering a combination of models from References [29–31], addressed a configuration with an expected more uniform and predictable impact velocity caused by non-breaking standing waves and obtained a closer confirmation of the theory.

Several theories exist regarding standing wave motion at vertical walls. Besides linear wave theory, earlier theories used in engineering to predict wave loads of standing waves are the ones introduced by Sainflou [36] and Miche [37]. Later, following the work for infinite depth and lower orders [38,39], a fourth order Stokes-like expansion for standing waves in finite water depth was developed by Goda [40]. This solution was tested for a wide range of conditions, and the load were found to be predicted well. Several further adaptations of these theories were made to partial reflection [41] and short-crested waves [42]. Similar to progressive waves, higher standing waves (compared to water depth and wave length), exhibit more non-linear effects. Hedges [43] presents the regions of applicability for wave theories, based on the Ursell Number. Fenton [44] suggests that equal to progressive waves, the Ursell Number governs the region of application of the higher order wave theories, and that the same limiting values might apply. Similarly, for long waves compared to the water depth, cnoidal wave theory applies [45]. Romanczyk [46] describes that steep standing waves become remarkably unstable. The majority of the mentioned studies refer to regular standing waves. Furthermore, most validating experiments focus on the load exerted on the wall, and not the velocity of the surface that is required in the present study. Lastly, no theories were found that focussed on water motion at a vertical wall with a protruding element near the water surface.

Regarding the preliminary design of hydraulic structures under impulsive loadings, Reference [47] highlighted the advantages of using the pressure-impulse and the force-impulse in design, instead of the peak pressures and peak force. Also, Reference [47] proposed a model for estimating the reaction forces from impulsive wave impact loads. Moreover, Reference [48] introduced a semi-analytical model which is capable of predicting the bending vibrations of flood gates and other elastic hydraulic structures subjected to impulsive wave impact loads.

1.2. Paper Aims

The previously described existing literature highlights the need for extended knowledge on wave impacts on vertical structures with overhangs. In consequence, two processes have a remarkable relevance: the impact velocity and the entrapped air. These two processes are addressed in this study by means of experimental observations with regular waves. Laboratory data includes the incident wave field, pressure measurements, wall wave gauge measurements and camera recording measurements of water level and wave surface velocity. Section 2 describes the laboratory experiments carried out. The wave impact velocity is addressed in Section 3, while the entrapped air is addressed in Section 4. Section 5 summarizes the main conclusions of this paper.

2. Laboratory Experiments

This study analyses regular wave experimental data obtained from a test campaign carried out in 2019, at the wave flume of the Hydraulic Engineering Laboratory at Delft University of Technology, see Figure 1. This test campaign included different structure configurations (i.e., vertical walls and vertical walls with overhangs), various regular incident wave conditions and different instrumentation (i.e., wave gauges, camera and a pressure sensor). The wave flume used is 42 m long, 1 m high and 0.8 m wide. The piston-type wave generation system includes second order steering (i.e., second order effects of the first higher and lower harmonics are considered in the wave paddle motion, resembling waves that occur in nature) and active reflection compensation (ARC) (i.e., the wave paddle compensates for the waves reflected by the structure preventing them to re-reflect back into the test area). Figure 1a shows an overview of the experimental test area, Figure 1b illustrates in more detail the structure during a wave impact, while Figure 1c presents a front view of the vertical wall configuration with an integrated wall wave gauge. More details on the experimental setup are presented hereafter.

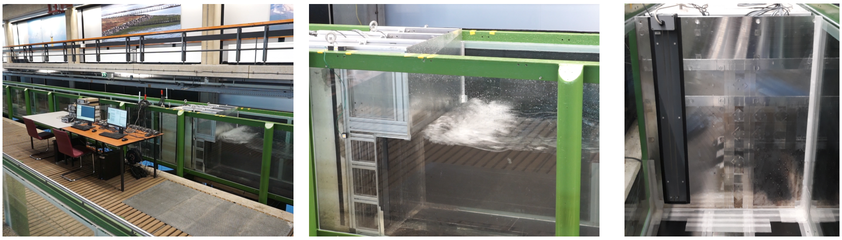

(**a**) Experimental test area. (**b**) Overhang setup at impact. (**c**) Front view vertical wall.

Figure 1. Overview of the experimental facility and model setup.

2.1. Experiment Description

The test setup was located at 23.3 m away from the wave paddle, see Figure 1. At this location, the aluminium test structure was mounted on a 1500 kg concrete block. The function of this concrete block (0.8 m wide, 0.8 m long and 1 m high) was to provide stability for the structure subjected to wave impacts. The test structure was built with 10 mm thick aluminium plates supported by aluminium profiles connected to the concrete block. Three different configurations were tested: a vertical wall with no overhang, a vertical wall with a shorter overhang ($W = 0.1$ m) and a vertical wall with a longer overhang ($W = 0.2$ m). In total, 15 tests were carried out: five with no overhang, five with a shorter overhang (named with the addition of "S") and five with a longer overhang (named with the addition of "L"). Table 1 summarizes the regular incident wave conditions, including the overhang length (W), the overhang height (h), the water level (d), the mean incident wave height (H), the variability of the incident wave height (σ_H/μ_H), the mean wave period (T), the mean local wave length according to linear wave theory for transitional depth (L), the mean steepness ($s = H/L$), the reflection coefficient (c_r), the Ursell Number ($U_r = HL^2/d^3$) and the impact type as described in Reference [1]. For the tests with overhangs, the still water depth was equal to the overhang height ($d = h = 0.6$ m), which can also de described as a situation of zero freeboard, see Figure 2. Under these circumstances, the wave surface is expected to have the maximum upward velocity when impacting the overhang. Consequently, this is expected to lead to the highest impact loads. For all configurations, 50 regular waves were analysed in each test, so the variability and repeatability of wave magnitudes could be evaluated.

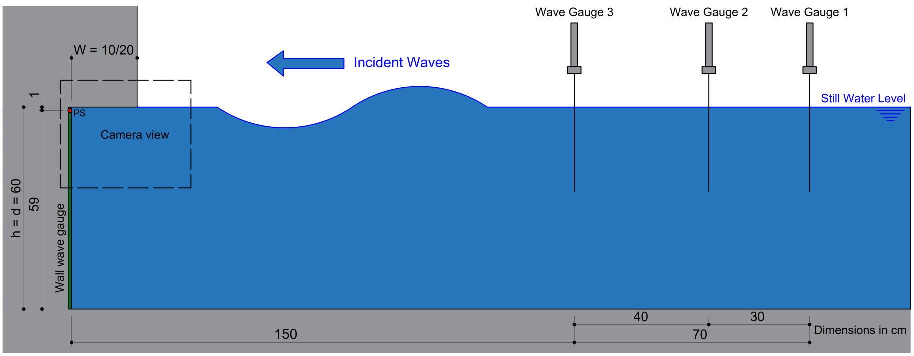

Figure 2. Test setup and instrumentation, adapted from Reference [1]. All dimensions in centimetres.

3

Table 1. Summary of measured incident wave conditions.

Test	W [m]	h [m]	d [m]	H [m]	$\frac{\sigma_H}{\mu_H}$ [%]	T [s]	L [m]	s [-]	c_r [-]	U_r [-]	Impact Type [-]
A	-	-	0.6	0.060	3.3	1.30	2.42	0.025	0.98	1.6	No impact
B	-	-	0.6	0.081	1.7	1.60	3.27	0.025	0.99	4.0	No impact
C	-	-	0.6	0.099	3.1	1.30	2.43	0.041	0.98	2.7	No impact
D	-	-	0.6	0.101	2.3	1.60	3.27	0.031	0.99	5.0	No impact
E	-	-	0.6	0.097	0.5	2.00	4.36	0.022	0.99	8.5	No impact
AS	0.1	0.6	0.6	0.061	2.3	1.30	2.42	0.025	0.84	1.7	Type I
BS	0.1	0.6	0.6	0.084	1.8	1.60	3.27	0.026	0.93	4.1	Type II
CS	0.1	0.6	0.6	0.103	3.7	1.31	2.43	0.042	0.81	2.8	Type I
DS	0.1	0.6	0.6	0.104	2.4	1.60	3.27	0.032	0.94	5.2	Type II
ES	0.1	0.6	0.6	0.101	0.4	2.00	4.36	0.023	0.92	8.9	Type III
AL	0.2	0.6	0.6	0.060	1.3	1.30	2.42	0.025	0.67	1.6	Type IV
BL	0.2	0.6	0.6	0.085	3.1	1.60	3.27	0.026	0.78	4.2	Type V
CL	0.2	0.6	0.6	0.100	2.0	1.30	2.43	0.041	0.63	2.7	Type IV
DL	0.2	0.6	0.6	0.108	3.5	1.60	3.27	0.033	0.74	5.4	Type V
EL	0.2	0.6	0.6	0.103	0.6	2.00	4.36	0.024	0.82	9.0	Type VI

2.2. Instrumentation

The incident and reflected waves were obtained at 1.5 m away from the vertical wall, following the method described by Zelt and Skjelbreia [49]. To this end, an array of 3 wave gauges with a sampling rate of 100 Hz were used, see their location in Figure 2. In addition, a wall wave gauge with its electrodes integrated flush in the wall (identical to wave gauges placed at wave generation paddles with ARC systems, see Figure 1c) was installed in the vertical wall, located at 12 cm away from the wave flume glass wall. This wall wave gauge had a sampling rate of 1000 Hz and was used for the measurement of the water level and the wave surface velocity at the vertical wall. All wave gauges included water conductivity compensation devices, to guarantee the accuracy of the measurements in all circumstances, correcting for temperature variations throughout the tests.

The recordings of an Olympus Tough TG-5 camera are used in this study for the tests with overhangs, see camera field of view in Figure 2. The camera was used with a frame rate of 59.94 fps and a resolution of 1920 × 1080, located slightly below the overhang level and 50 cm away from the wave flume glass wall. These camera recordings are synchronized with the measurements from the pressure sensor and wave gauges through LED light pulses recorded by the camera. The camera recordings are available for a limited number of waves, including the five first consecutive waves (tests AS, BS, ES, AL, BL, EL) or the three first consecutive waves (tests CS, DS, CL, DL). From these camera recordings, the wave surface is manually recognized by defining several wave surface points on each image frame using Matlab. These pixel coordinates are calibrated with the help of markers on the inner side of the flume glass wall. From this, the water level and wave surface velocity are derived. Furthermore, the use of transparent overhangs to capture air dynamics from inside the structure were considered. Nevertheless, the larger deformations of the polycarbonate elements under wave impacts and its expected influence on the pressure evolution favoured maintaining a full aluminium structure.

A Kulite HKM-375M-SG pressure sensor with 1 bar measurement range and sealed gauge is used in this study, screwed flush in the aluminium surface. The pressure sensor is located in the middle of the wave flume (40 cm away from the flume glass wall) and in the corner between wall and overhang, see 'PS' in Figure 2. The sampling frequency was 20 kHz. The calibrations obtained before the test campaign were regularly checked during and after the test campaign, with before-after differences in calibration factors of 0.12%. The pressures shown in this study are dynamic pressures, which are obtained after removing the hydrostatic pressures (i.e., pressures recorded prior to the wave motion) from the pressure measurements.

3

3. Impact Velocity

The wave impact velocity is a key parameter for determining the magnitudes and characteristics of the loads generated by a given wave impact. Furthermore, the wave impact velocity is also required in order to obtain dimensional values from theoretical estimations based on the pressure-impulse theory. Thus, this section addresses the study of the wave impact velocity considering theoretical expressions and experimental measurements.

3.1. Theoretical Estimation

A theoretical method to estimate standing wave impact velocities was presented in Reference [1] based on linear wave theory. Considering the Ursell Number obtained for the different tests (see Table 1), the use of linear wave theory is suitable according to the criteria presented in Reference [43]. Thus, the advantages of this method are the suitability for describing the wave motion and the simplicity of the expressions that can be used in future design guidance. According to Reference [1], the wave impact velocity (U) can be obtained from Equation (1), for the condition of zero freeboard ($d = h$) and considering a 100% of wave reflection at the wall (reflection coefficient $cr = 1$). A 100% of wave reflection is applicable in this case as the incident wave is not affected by the presence of the overhang within the period $T/2$ prior to the instant when the wave impact takes place.

$$U = \omega H_i, \tag{1}$$

where U is the wave impact velocity, ω is the angular wave frequency ($\omega = 2\pi/T$, where T is the incident wave period) and H_i is the incident wave height.

3.2. Impact Velocity without Overhangs

This section compares the theoretical expression for the wave impact velocity based on linear wave theory (see Section 3.1) with the measurements by the wall wave gauge in the tests without an overhang. Figure 3 show the comparison between measurements and theoretical estimations for the water level and wave surface velocity. For the theoretical estimations, a reflection coefficient of 100% ($cr = 1$) is considered. In addition to linear wave theory, the water level and wave surface velocity estimated by the third order wave theory from Reference [38] is also presented in Figure 3.

As shown in Figure 3, the theoretical estimations based on the linear wave theory describe rather accurately the water level and wave surface velocity at the wall. Given its accuracy and simplicity, this theoretical method is recommended to describe this wave field. Table 2 shows the differences between the impact velocity estimated by the linear wave theory (U_T), with the measured maximum upward velocity (U_{EMax}), the measured zero-crossing upward velocity (U_{EZero}) and the zero-crossing upward velocity estimated by the third order wave theory (U_{3Zero}). It is observed that the maximum upward velocities deviate more from linear wave theory (i.e., between +5.5% and +13.0%), while the zero-crossing upward velocities deviate less from linear wave theory (i.e., between +1.9% and +7.0%). The zero-crossing upward velocities estimated by the third order wave theory deviate slightly from the linear wave theory (i.e., between +1.8% and +4.7%).

Table 2. Impact velocity for tests without overhang.

Test	U_T [m/s]	U_{EMax} [m/s]	U_{EMax} to U_T [%]	U_{EZero} [m/s]	U_{EZero} to U_T [%]	U_{3Zero} [m/s]	U_{3Zero} to U_T [%]
A	0.290	0.316	+9.2	0.310	+7.0	0.295	+1.8
B	0.319	0.345	+8.0	0.332	+3.8	0.329	+3.0
C	0.475	0.502	+5.5	0.499	+4.9	0.498	+4.7
D	0.397	0.449	+13.0	0.423	+6.5	0.416	+4.6
E	0.304	0.334	+9.9	0.310	+1.9	0.317	+4.2

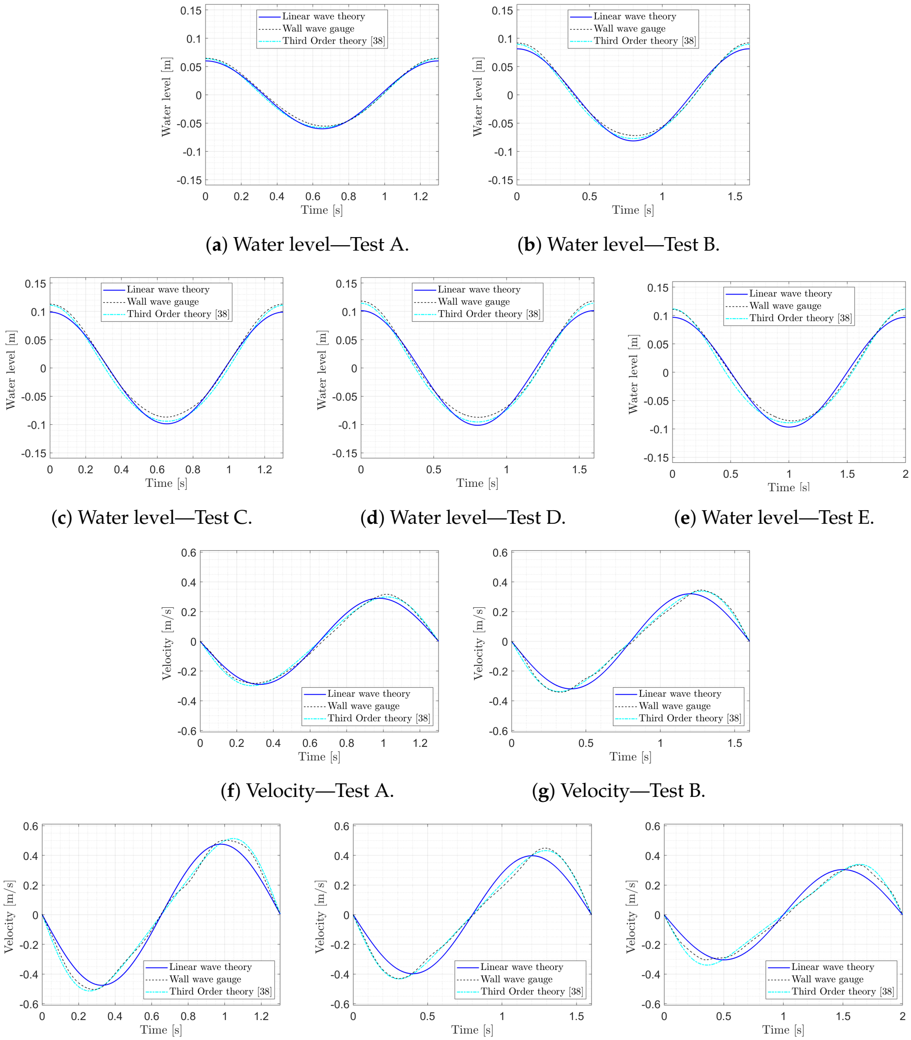

(**a**) Water level—Test A. (**b**) Water level—Test B.

(**c**) Water level—Test C. (**d**) Water level—Test D. (**e**) Water level—Test E.

(**f**) Velocity—Test A. (**g**) Velocity—Test B.

(**h**) Velocity—Test C. (**i**) Velocity—Test D. (**j**) Velocity—Test E.

Figure 3. Water level and wave surface velocity for tests without overhangs. Comparison between linear wave theory (solid blue lines), measurements at the vertical wall with a wall wave gauge (dashed black lines) and third order wave theory based on Reference [38] (point-dashed cyan lines).

3.3. Impact Velocity with Overhangs

This section addresses the wave impact velocity for tests with an overhang. The measurements of the wall wave gauge are only obtained locally at the wall, without fully representing the complete wave (velocity) field beneath the overhang and includes local velocities created by splashes and other oscillations. Thus, camera recording measurements are used instead, which are able to describe the velocity along the wave surface beneath the overhang. Nevertheless, the velocity measurements from the camera recording measurements at the wall (averaged within 10 mm from the wall) are first compared in Figure 4 with the wall wave gauge measurements to validate the camera recordings.

Figure 4 shows that a close agreement is found from this comparison, so the camera recording measurements can be used hereafter for the study of the impact velocity for tests with the presence of an overhang. Nevertheless, four minor discrepancies in this comparison should be explained. Firstly, discrepancies in the negative velocities in various tests are found to be caused by conditions where a thin layer of water remains at the wall, captured by the camera as a sudden fall and by the wall wave gauge as a progressive fall. Secondly, discrepancies in positive velocities are found to be caused by conditions with a highly aerated water portion at the wall, captured by the camera as a sudden rise and by the wall wave gauge as a progressive rise (e.g., higher peak for test AL). Thirdly, discrepancies in the water level for test AS and DL are caused by a stationary air bubble located under the overhang throughout the wave cycle. Fourth, high short velocity peaks for the wall wave gauge data is considered to be caused by sudden air bubbles displacement affecting the conductivity at the wall wave gauge (e.g., tests CL, DS and ES). Furthermore, this comparison is used to better adjust the synchronization of the camera recording measurements in all the tests, taking as reference the wall wave gauge wave surface velocity measurements.

The camera recordings are used in this study to characterize the displacement of water surface before the wave impact. From each image frame from the camera recordings, the water surface was recognized. This is used to estimate the wave impact velocity and the non-uniformity of the wave surface before and during the wave impact. The water level and wave surface velocity presented hereafter are calculated as the average along the length of the overhang, 0.1 m for the shorter overhang and 0.2 m for the longer overhang. Figure 5 presents the results for the shorter overhang, while Figure 6 presents the results for the longer overhang. Table 3 summarizes the results for tests with overhangs, describing the differences between the impact velocity estimated by the linear wave theory (U_T), with the measured maximum upward velocity (U_{EMaxOH}). In this study, U_T is calculated and showed in all graphs as the value obtained at the wall position, without averaging over the overhang length. This leads to a difference of between 0.11% to 0.35% in the obtained velocities for shorter overhangs and to a difference of between 0.39% to 1.26% in the obtained velocities for longer overhangs. This method allows consistency and simplicity in this study, with impact velocities obtained from Equation (1).

From Figures 5 and 6 a few observations can be made. As shown in the third column in both figures, the wave surface motion before the impact presents large variability between the different tests. This illustrates the complex hydrodynamics that affects the wave surface displacement before the wave impacts, influenced by the incident wave conditions and structural characteristics. These complex hydrodynamics are observed both for the shorter and the longer overhang. As a consequence, the wave surface velocity and water level shown in the first and second columns also present a significant variability and differences from the theoretical estimations. Table 3 summarizes the differences between the experimental measurements for the wave surface velocity compared with linear wave theory, ranging between −11.8% and +13.4%. This table also presents the effective bounce-back factor β_{U_T} as calculated in Reference [1] considering the wave impact velocity according to linear wave theory, and the effective bounce-back factor $\beta_{U_{EMaxOH}}$ considering the wave impact velocity according to camera recordings. For the 10 tests considered in this study the effective bounce-back factor $\beta_{U_{EMaxOH}}$ presents a higher mean and standard deviation ($\mu = 1.21$ and $\sigma = 0.16$) than β_{U_T} ($\mu = 1.19$ and $\sigma = 0.12$). These experimental results illustrate that when considering the impact velocity from camera recordings, the mean effective bounce-back factor deviates relatively little from when linear wave theory is used (1.21 instead of 1.19, ≈1% difference) while the uncertainty described by the standard deviation increases significantly (0.16 instead of 0.12, ≈35% difference). The values of β_{U_T} presented in this study are slightly different than in Reference [1] ($\mu = 1.17$ and $\sigma = 0.11$) since a reduced amount of tests are used here. Thus, the values of β_{U_T} from Reference [1] are recommended to be considered as a reference.

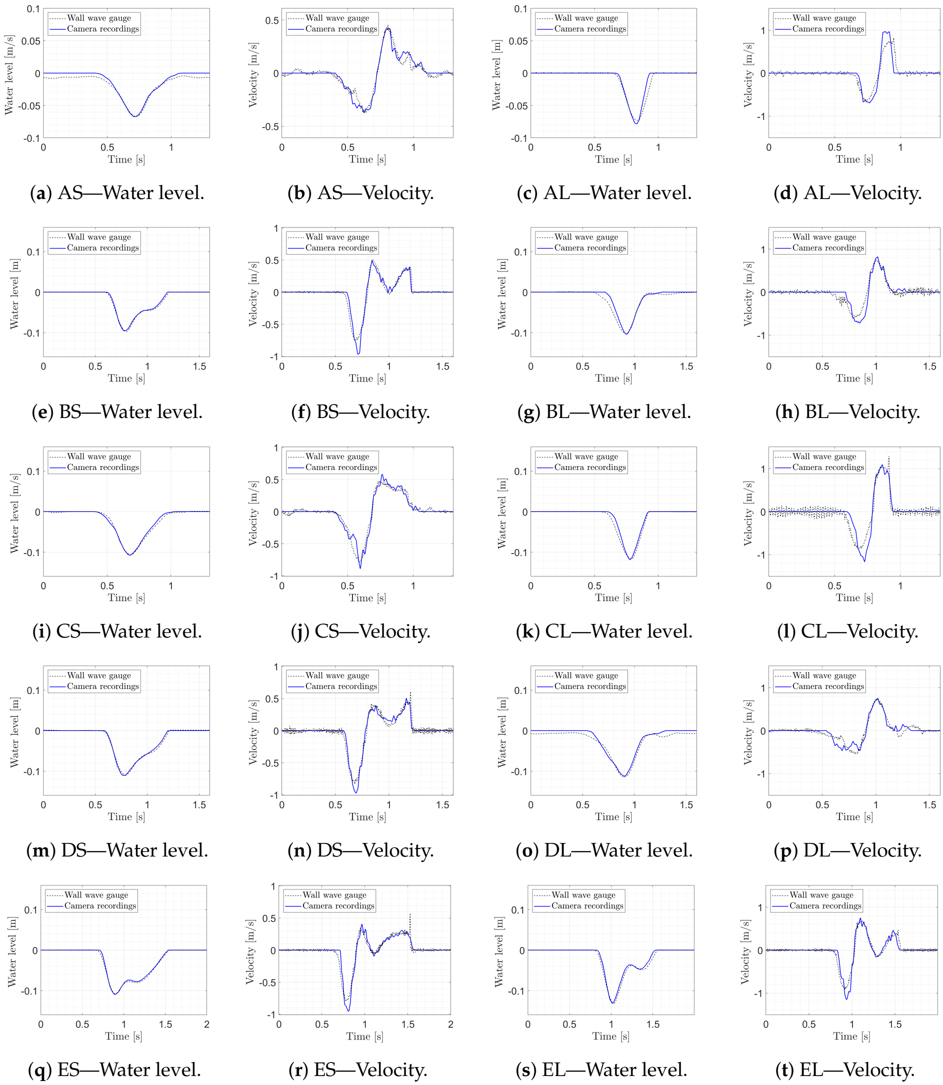

(**a**) AS—Water level. (**b**) AS—Velocity. (**c**) AL—Water level. (**d**) AL—Velocity.

(**e**) BS—Water level. (**f**) BS—Velocity. (**g**) BL—Water level. (**h**) BL—Velocity.

(**i**) CS—Water level. (**j**) CS—Velocity. (**k**) CL—Water level. (**l**) CL—Velocity.

(**m**) DS—Water level. (**n**) DS—Velocity. (**o**) DL—Water level. (**p**) DL—Velocity.

(**q**) ES—Water level. (**r**) ES—Velocity. (**s**) EL—Water level. (**t**) EL—Velocity.

Figure 4. Water level and wave surface velocity at the wall for tests with overhangs. Comparison between wall wave gauge measurements (dashed black lines) and camera measurements averaged within 10 mm from the wall (solid blue lines).

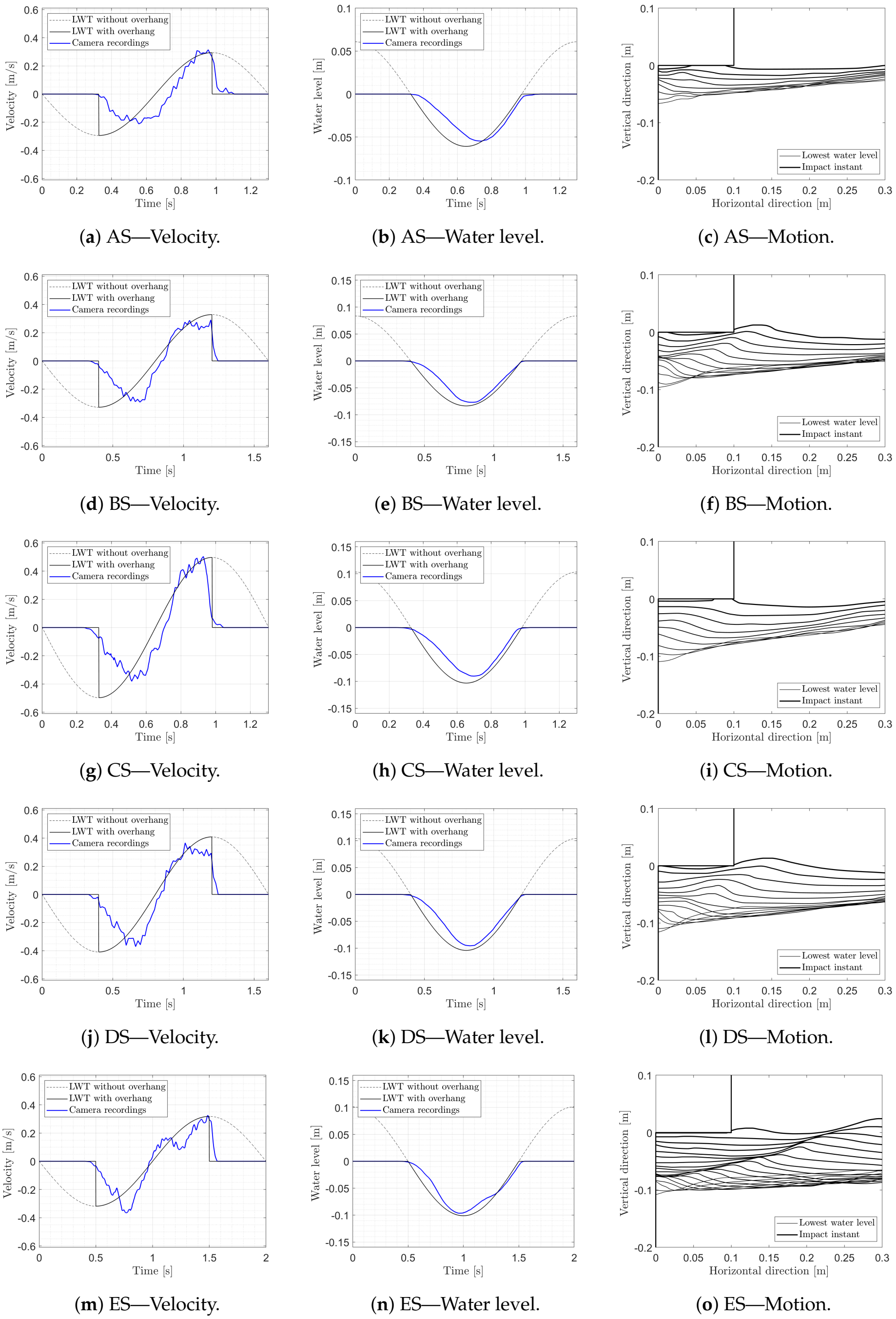

(**a**) AS—Velocity. (**b**) AS—Water level. (**c**) AS—Motion.

(**d**) BS—Velocity. (**e**) BS—Water level. (**f**) BS—Motion.

(**g**) CS—Velocity. (**h**) CS—Water level. (**i**) CS—Motion.

(**j**) DS—Velocity. (**k**) DS—Water level. (**l**) DS—Motion.

(**m**) ES—Velocity. (**n**) ES—Water level. (**o**) ES—Motion.

Figure 5. Tests with shorter overhangs. Left and centre: water level and wave surface velocity from camera recordings averaged over the overhang width (solid blue lines) compared with theoretical estimations (black lines). Right: wave motion before wave impact.

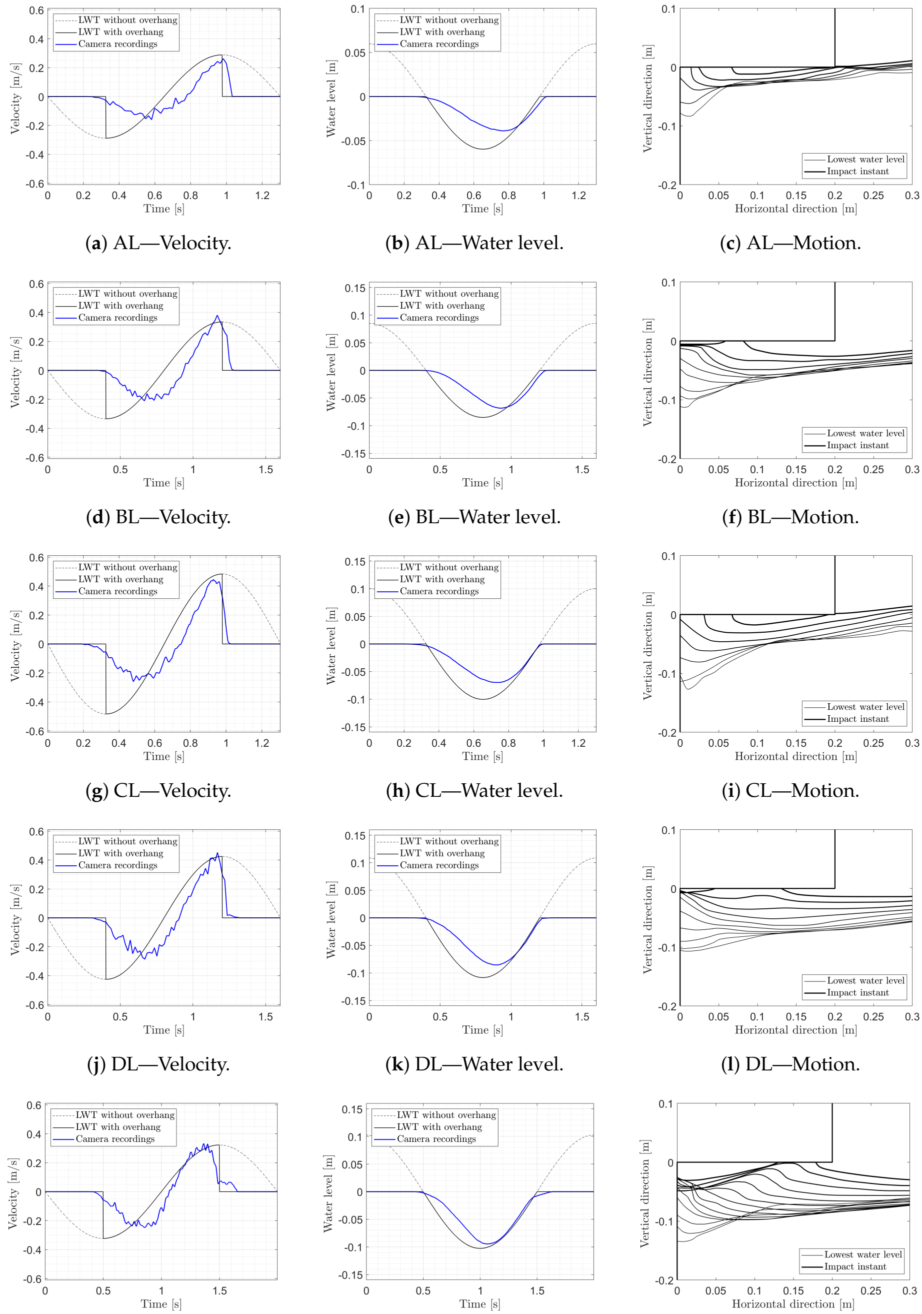

(**a**) AL—Velocity. (**b**) AL—Water level. (**c**) AL—Motion.

(**d**) BL—Velocity. (**e**) BL—Water level. (**f**) BL—Motion.

(**g**) CL—Velocity. (**h**) CL—Water level. (**i**) CL—Motion.

(**j**) DL—Velocity. (**k**) DL—Water level. (**l**) DL—Motion.

(**m**) EL—Velocity. (**n**) EL—Water level. (**o**) EL—Motion.

Figure 6. Tests with longer overhangs. Left and centre: water level and wave surface velocity from camera recordings averaged over the overhang width (solid blue lines) compared with theoretical estimations (black lines). Right: wave motion before wave impact.

Table 3. Impact velocity for tests with overhangs.

Condition	U_T [m/s]	U_{EMaxOH} [m/s]	U_{EMaxOH} to U_T [%]	β_{U_T} [-]	$\beta_{U_{EMaxOH}}$ [-]
AS	0.294	0.313	+6.6	1.04	0.98
BS	0.328	0.289	−11.8	1.10	1.25
CS	0.497	0.502	+1.1	1.35	1.34
DS	0.409	0.365	−10.8	1.23	1.38
ES	0.318	0.326	+2.4	1.03	1.01
AL	0.288	0.261	−9.3	1.10	1.21
BL	0.335	0.379	+13.4	1.19	1.05
CL	0.483	0.445	−8.0	1.36	1.48
DL	0.426	0.451	+6.1	1.25	1.18
EL	0.323	0.333	+3.1	1.29	1.25

3

4. Entrapped Air Size Quantification

The presence of air is regarded as a source of dynamic processes which has led to a high degree of uncertainty in the study of wave impacts [2], including a decisive influence on the magnitudes and characteristics of wave impacts. Thus, the presence of air affects the variability and predictability of wave impact magnitudes and the characteristics of the pressure/force time-series, including their pressure/force peaks and impact durations. Moreover, the presence of air pockets in wave impacts may lead to pressure oscillations in the water column caused by the compression and decompression of air bubbles [27]. This section aims to extend the knowledge on wave impacts by quantifying the amount of entrapped air in the experiments with wave impacts caused by the presence of an overhang. The complex hydrodynamics shown in Figures 5 and 6 affects directly these characteristics and variabilities of the entrapped air dimensions.

Figures 7 and 8 show the wave surface at the instant of wave impact and the corresponding pressure signal, for shorter and longer overhang respectively. In these figures, the first column shows the water level at the impact instant for the various recorded waves and the average impact instant position from these waves. In the second column, the impact instant is shown for the first of these waves, while in the third column the pressure signal is shown also for this first wave impact. Entrapped air dimensions were determined from the contours of the average impact instant position. These are presented in Table 4, including the mean entrapped air length (l_A), the variability of the entrapped air length (σ_{l_A}/μ_{l_A}), the mean entrapped air height (h_A), the variability of the entrapped air height (σ_{h_A}/μ_{h_A}), the mean entrapped air area (A_A) and the variability of the entrapped air area (σ_{A_A}/μ_{A_A}). The impact duration (d_t) determined from the pressure signal (according to Reference [1]) is also included.

Table 4. Summary of entrapped air dimensions.

Test	l_A [mm]	$\frac{\sigma_{l_A}}{\mu_{l_A}}$ [%]	h_A [mm]	$\frac{\sigma_{h_A}}{\mu_{h_A}}$ [%]	A_A [mm^2]	$\frac{\sigma_{A_A}}{\mu_{A_A}}$ [%]	d_t [ms]
AS	46.1	6.6	4.6	8.3	210.0	9.6	37
BS	71.4	6.4	3.4	12.9	242.4	7.6	52
CS	71.1	3.4	3.6	7.5	255.7	10.5	36
DS	90.4	5.0	3.7	12.5	335.5	9.1	42
ES	91.2	9.6	0.6	22.4	59.2	14.0	10
AL	132.8	2.8	8.9	14.5	1184.0	16.5	110
BL	53.5	11.3	4.4	24.3	233.3	32.6	69
CL	120.1	9.2	10.9	6.5	1304.8	15.3	101
DL	51.8	16.0	4.9	12.1	252.0	10.0	57
EL	128.3	3.4	17.2	12.5	2207.6	15.1	37

A few observations can be made on the characteristics of the entrapped air measured in the laboratory experiments, as shown in Figures 7 and 8. It is found that the different tests lead to radically different dimensions and characteristics of entrapped air, caused by the interaction of incident wave parameters with structural configurations. For the tests with a shorter overhang, the differences in entrapped air area are up to a factor of 5.7 (factors of 2.0 for entrapped air length and 7.7 for entrapped air height), while for the tests with a longer overhang these differences in entrapped air area are up to a factor of 9.5 (factors of 2.6 for entrapped air length and 3.9 for entrapped air height). This variability on the entrapped air is expected to be the main cause of the radically different pressure time-series in the different tests, as shown in the pressure sensor measurements. Furthermore, it is observed that the entrapped air pockets are rather flat, in contrast to what can be observed in breaking waves, and more similar to the piston model from Bagnold [2].

For tests with shorter overhangs, Figures 5 and 7 are analysed together, considering also the six impacts types from Reference [1]. For tests AS and CS an air pocket is found directly at the wall. This is named as Type I impact, which has one single peak, an intermediate level of vibrations and an intermediate impact duration. For tests BS and DS an air pocket is found away from the wall. This is named as Type II impact, which has one single peak, almost no vibrations and an intermediate impact duration. The presence of an air pocket away from the wall is caused by a previous run-up of the wave at the wall and a first pre-impact observed in the pressure signal for tests BS and DS. For test ES, a minimum air pocket is found below the overhang. This is named as Type III impact, which has one single peak, a reduced level of vibrations and a very short impact duration. For tests with longer overhangs, Figures 6 and 8 are also analysed together. For tests AL and CL an air pocket is found away from the wall. This is named as Type IV impact, which has one stepped wide peak, an intermediate level of low frequency vibrations and a very long impact duration. The presence of this air pocket away from the wall is caused by a previous run-up of the wave at the wall and a first pre-impact observed in the pressure signal for tests AL and CL. For tests BL and DL an air pocket is found directly at the wall. This is named as Type V impact, which has one peak with a close secondary peak, large vibrations and a long impact duration. For test EL, an extremely large air pocket is found below the overhang. This is named as Type VI impact, which has two peaks within an interval of 0.2 s ($\approx T/10$), an intermediate level of vibrations and an intermediate impact duration. This double impact (see Figures 6o and 8o) occurs as the wave surface first hits the outer edge of the overhang, before a second pressure peak occurs when the wave surface at the wall impacts the overhang.

Figure 9 presents a comparison between the entrapped air dimensions (i.e., length, height and area) and the impact duration. According to these results, the increase in the entrapped air dimensions is closely related to an increase in the impact duration. This relation is caused by the compression of air during the wave impact, as it is predicted by References [2,6]. The discrepancy for the double peak EL test is explained by the fact that the impact duration is calculated as the impact duration of the first of the two pressure peaks. For the tests AL and CL with a strong pre-peak, it is important to mention that the impact duration is much longer due to this pre-peak. Nevertheless, for all the tests (besides for test EL) a rather strong correlation exists between impact duration and entrapped air dimensions. Among the entrapped air dimensions, the entrapped air height (h_A) shows the strongest correlation with the impact duration. The entrapped air area (A_A) also show a high correlation with the impact duration, while the entrapped air length (l_A) does not show any clear trend. Furthermore, Figure 9 also shows that the entrapped air height and entrapped air length are related to the overhang length (W). It is observed that for the tests with the longer overhangs, the entrapped air pockets are thicker and longer. This suggests that the overhang length may determine both the maximum entrapped air length and the maximum entrapped air height.

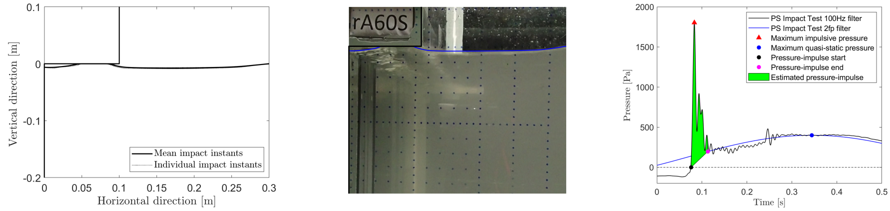

(**a**) AS—Impacts. (**b**) AS—Illustration. (**c**) AS—Pressure [1].

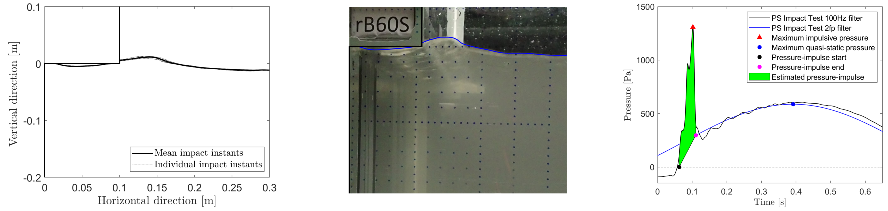

(**d**) BS—Impacts. (**e**) BS—Illustration. (**f**) BS—Pressure [1].

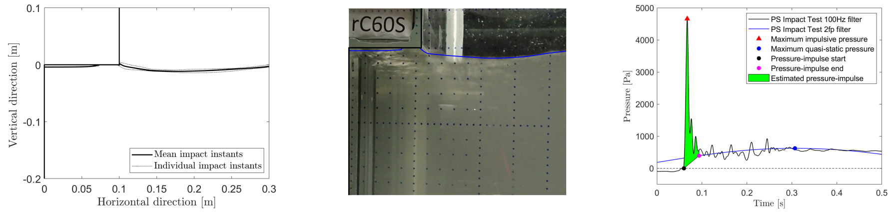

(**g**) CS—Impacts. (**h**) CS—Illustration. (**i**) CS—Pressure [1].

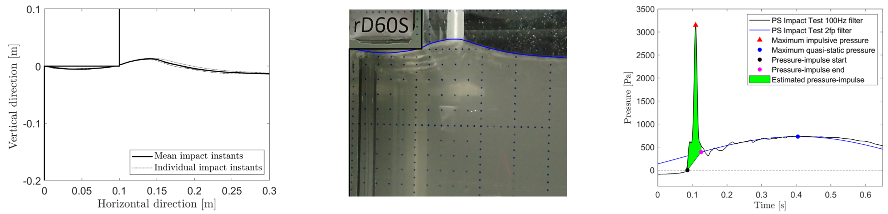

(**j**) DS—Impacts. (**k**) DS—Illustration. (**l**) DS—Pressure [1].

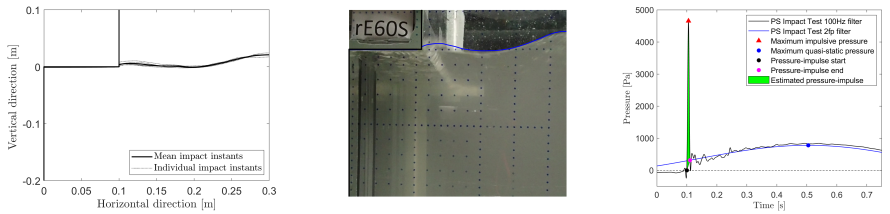

(**m**) ES—Impacts. (**n**) ES—Illustration. (**o**) ES—Pressure [1].

Figure 7. Wave surface and entrapped air at wave impact instant for tests with a shorter overhang. The impact instant shown in the images (left and center column) corresponds to the camera frame intermediately before the pressure-impulse start point shown in the pressure plots in the right column.

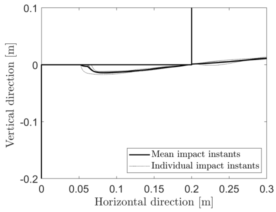

(**a**) AL—Impacts.

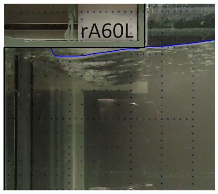

(**b**) AL—Illustration.

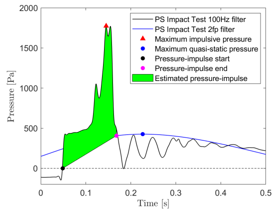

(**c**) AL—Pressure [1].

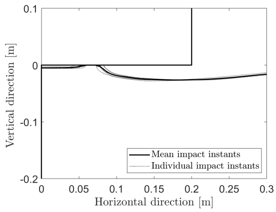

(**d**) BL—Impacts.

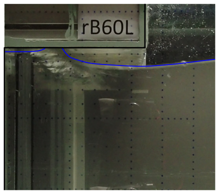

(**e**) BL—Illustration.

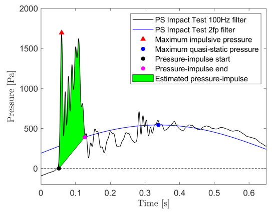

(**f**) BL—Pressure [1].

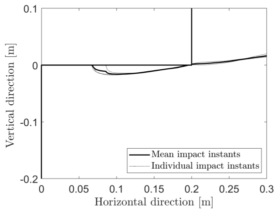

(**g**) CL—Impacts.

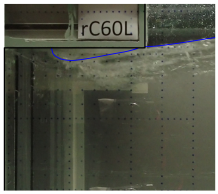

(**h**) CL—Illustration.

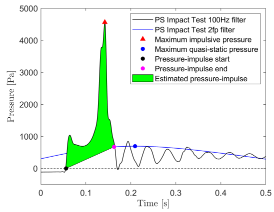

(**i**) CL—Pressure [1].

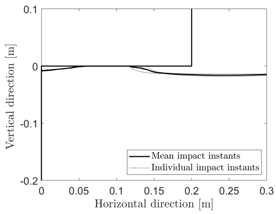

(**j**) DL—Impacts.

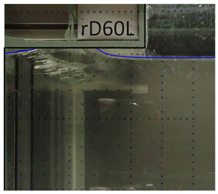

(**k**) DL—Illustration.

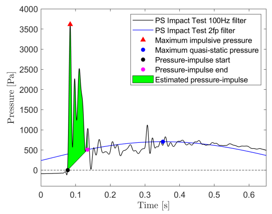

(**l**) DL—Pressure [1].

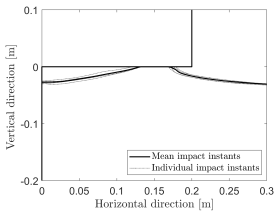

(**m**) EL—Impacts.

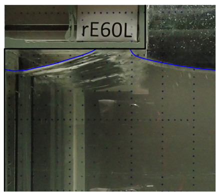

(**n**) EL—Illustration.

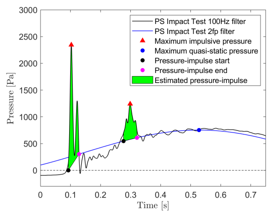

(**o**) EL—Pressure [1].

Figure 8. Wave surface and entrapped air at wave impact instant for tests with a longer overhang. The impact instant shown in the images (left and center column) corresponds to the camera frame intermediately before the pressure-impulse start point shown in the pressure plots in the right column (for test EL, the impact instant corresponds to the first peak).

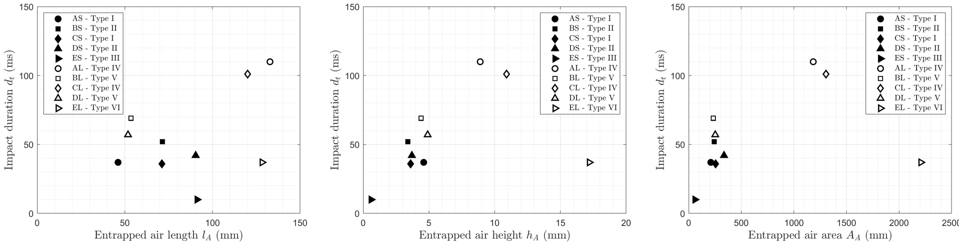

(**a**) Air length vs d_t. (**b**) Air height vs d_t. (**c**) Air area vs d_t.

Figure 9. Entrapped air dimensions in comparison with impact duration.

Figure 10 presents a comparison between the entrapped air dimensions (i.e., length, height and area) and the effective bounce back factor β (including β_{U_T} and $\beta_{U_{EMaxOH}}$). For all cases, larger β values are found for larger entrapped air dimensions. These relations highlight that the effective bounce-back factor β accounts for the entrapped air dimensions, but the associated scatter also shows that β is affected by other processes and uncertainties. Furthermore, this scatter in the observed trends between β and entrapped air height is larger in Figures 10d/e/f for $\beta_{U_{EMaxOH}}$ (where the impact velocity is obtained from camera recordings) than in Figure 10a/b/c for β_{U_T} (where the impact velocity is obtained from linear wave theory). In summary, according to experiments analysed in this study, the increase in the entrapped air dimensions is linked to an increase of the variability of wave impact magnitudes, an increase of pressure/force impulses, an increase of the impact durations and a decrease of the pressure/force peaks.

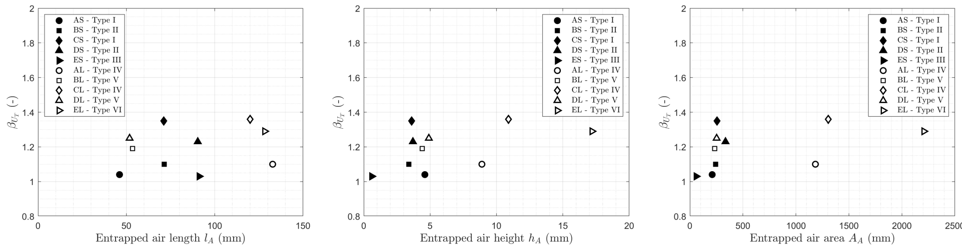

(**a**) Air length vs β_{U_T}. (**b**) Air height vs β_{U_T}. (**c**) Air area vs β_{U_T}.

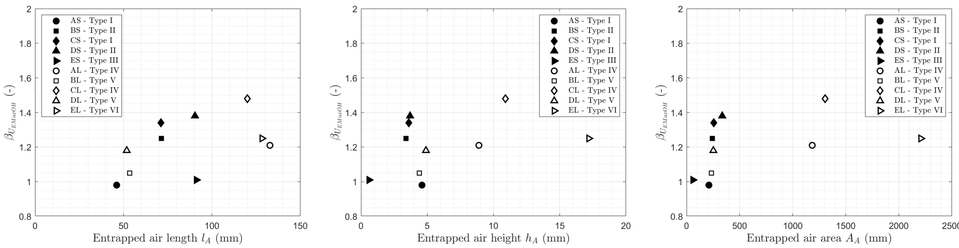

(**d**) Air length vs $\beta_{U_{EMaxOH}}$. (**e**) Air height vs $\beta_{U_{EMaxOH}}$. (**f**) Air area vs $\beta_{U_{EMaxOH}}$.

Figure 10. Entrapped air dimensions in comparison with effective bounce-back factor.

3

5. Conclusions

The impact velocity and the entrapped air are two main processes with a significant effect on the loading characteristics (e.g., impact magnitudes, duration, oscillations and variability) for wave impacts on vertical structures with overhangs. Furthermore, these loading characteristics are particularly important for slender structures which are especially susceptible to dynamic behaviour under such impulsive loads. Thus, impact velocity and entrapped air are studied by means of laboratory experiments. This study analysed laboratory data for relatively short overhangs with respect to the wave length ($12.1 < L/W < 43.6$) and with respect to the overhang height ($3 < h/W < 6$). These structures were tested in a wave flume subjected to low-steepness, non-breaking regular waves.

The impact velocity according to linear wave theory is reasonably in agreement with experimental measurements from a wall wave gauge for tests without overhangs, with maximum upward velocities deviating from linear wave theory between +5.5% and +13.0%, while the zero-crossing upward velocities deviate from linear wave theory between +1.9% and +7.0%. The zero-crossing upward velocities estimated from third order wave theory deviate from the linear wave theory between +1.8% and +4.7%. In the tests with overhangs, the maximum upward velocity below the overhang estimated by camera recording measurements deviates from linear wave theory between −11.8% and +13.4%. These larger deviations for the tests with overhangs illustrate the complex hydrodynamics that affects the wave surface displacement before the wave impacts, influenced by the incident wave conditions and structural characteristics. It was also found that when considering the impact velocity from camera recordings, the mean effective bounce-back factor β deviates relatively little from when linear wave theory is used (1.21 instead of 1.19, ≈1% difference) while the uncertainty described by the standard deviation increases significantly (0.16 instead of 0.12, ≈35% difference).

The entrapped air dimensions also present large variations between the tests, caused by the interaction between incident wave parameters and structural configurations. It was found differences in the entrapped air area up to a factor of 5.7 for shorter overhangs and a factor of 9.5 for longer overhangs. This variability in the entrapped air characteristics is expected to lead to significant effects on the loading on the structure caused by these wave impacts, as observed by the pressure measurements. Furthermore, the relation between the increase of impact durations caused by increased entrapped air dimensions is found in the experimental measurements. Among the entrapped air dimensions, the entrapped air height shows the strongest correlation with the impact duration. The entrapped air area also show a high correlation with the impact duration, while the entrapped air length does not show any clear trend. A relation is also found between increasing effective bounce-back factor β for increasing entrapped air dimensions. This relation highlights that the effective bounce-back factor β accounts for the entrapped air dimensions, but the associated scatter also shows that β is affected by other processes and uncertainties. Furthermore, this scatter in the observed trend between β and entrapped air length is larger for $\beta_{U_{EMaxOH}}$ (where the impact velocity is obtained from camera recordings) than for β_{U_T} (where the impact velocity is obtained from linear wave theory).

This study highlights the importance of the details of the impact velocity and entrapped air for determining the standing wave impact load on vertical structures with overhangs. These two factors show a large variability caused mainly by the interaction between the structure and the incident wave field. Thus, more extensive research in this area is recommended, including the use of numerical methods. The combination of analytical, experimental and numerical methods would allow to further reduce the existing uncertainties and increase the reliability in the design of vertical hydraulic structures with overhangs. This is particularly important for thin structures such as steel gates which are especially susceptible to a dynamic behaviour under such impulsive loads.

Author Contributions: Conceptualization, methodology, validation, investigation, writing-review and editing: E.d.A and B.H.; formal analysis, data curation, writing-original draft preparation, visualization: E.d.A.; resources, supervision, project administration, funding acquisition: B.H. All authors have read and agreed to the published version of the manuscript.

Funding: This study is part of the DynaHicS (Dynamics of Hydraulic Structures) research programme, supported by NWO (Nederlandse Organisatie voor Wetenschappelijk Onderzoek) grant ALWTW.2016.041.

Conflicts of Interest: The authors declare no conflict of interest.

References

1. De Almeida, E.; Hofland, B. Validation of pressure-impulse theory for standing wave impact loading on vertical hydraulic structures with short overhangs. *Coast. Eng.* **2020**, *159*, 103702. [CrossRef]
2. Bagnold, R.A. Wave-pressure research. *Inst. Civ. Eng.* **1939**, *12*, 202–226. [CrossRef]
3. Minikin, R.R. *Winds, Waves and Maritime Structures*; Griffin: London, UK, 1950.
4. Goda, Y. A new method of wave pressure calculation for the design of composite breakwater. In Proceedings of the Coastal Engineering Conference, Copenhagen, Denmark, 24–28 June 1974.
5. Takahashi, S.; Tanimoto, K.; Shimosako, K. A Proposal of impulsive pressure coefficient for design of composite breakwaters. In Proceedings of the International Conference of Hydro-Technical Engineering for Port and Harbour Construction, Yokosuka, Japan, 19–21 October 1994.
6. Mitsuyasu, H. Shock pressure of breaking wave. In Proceedings of the Coastal Engineering Conference, Orlando, FL, USA, 2–6 September 1996.
7. Partenscky, H.W. Dynamic forces due to waves breaking at vertical coastal structures. In Proceedings of the Coastal Engineering Conference, Sol-Malaga, Spain, 20–25 June 1988.
8. Oumeraci, H.; Kortenhaus, A.; Allsop, W.; de Groot, M.; Crouch, R.; Vrijling, H.; Voortman, H. *Proverbs: Probabilistic Design Tools for Vertical Breakwaters*; Balkema: Lisse, The Netherlands, 2001.
9. Cuomo, G.; Allsop, W.; Bruce, T.; Pearson, J. Breaking wave loads at vertical seawalls and breakwaters. *Coast. Eng.* **2010**, *57*, 424–439. [CrossRef]
10. Kisacik, D.; Troch, P.; Bogaert, P.V.; Caspeele, R. Investigation of uplift impact forces on a vertical wall with an overhanging horizontal cantilever slab. *Coast. Eng.* **2014**, *90*, 12–22. [CrossRef]
11. Chen, X.; Hofland, B.; Altomare, C.; Suzuki, T.; Uijttewaal, W. Forces on a vertical wall on a dike crest due to overtopping flow. *Coast. Eng.* **2015**, *95*, 94–104. [CrossRef]
12. Chen, X.; Hofland, B.; Uijttewaal, W. Maximum overtopping forces on a dike-mounted wall with a shallow foreshore. *Coast. Eng.* **2016**, *116*, 89–102. [CrossRef]
13. McConnell, K.; Allsop, W.; Cruickshank, I. *Piers, Jetties and Related Structures Exposed to Waves: Guidelines for Hydraulic Loadings*; Thomas Telford Publishing: London, UK, 2004.
14. Cuomo, G.; Tirindelli, M.; Allsop, W. Wave-in-deck loads on exposed jetties. *Coast. Eng.* **2007**, *54*, 657–679. [CrossRef]
15. Seiffert, B.; Hayatdavoodi, M.; Ertekin, R.C. Experiments and computations of solitary-wave forces on a coastal-bridge deck. Part I: Flat Plate. *Coast. Eng.* **2014**, *88*, 194–209. [CrossRef]
16. Hayatdavoodi, M.; Seiffert, B.; Ertekin, R.C. Experiments and computations of solitary-wave forces on a coastal-bridge deck. Part II: Deck with girders. *Coast. Eng.* **2014**, *88*, 210–228. [CrossRef]
17. Dias, F.; Ghidaglia, J.M. Slamming: Recent Progress in the Evaluation of Impact Pressures. *Annu. Rev. Fluid Mech.* **2018**, *50*, 243–273. [CrossRef]
18. Sonneville, B.; Hofland, B.; Mowinckel, A.; Paulsen, B. Wave impact loads on offshore gravity based structure. In Proceedings of the OMAE Conference, St. John's, NL, Canada, 31 May–5 June 2015.
19. Bogaert, H. An experimental investigation of sloshing impact physics in membrane LNG tanks on foating structures. Ph.D. Thesis, Delft University of Technology, Delft, The Netherlands, 2018.
20. Ramkema, C. A model law for wave impacts on coastal structures. In Proceedings of the Coastal Engineering Conference, Hamburg, Germany, 27 August–3 September 1978.
21. Castellino, M.; Sammarco, P.; Romano, A.; Martinelli, L.; Ruol, P.; Franco, L.; Girolamo, P.D. Large impulsive forces on recurved parapets under non-breaking waves. A numerical study. *Coast. Eng.* **2018**, *136*, 1–15. [CrossRef]
22. Martinelli, L.; Ruol, P.; Volpato, M.; Favaretto, C.; Castellino, M.; Girolamo, P.D.; Franco, L.; Romano, A.; Sammarco, P. Experimental investigation on non-breaking wave forces and overtopping at the recurved parapets of vertical breakwaters. *Coast. Eng.* **2018**, *141*, 52–67. [CrossRef]
23. de Almeida, E.; Hofland, B.; Jonkman, S. Wave impact pressure-impulse on vertical structures with overhangs. In Proceedings of the Coastal Structures Conference, Hannover, Germany, 30 September–2 October 2019.

24. WL. Wave impacts on the gate in the Eastern Scheldt caisson. In *Dutch: Golfklappen op de Schuif in de Oosterschelde-Caisson*; Verslag M 1335 deel I; WL Delft Hydraulics (Presently Deltares): Delft, The Netherlands, 1977.
25. WL. Wave impacts against concrete perforated gates. In *Dutch: Golfklappen Tegen Betonnen Roosterschuiven*; Verslag M 1381 deel II; WL Delft Hydraulics (Presently Deltares): Delft, The Netherlands, 1978.
26. WL. Wave impacts: A piston model with compressible water. In *Dutch: Golfklappen: Een Zuigermodel Met Samendrukbaar Water*; Verslag M 1335 deel II; WL Delft Hydraulics (Presently Deltares): Delft, The Netherlands, 1979.
27. WL. Wave impacts: A literature review and scale effects in model studies. In *Dutch: Golfklappen: Een Literaturroverzicht en Schaaleffekten in Modelonderzoek*; Verslag M 1335 deel III; WL Delft Hydraulics (Presently Deltares): Delft, The Netherlands, 1979.
28. Hofland, B. *Modeltesten Golfkrachten Spuisluizen Afsluitdijk*; Meetrapport 1220263; Deltares: Delft, The Netherlands, 2015.
29. Cooker, M.J.; Peregrine, D.H. A model for breaking wave impact pressures. In Proceedings of the Coastal Engineering Conference, Delft, The Netherlands, 2–6 July 1990.
30. Cooker, M.J.; Peregrine, D.H. Pressure-impulse theory for liquid impact problems. *J. Fluid Mech.* **1995**, *297*, 193–214. [CrossRef]
31. Wood, D.J.; Peregrine, D.H. Wave impact beneath a horizontal surface. In Proceedings of the Coastal Engineering Conference, Orlando, FL, USA, 2–6 September 1996.
32. Peregrine, D.H.; Thais, L. The effect of entrained air in violent wave impacts. *J. Fluid Mech.* **1996**, *325*, 377–397. [CrossRef]
33. Wood, D.J.; Peregrine, D.H.; Bruce, T. Study of wave impact against a wall with pressure-impulse theory. I: Trapped air. *J. Waterw. Port Coast. Ocean. Eng.* **2000**, *126*, 182–190. [CrossRef]
34. Bredmose, H.; Peregrine, D.; Bullock, G. Violent breaking wave impacts. Part 2: Modelling the effect of air. *J. Fluid Mech.* **2009**, *641*, 389–430. [CrossRef]
35. Peregrine, D.H. Water-wave impact on walls. *Annu. Rev. Fluid Mech.* **2003**, *35*, 23–43. [CrossRef]
36. Sainflou, M. Essai sur les digues maritimes verticales. *Ann. Des Ponts Chaussées* **1928**, *98*, 5–48.
37. Miche, M. Mouvement ondulatoire de la mer en profondeur constante ou decroissante. *Ann. Des. Ponts Chaussées* **1944**, *121*, 285–318.
38. Tadjbakhsh, I.; Keller, J.B. Standing surface waves of finite amplitude. *J. Fluid Mech.* **1960**, *8*, 442–451. [CrossRef]
39. Penney, W.G.; Price, A.T.; Martin, J.C.; Moyce, W.J.; Thornhill, C.K. Finite periodic stationary gravity waves in a perfect liquid. *Philos. Trans. R. Soc. Lond.* **1952**, *244*, 254–284.
40. Goda, Y. Finite periodic stationary gravity waves in a perfect liquid. *Coast. Eng. Jpn.* **1967**, *10*, 1–11. [CrossRef]
41. Jeng, D. Wave kinematics of partial reflection from a vertical wall. *Ocean. Eng.* **2002**, *29*, 1711–1724. [CrossRef]
42. Teo, H. Wave pressures on a vertical wall due to short-crested waves: Fifth-order approximation. *Ocean. Eng.* **2003**, *30*, 2157–2166. [CrossRef]
43. Hedges, T. Regions of validity of analytical wave theories. *ICE Water Marit. Energy* **1995**, *112*, 111–114. [CrossRef]
44. Fenton, J.D. Wave Forces on Vertical Walls. *J. Waterw. Port Coast. Ocean. Eng.* **1985**, *111*, 693–718. [CrossRef]
45. Bridges, T.J. Wave Forces on Vertical Walls. *J. Waterw. Port Coast. Ocean. Eng.* **1986**, *29*, 2819–2827.
46. Romanczyk, W. Instability of nonlinear standing waves in front of a vertical wall. *J. Fluids Struct.* **2007**, *23*, 733–753. [CrossRef]
47. Chen, X.; Hofland, B.; Molenaar, W.; Capel, A.; Gent, M.R.V. Use of impulses to determine the reaction force of a hydraulic structure with an overhang due to wave impact. *Coast. Eng.* **2019**, *147*, 75–88. [CrossRef]
48. Tieleman, O.C.; Tsouvalas, A.; Hofland, B.; Jonkman, S.N. A three dimensional semi-analytical model for the prediction of gate vibrations. *Mar. Struct.* **2019**, *65*, 134–153. [CrossRef]

49. Zelt, J.; Skjelbreia, J. Estimating Incident and Reflected Wave Fields Using an Arbitrary Number of Wave Gauges. In Proceedings of the Coastal Engineering Conference, Venice, Italy, 4–9 October 1992.

Publisher's Note: MDPI stays neutral with regard to jurisdictional claims in published maps and institutional affiliations.

4

VARYING INCIDENT WAVE FIELDS AND CONFIGURATIONS

This chapter has been published in "Standing wave impacts on vertical hydraulic structures with overhangs for varying wave fields and configurations" in the Journal of Coastal and Hydraulic Structures (De Almeida & Hofland 2021).

JCHS TU Delft OPEN

JOURNAL OF COASTAL AND HYDRAULIC STRUCTURES

Vol. 1, 2021, 10

Standing wave impacts on vertical hydraulic structures with overhangs for varying wave fields and configurations

4

Ermano de Almeida[1] and Bas Hofland[2]

Abstract

This study focuses on standing wave impacts on vertical hydraulic structures with relatively short overhangs. It addresses the demand for extended knowledge and loading prediction expressions for these structures. Based on laboratory experimental data from 146 tests, this paper works on two complementary objectives. Firstly, this study extends the knowledge on this type of wave impact addressing the following aspects: changes in hydraulic loading conditions (regular/irregular waves and varying freeboards) and changes in the structure geometry (lateral constriction and loading reducing ventilation gaps). All laboratory tests consider relatively short overhangs, with ratios of wave length to overhang length between 10 and 40, and ratios of overhang height to overhang length of 3 and 6. The regular wave tests showed that the tests with the longer overhang were related to longer impact durations and larger loading variability compared to the tests with the shorter overhang. Also, tests with reduced freeboards produced larger impact loads. In addition, repeated tests presented equal impulse values (I, β, t_d, Λ). Furthermore, the pressure peaks measured at one location were found to not represent the pressure peaks averaged over the structure width, while the pressure-impulses measured at one location were found to properly represent the pressure-impulses averaged over the width. The constriction tests showed that a lateral constriction amplifies pressure peaks and pressure-impulses at the constriction edge. The ventilation gap tests showed that ventilation gaps are effective in reducing force peaks and force-impulses. The irregular wave tests highlighted that the dynamic interactions of the incident waves with the structural configurations are even more dynamic and variable in tests with irregular wave conditions. Secondly, this study presents loading prediction expressions for preliminary loading estimations built up by the previously developed pressure-impulse theory that is empirically calibrated using the presently acquired experimental data. To that end, the relation between the effective bounce-back factor $(1 < \beta < 2)$ with the Gamma Parameter (Γ) is described. These loading prediction expressions may be used for preliminary load estimations and in combination with structural response models.

[1]E.deAlmeida@tudelft.nl, Delft University of Technology, Delft, The Netherlands
[2]B.Hofland@tudelft.nl, Delft University of Technology, Delft, The Netherlands

This paper was submitted 11 July 2021. It was accepted after double-blind review on 27 November 2021 and published online on 24 December 2021"

DOI: https://doi.org/10.48438/jchs.2021.0010

Cite as: "De Almeida, E., Hofland, B. Standing wave impacts on vertical hydraulic structures with overhangs for varying wave fields and configurations. Journal of Coastal and Hydraulic Structures, 1, p.10. https://doi.org/10.48438/jchs.2021.0010"

Keywords:

wave impacts, hydraulic structures, impulsive loading, overhangs

1 Introduction

During the coming years and decades, numerous hydraulic structures will be constructed worldwide. Also, various existing hydraulic structures will be renovated after reaching the end of their design lifetime or due to increasing safety standards and/or loading conditions. Figure 1 shows one of such singular hydraulic structures, the flood gate complexes in the Afsluitdijk in The Netherlands. The Afsluitdijk is currently being fully renovated after almost 90 years of operation. The renovation of the Afsluitdijk includes the complete renewal of the existing flood gate complexes, and the construction of additional flood gate complexes to cope with sea level rise and more extreme weather scenarios. Such construction and renovation projects require the development of design guidelines and prediction methods for determining wave impact characteristics and magnitudes.

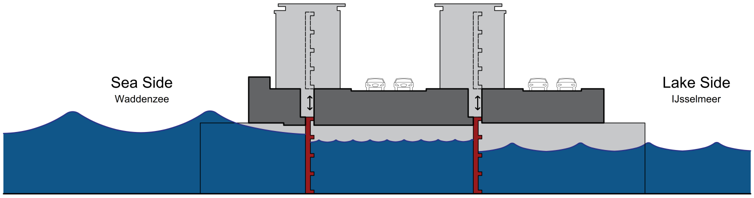

Figure 1: Existing Afsluitdijk flood gate, during high water at the sea side (de Almeida and Hofland, 2020*a*).

Three types of wave impacts are described in de Almeida and Hofland (2020*a*): breaking waves acting on a vertical wall, overtopping waves acting on a crest wall and non-breaking waves acting on a vertical wall with a horizontal overhang. This study focuses on this third type of wave impact (i.e. standing wave impacts on vertical structures with overhangs). This type of wave impact is determinant for structures as shown in Figure 1, but also for many others such as crest walls, lock gates, sluice gates, dewatering sluices, flood gates and storm surge barriers. Until recently, only a few studies were conducted on wave impact loads acting on vertical hydraulic structures with overhangs (Ramkema, 1978; Kisacik et al., 2014). Nevertheless, this wave impact type is gaining increasing attention in the past years. Recent developments on the study of standing wave impacts on hydraulic structures were presented by Castellino et al. (2018), Martinelli et al. (2018), de Almeida and Hofland (2020*a*), de Almeida and Hofland (2020*b*), Castellino et al. (2021) and Dermentzoglou et al. (2021), among others. Furthermore, recent studies have also addressed wave impacts on overhang configurations that occur in nature, for example on cliffs and shore platforms (Renzi et al., 2018).

Bagnold (1939) contributed to the study of impulsive loading caused by breaking waves, including two key findings. Firstly, the highest pressure magnitudes were measured when the air cushion between the wave front and the impact surface was small, but not zero. Secondly, although maximum peak pressures present large fluctuations, the area enclosed by the pressure-time curve (i.e. the pressure-impulse P) was remarkably constant. Further research on impulsive loadings caused by wave impacts has mainly focused on breaking wave impacts on vertical structures (Minikin, 1950; Goda, 1974; Takahashi et al., 1994; Oumeraci et al., 2001; Cuomo et al., 2010). In addition, breaking wave impacts have also been studied for structures with relatively long overhangs (Kisacik et al., 2014). Regarding overtopping wave impacts, this wave impact type has also been studied recently by Chen et al. (2015, 2016).

A comprehensive series of laboratory tests took place in The Netherlands for the design and construction of the Delta Works (1953-1997). A large number of those laboratory tests focussed on wave impact loadings on the Eastern Scheldt Storm Surge Barrier, including standing wave impacts in configurations with overhangs (Ramkema, 1978; WL, 1977, 1978). However, those studies focussed on design optimization and scaling laws and did not introduce general design criteria for such types of hydraulic structures. More recently, Hofland (2015) studied impulsive wave impact loading acting on the existing Afsluitdijk flood gates, including the effect of the existing overhang and ventilation gap. Nevertheless, those tests were once more focused on representing a particular structural configuration and did not introduce general design guidelines.

The pressure-impulse theory applied to wave impacts was first presented by Cooker and Peregrine (1990, 1995). This theoretical model allows calculating the pressure-impulse caused by a wave impact and was developed based on the Navier-Stokes equations of motion. This theory was first presented considering a horizontally moving volume of water (describing a simplified breaking wave) impacting on a vertical wall. Later on, Wood and Peregrine (1996) extended this theory considering a vertically moving volume of water (describing a simplified reflecting wave) impacting on a horizontal overhang. This theory was validated by de Almeida and Hofland (2020*a*), combining the models from Cooker and Peregrine (1990, 1995) and Wood and Peregrine (1996). This validation was done for a vertical wall with a horizontal overhang subjected to standing incident waves and obtained a close confirmation of the theory. The advantages of using the pressure-impulse and force-impulse for preliminary load estimations instead of pressure and force peaks were presented by Chen et al. (2019). Furthermore, a model to estimate reaction forces from impulsive wave impact loads was also introduced. Tieleman et al. (2019, 2021) developed a semi-analytical model for predicting the bending vibrations of vertical hydraulic structures subjected to impulsive wave impact loadings, including the configuration of a vertical wall with a horizontal overhang (e.g. flood gates shown in red in Figure 1).

Various authors have focussed on the study of impulsive wave loads on recurved crest walls on vertical breakwaters (Castellino et al., 2018, 2021; Martinelli et al., 2018; Dermentzoglou et al., 2021). Those authors have addressed both the loading and response aspects, considering both experimental and numerical methods. In addition to de Almeida and Hofland (2020*a*), de Almeida and Hofland (2020*b*) has also studied standing wave impacts with a focus on the wave impact velocity and entrapped air characteristics. There, the details of the entrapped air and the kinematics of the impacting wave surface were seen to determine the impact duration. This study confirmed the observations from WL (1979), which highlighted that the presence of air pockets has a decisive effect on the characteristics and magnitudes of wave impact loadings. Wave impact loads acting on similar structures such as piers and bridge decks were also studied recently (McConnell et al., 2004; Cuomo et al., 2007; Seiffert et al., 2014; Hayatdavoodi et al., 2014). In addition, other studies present recent experimental and numerical models and tools for assessing slamming loads on offshore structures, natural gas tanks and ship hulls (Dias and Ghidaglia, 2018; Sonneville et al., 2015; Bogaert, 2018). Those contributions show that, besides significant differences, common processes are observed in confined wave impacts in hydraulic structures, piers, bridge decks, offshore structures/platforms and during sloshing impacts inside gas tankers. One key difference is that de Almeida and Hofland (2020*a*) has focused on describing the confined wave impact load by the pressure/force-impulse based on regular wave laboratory tests and the pressure-impulse theory. This is different to many other studies that focused on describing wave impact loads mostly in terms of pressure/force peaks. Thus, a knowledge gap still exists in describing confined wave impact loads on realistic configurations loaded by irregular wave fields considering the pressure/force-impulses and based on the pressure-impulse theory.

The previously described literature presented a range of contributions on wave impacts in general and confined wave impacts in particular. Nevertheless, important knowledge gaps remain in the study of standing wave impacts on vertical hydraulic structures with relatively short overhangs. Mainly, there is a lack of loading prediction expressions for this type of wave impact. Knowledge gaps also exist on the influence of irregular incident waves, the effect of different water levels, the spatial distribution of loading and load reducing ventilation gaps. This paper addressed those knowledge gaps, based on experimental data and the pressure-impulse theory.

The aims of this paper are divided into two objectives. Firstly, to extend the knowledge on this type of wave impact addressing the following four aspects: regular and irregular incident waves, the effect of different water levels, the spatial distribution of loading in configurations with and without realistic geometrical variations like lateral constrictions and load reducing ventilation gaps. Secondly, to present loading prediction expressions for preliminary loading estimations based on laboratory experimental data and the pressure-impulse theory. Section 2 describes the theoretical expressions used in this study. Section 3 describes the setup, characteristics and configurations of the laboratory experiments. Section 4 presents all experimental results, including the loading prediction expressions based on laboratory experimental data and the pressure-impulse theory. Section 5 discusses the main aspects of this work, while Section 6 summarizes the main conclusions of this study.

2 Theoretical methods

This section summarizes the most important theoretical expressions and concepts used in this study. It includes the main expressions of the pressure-impulse theory, the estimation of the wave impact velocity based on linear wave theory and the characteristics of the Rayleigh distribution. Figure 2 describes the main hydraulic and structural parameters used in this study. Furthermore, the pressure-impulse expression is shown in Equation 1.

$$P = \int_{t_d} p \, dt \tag{1}$$

where P [Pa s] is the pressure-impulse, p [Pa] is the pressure and t_d [s] is the impact duration.

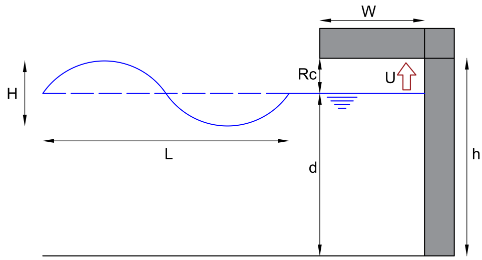

Figure 2: Hydraulic and structural parameters: incident wave height H [m]; incident wave length L [m]; still water depth d [m]; overhang height h [m], overhang width W [m]; freeboard R_c [m]; impact velocity U [m/s].

4

Pressure-impulse theory

In this paper, the pressure-impulse model is used in a dimensionless form, as presented by Wood and Peregrine (1996) and validated in de Almeida and Hofland (2020*a*). The dimensionless model is obtained by considering the overhang length W as the geometric scaling magnitude. This is justified by the fact that the overhang length W is the length over which the vertically-moving water surface impacts the horizontal overhang. Then, W is used for obtaining the dimensionless geometric magnitudes, such as the dimensionless overhang length ($\bar{W} = 1$) and the dimensionless overhang height ($\bar{h} = h/W$). For the conversion between dimensionless and dimensional impulse results, Equations 2 and 3 are used. Equation 2 is used for the pressure-impulse P obtained at any point in the fluid domain. Equation 3 is used for the total force-impulse I integrated over a given boundary, such as the vertical wall that extends from beneath the overhang to the bottom. In these equations and throughout this study, the overbar sign "$^-$" represents dimensionless values.

$$\bar{P} = \frac{P}{\rho U W} \tag{2}$$

$$\bar{I} = \frac{I}{\rho U W^2} \tag{3}$$

where ρ [kg/m^3] represents the fluid density and U [m/s] represents the wave impact velocity.

A summary of the validated pressure-impulse theory is presented hereafter. For the detailed theoretical descriptions of the model and full validation process, please refer to de Almeida and Hofland (2020*a*). All three Equations 4-6 shown here were obtained as fits in de Almeida and Hofland (2020*a*) from the analytical model by Wood and Peregrine (1996). The total dimensionless force-impulse $\bar{I}$ applied along the vertical wall can be calculated for any value of dimensionless overhang height $\bar{h}$ and effective bounce-back factor β according to the expression presented in Equation 4. C_I represents the total theoretical dimensionless force-impulse (i.e. $\beta = 1$), obtained as a fit to the pressure-impulse analytical model. Equations 5-6 present the expressions for the maximum (i.e. at the top of the wall) and minimum (i.e. at the bottom of the wall) dimensionless pressure-impulse $\bar{P}$ as function of the dimensionless overhang height $\bar{h}$ and the effective bounce-back factor β. The factor β was introduced by Wood et al. (2000) to describe the increase in impact pressure-impulse due to the bounce-back of entrapped air, with values in the range $1 < \beta < 2$. In this paper, β is used as described in de Almeida and Hofland (2020*a*), to account for all differences between theory and measurement, so it is used as the effective bounce-back factor. From the experimental tests, β is calculated as follows: $\beta = \bar{I}/C_I$. Furthermore, based on Wood et al. (2000), de Almeida and Hofland (2020*a*) introduced the Peregrine Number ($\Lambda = t_d U/W$). This parameter assesses the validity of the pressure-impulse theory. According to Wood et al. (2000) and based on breaking wave impacts, the pressure-impulse theory is applicable for describing wave impacts with lower values of the Peregrine Number ($\Lambda << 1$). The value of $\Lambda = 0.4$ is adopted as an approximate upper limit for the theory validity, while more violent wave impacts with lower values of the Peregrine Number Λ are expected to show better agreement with the pressure-impulse theory.

$$\bar{I} \approx \beta C_I \approx \beta(2\bar{h}^{0.18} - 1.14) \qquad \text{for} \quad 1 \leq \bar{h} \leq 10 \tag{4}$$

$$\bar{P}_{max} \approx \beta(0.18\bar{h}^{-1.9} + 1) \qquad \text{for} \quad 1 \leq \bar{h} \leq 10 \tag{5}$$

$$\bar{P}_{min} \approx \beta(0.75\bar{h}^{-0.97}) \qquad \text{for} \quad 1 \leq \bar{h} \leq 10 \tag{6}$$

Impact velocity

The proposed method to estimate the standing wave impact velocity is linear wave theory. This was used by de Almeida and Hofland (2020*b*) as it is considered suitable for the undisturbed waves within the ranges of steepness and relative depth applied in this study (Hedges, 1995) and it is a well-known theory that can be implemented in future design guidelines. According to this theory, and as presented in the previously mentioned studies, a linear wave reflecting against a vertical wall can be described as in Equation 7.

$$\eta = (1 + cr)\frac{H}{2}\sin\omega t = A_w \sin\omega t \tag{7}$$

where η [m] represents the surface elevation, cr [-] represents the wave reflection coefficient, H [m] represents the incident wave height, ω [rad/s] represents the angular wave frequency ($\omega = 2\pi/T$, where T [s] represents the incident wave period) and A_w [m] represents the total wave amplitude at the wall.

Equation 7 (water surface position) was combined with its derivative (water surface velocity), so the water surface velocity $\dot{\eta}$ is described as function of the water surface position η: $\dot{\eta} = \omega\sqrt{A_w^2 - \eta^2}$ (de Almeida and Hofland, 2020*a*). In addition, a reflection coefficient of $cr = 1$ is used in this method, as the incident wave is not influenced by the presence of the overhang during the period $T/2$ prior to the wave impact. The results presented in de Almeida and Hofland (2020*b*) showed that the wave surface position/velocity estimated with this method is in agreement with the laboratory measurements. A reflection coefficient of $cr = 1$ leads to a total wave amplitude at the wall equal to the incident wave height ($A_w = H$). The wave surface impact velocity U on an overhang with a freeboard ($R_c < H$) can then be obtained from Equation 8.

$$U = \omega\sqrt{H^2 - R_c^2} \tag{8}$$

Rayleigh distribution

For irregular wave fields, the incident wave height of the single waves (H) in Equation 8 should be obtained from the wave field parameters (i.e. significant wave height H_s) and given a certain exceedance probability (i.e. pr). The Rayleigh distribution is used in this study to describe the wave height distribution for a set of given incident wave parameters (Longuet-Higgins, 1952). The Rayleigh distribution is a particular type of Weibull distribution in which the shape parameter is equal to 2. Further, with a scale parameter of 0.5, the cumulative distribution function of the Rayleigh distribution can be re-arranged as in Equation 9. This equation allows obtaining the incident wave heights associated with a given exceedance probability (pr), or a given return period. This can then be used to describe the wave impact velocity of each wave according to Equation 8.

$$H = H_s\sqrt{-\frac{\log(pr)}{2}} \tag{9}$$

3 Laboratory experiments

This section presents the experiments carried out for this study, which includes a total of 146 laboratory tests. This large amount of tests constitutes a robust dataset on this type of wave impact, including a wide range of structural and hydraulic combinations. This experimental dataset is used to draw a wide range of new conclusions and to carry out the validation of the load prediction expressions. Hereafter in this section, the experimental setup, the experiment conditions and the instrumentation are described in more detail.

3.1 Experimental Setup

This study analyses the results of 146 laboratory tests carried out during three test campaigns (2018, 2019, 2020) at the wave flume at the Hydraulic Engineering Laboratory at the Delft University of Technology. Figure 3 illustrates the laboratory test area during the 2019 test campaign. The wave flume used in all tests is 42 m long, 1 m high and 0.8 m wide. The wave generation equipment consists of a piston-type wave maker able to generate regular and irregular waves and is equipped with active reflection compensation (ARC) and second order wave steering. The test setup was fully built with aluminium elements, supported by a 1500 kg concrete block placed inside the wave flume. This concrete block was 0.8 m wide, 0.8 m long and 1 m high and provided the required stability for the structure subjected to wave impacts. Furthermore, this laboratory model does not represent a precise real structure. It is a schematic configuration, inspired by structures such as the Afsluitdijk sluice gates. For orientation purposes, the dimensions of the laboratory setup would correspond to an approximate 1:15 scale to a structure such as the Afsluitdijk sluice gates. The details on the various structural configurations and test conditions are described in more detail hereafter.

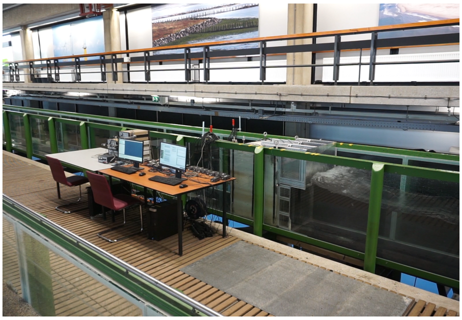

(a) Experimental test area.

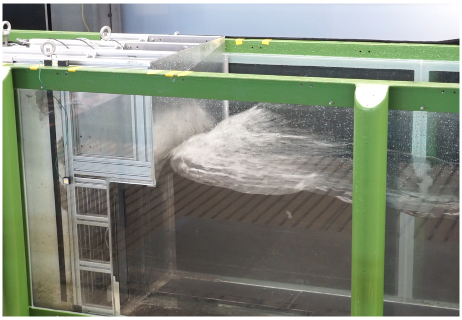

(b) Overhang structure model setup.

Figure 3: Overview of experiments(images taken from de Almeida and Hofland (2020*a*)).

3.2 Experiment Conditions

Table 1 briefly summarizes all laboratory tests used in this study. As shown in Table 1 and Figure 4, three main structural configurations were tested. A common feature of all tests in this study is the constant width of the structure ($M = 0.8$ m) which is equal to the flume width, the constant height of the overhang ($h = 0.6$ m) and the use of two overhang lengths: a shorter overhang “S” ($W = 0.1$ m) and a longer overhang “L” ($W = 0.2$ m). 106 out of the 146 tests were done for the standard configuration, consisting of a vertical wall and a horizontal overhang. For this configuration tests with regular and irregular waves were carried out with variations of wave height (H), wave period (T), wave steepness (s), water depth (d) and freeboard (R_c). This large number of tests fulfilled the goal of allowing a wide range of conclusions on this type of wave impact and providing a robust dataset for the validation of the prediction expressions. Furthermore, two additional configurations were tested, to extend the knowledge on the effects of lateral constrictions and ventilations gaps on the wave impact loads. Those experiments included the remaining 40 tests with only regular waves and a shorter number of variations in the incident wave conditions. More details on the tests carried out (i.e. variations of structural configurations and incident wave conditions) are shown in the Annexes in Table A1.

Table 1: Number of laboratory tests.

Condition	Regular wave	Irregular wave	Total
Standard configuration	54	52	106
Lateral constriction	10	-	10
Ventilation gaps	30	-	30

3.3 Instrumentation

The incident waves parameters were measured at 1.5 metres away from the vertical wall. To this end, an array of three wave gauges with a 100 Hz sampling rate were used, see Figure 4b. Based on the wave gauge measurements, the method from Zelt and Skjelbreia (1992) was used to obtain the incident wave spectra, time-series and parameters (i.e. wave height H and wave period T). These wave gauges were equipped with water conductivity compensation systems to ensure the accuracy of the measurements in all circumstances, adjusting for temperature variations during the tests.

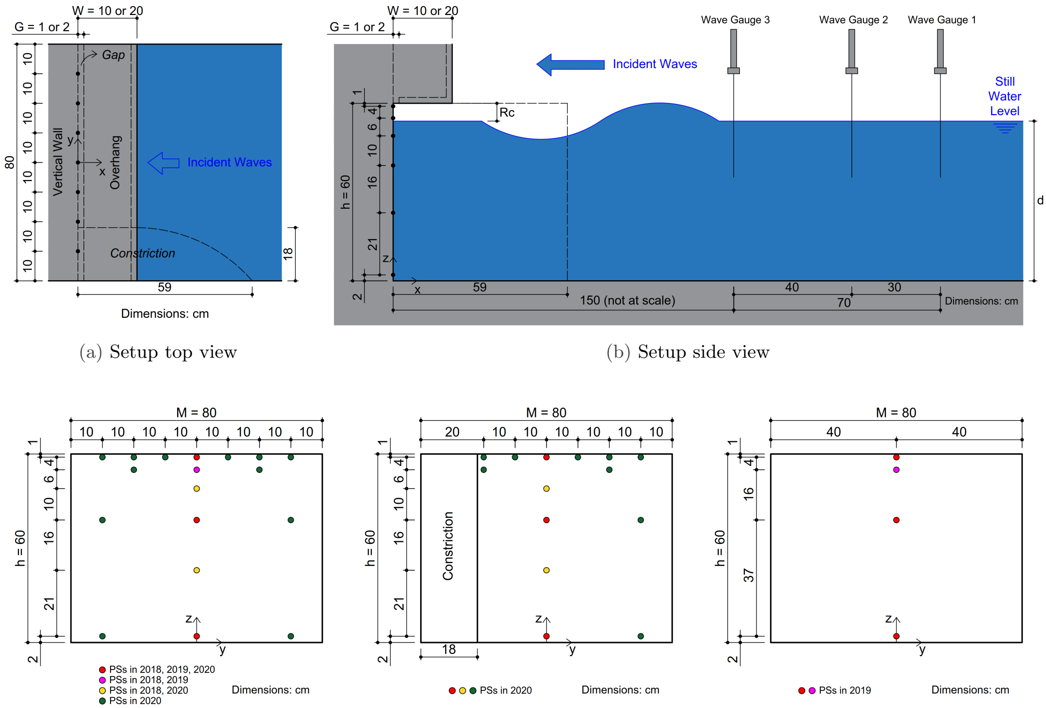

(a) Setup top view

(b) Setup side view

(c) Standard configuration front view

(d) Constriction tests front view

(e) Gap tests front view

Figure 4: Experimental setup characteristics.

Pressures were measured in this study with pressure sensors Kulite HKM-375M-SG with 1 bar measurement range and sealed gauge, screwed flush on the structure aluminium surface. During all tests, a sampling rate of 20 kHz was used for these dynamic pressure measurements. By integrating the pressures measured over the vertical wall, the total forces were obtained. All pressure and force peaks presented throughout this study were calculated from the original unfiltered time series. Furthermore, this study uses the method presented by de Almeida and Hofland (2020*a*) for calculating the pressure-impulses, force-impulses and impact durations generated by the wave impacts. In this method, the original time series is filtered with a low-pass third order Butterworth filter with a cut-off frequency of 100Hz. This cut-off frequency allows to remove higher frequency components but it is sufficiently large to not affect the impulse measurements. Further, the wave impact start is defined as when the pressure becomes larger than zero (i.e. hydrostatic pressure), and the impact end is defined as when the pressure becomes smaller than the quasi-static component. The impact duration (t_d) is then obtained as the time interval between the impact start and the impact end. Next, pressure-impulses are calculated by integrating the pressures between the previously defined impact start and the impact end. Lastly, force-impulses are then calculated by integrating the obtained pressure-impulse profile over the vertical wall height. During the different test campaigns, a different number of pressure sensors (PS) were used: 6 in 2018, 4 in 2019 and 17 in 2020. The locations of these pressure sensors in the three test campaigns are shown in Figures 4c, 4d and 4e for the different test configurations. The calibrations of these pressure sensors obtained at the start of the test campaign were regularly checked during and after the test campaign, with before-after variations in calibration factors around 0.12%. Furthermore, this study uses in all analyses the dynamic values for pressures and forces, which are obtained after the hydrostatic pressure/forces (i.e. the ones measured before wave motion) are removed from the measurements.

4 Experimental results

This section presents and discusses the results of the laboratory experiments. Hereafter, these test results are separated into three parts. Firstly, the results of the regular wave tests with standard configuration are presented. Secondly, the results of the regular wave tests with the non-standard configurations (i.e. lateral constriction and ventilation gaps) are discussed. Lastly, the results of the irregular wave tests are presented.

4.1 Regular wave tests with standard configuration

This experimental set consists of a total of 54 tests, including four water levels, five incident wave conditions and two overhang lengths. Figures 5 and 6 illustrates the regular wave tests with standard configuration, including the combinations of water levels, incident wave conditions and overhang lengths. Here only three test conditions (A, C, E) are presented for simplicity. Nevertheless, these three test conditions (A, C, E) cover the full range of incident wave characteristics and measured wave impact loading. Figure 5 shows the results for the shorter overhang, while Figure 6 shows the results for the longer overhang. These figures show the pressure measurements from the pressure sensor located at the top-centre of the vertical wall ($x = 0$ m, $y = 0$ m, $z = 0.59$ m), see Figure 4c. Detailed results from all the regular wave tests are shown in the Annexes in Table A2.

From Figures 5 and 6, a series of observations can be highlighted. First, for the smallest incident wave condition (rA), no wave impact took place for the highest water level with negative freeboard ($d = 0.63$ m, $R_c = -0.03$ m), see Figures 5d and 6d. This reduces the number of tests with wave impacts in this experimental set to 52, which will be used further in this study. Second, it is observed that repeated tests (for $d = 0.60$ only, see Table A2 for details) showed similar impulsive load characteristics as described by I, β, t_d and Λ. Furthermore, given the reduced values of the Peregrine Number obtained in this study ($\Lambda \leq 0.30$), it is considered that all the tests in this study fall within the range of validity for the pressure-impulse theory (Wood et al., 2000). Third, the tests with longer overhangs presented longer impact durations compared to the tests with shorter overhangs. This can be observed in the results of impact duration (see Table A2 for details) and also visually in Figures 5 and 6. As highlighted in de Almeida and Hofland (2020*b*), this is explained by the fact that a longer overhang is directly related to larger air entrapments and thus directly related to longer impact durations (Mitsuyasu, 1966). In addition, it is also observed that lower water levels are strongly related to shorter impact durations in tests with shorter overhangs. For the tests with longer overhangs this relation between water level and impact duration is less evident but still present. This can be explained by a easier release of the air before wave impacts for lower water levels, leading to shorter impact durations. In the case of higher water levels and reduced freeboards, the air may be more easily entrapped between the wave surface and the structure, leading to longer impact durations. It can then be highlighted that in general the shorter wave impact durations will be expected for shorter overhangs at lower water levels. Fourth, it is also observed that for the same incident wave conditions, the impacts on the longer overhangs (Figure 6) show a more complex and variable behaviour compared to the tests with shorter overhangs (Figure 5). That more complex behaviour for tests with longer overhangs includes frequent vibrations (Figures 6a, 6e, 6i, 6j), pre-peaks (Figures 6b, 6f, 6l), very long impacts (Figures 6b, 6c, 6f, 6g), double peaks (Figure 6k) and even triple peaks (Figure 6h). This higher variability of wave impacts loading characteristics, is driven by the more complex interaction of structural configurations, incident wave conditions and air entrapment in configurations with longer overhangs. For the shorter overhangs, such complex behaviour is still present but less frequent, with less complex wave impact loading characteristics. The majority of tests with the shorter overhang showed a short and high wave impact (Figures 5a, 5b, 5e, 5i, 5j, 5k). Few exceptions include two tests with small vibrations (Figures 5c, 5g), a long impact (Figure 5h), an impact with a short pre-peak (Figure 5l) and a double peak (Figure 5f). Fifth, tests with identical incident wave conditions and different water levels showed a limited variation in the loading curves behaviour, see Figures 5i, 5j and 5k for the shorter overhang or Figures 6e, 6f and 6g for the longer overhang. Sixth, tests with identical water levels and different incident wave conditions showed a limited variation in the loading curves behaviour, see Figures 5a, 5e and 5i for the shorter overhang or Figures 6a, 6e and 6i for the longer overhang. Seventh, the tests with a negative freeboard showed a more complex loading behaviour: pre-peaks (Figures 5l, 6l), long peak (Figure 5h) and a triple peak (Figures 6h).

Figure 7 gives the values of dimensionless total force-impulse $\bar{I}$ obtained from the regular wave tests with standard configuration. This extends the validation of the pressure-impulse theory presented by de Almeida and Hofland (2020*a*), including a larger number of tests (52 tests instead of 14) and also four different water levels (instead of only one). Based on all regular wave tests with standard configuration, the obtained effective

$d = 0.56$ m $\Downarrow R_c = 0.04$ m | $d = 0.58$ m $\Downarrow R_c = 0.02$ m | $d = 0.60$ m $\Downarrow R_c = 0.00$ m | $d = 0.63$ m $\Downarrow R_c = -0.03$ m

$\Longrightarrow$ Cond. rA, $H = 0.06$ m, $s = 0.023$, $W = 0.1$ m

$\Longrightarrow$ Cond. rC, $H = 0.10$ m, $s = 0.038$, $W = 0.1$ m

$\Longrightarrow$ Cond. rE, $H = 0.10$ m, $s = 0.016$, $W = 0.1$ m

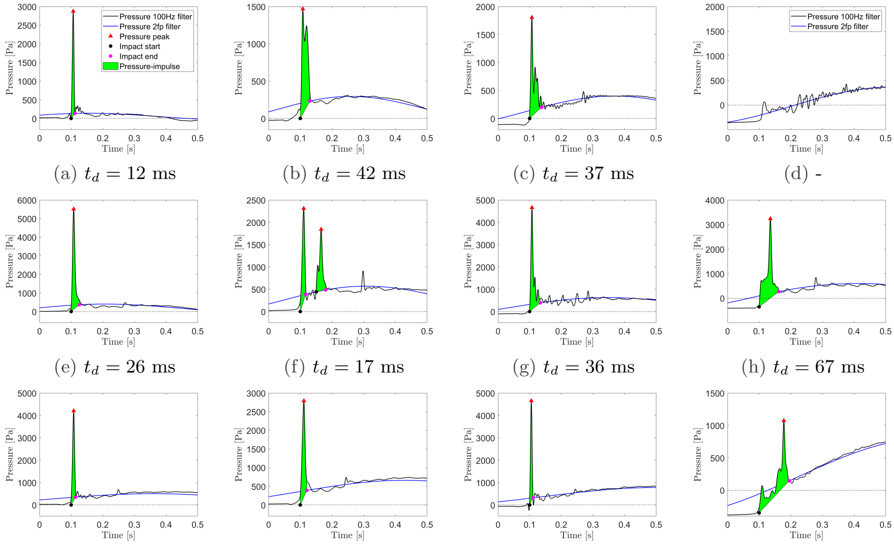

(a) $t_d = 12$ ms (b) $t_d = 42$ ms (c) $t_d = 37$ ms (d) -

(e) $t_d = 26$ ms (f) $t_d = 17$ ms (g) $t_d = 36$ ms (h) $t_d = 67$ ms

(i) $t_d = 16$ ms (j) $t_d = 22$ ms (k) $t_d = 10$ ms (l) $t_d = 90$ ms

Figure 5: Shorter overhang ($W = 0.1$ m) - Impact types for regular wave tests.

$d = 0.56$ m $\Downarrow R_c = 0.04$ m | $d = 0.58$ m $\Downarrow R_c = 0.02$ m | $d = 0.60$ m $\Downarrow R_c = 0.00$ m | $d = 0.63$ m $\Downarrow R_c = -0.03$ m

$\Longrightarrow$ Cond. rA, $H = 0.06$ m, $s = 0.023$, $W = 0.2$ m

$\Longrightarrow$ Cond. rC, $H = 0.10$ m, $s = 0.038$, $W = 0.2$ m

$\Longrightarrow$ Cond. rE, $H = 0.10$ m, $s = 0.016$, $W = 0.2$ m

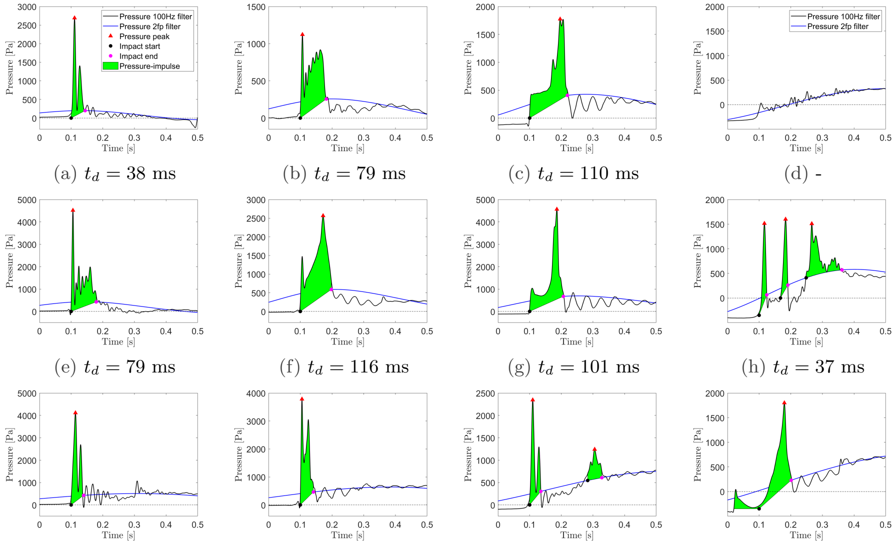

(a) $t_d = 38$ ms (b) $t_d = 79$ ms (c) $t_d = 110$ ms (d) -

(e) $t_d = 79$ ms (f) $t_d = 116$ ms (g) $t_d = 101$ ms (h) $t_d = 37$ ms

(i) $t_d = 34$ ms (j) $t_d = 41$ ms (k) $t_d = 37$ ms (l) $t_d = 95$ ms

Figure 6: Longer overhang ($W = 0.2$ m) - Impact types for regular wave tests.

bounce-back factor was $\beta = 1.19$ ($\sigma_\beta = 0.15$). This deviates slightly from the values obtained in de Almeida and Hofland (2020a) ($\beta = 1.17$ ($\sigma_\beta = 0.11$). The test with a remarkably large dimensionless impulse found in Figure 7 ($\bar{h} = 6$ and $\bar{I} = 2.61$) is showed in Figure 5h corresponding to a condition of negative freeboard, with a very high and long impact. The discussion on the effective bounce-back factor β and its applicability for preliminary load predictions continues in this study in Section 4.3, when the irregular wave tests are considered.

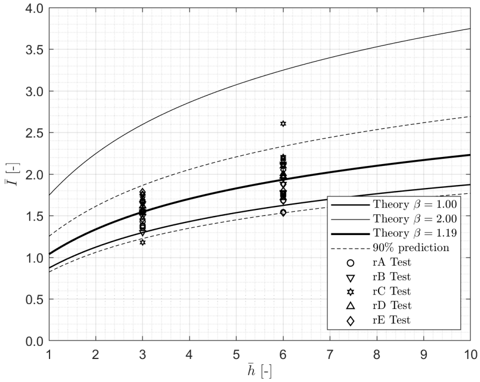

Figure 7: Dimensionless experimental results from regular wave tests with standard configuration.

Spatial variation over the width with standard configuration

The spatial distribution of pressures over the width of the structure was studied in the standard configuration tests. During 10 regular wave tests with standard configuration (5 with shorter overhang and 5 with longer overhang), 7 pressure sensors were placed at the top of the vertical wall along the structure width (see Figure 4c). At this location the wave impact and the highest pressures take place. In addition, an ensemble averaged pressure time series (noted by $\langle\,\rangle$) was calculated as the average pressures from the 7 individual pressure sensors.

Figure 8 summarizes the spatial distribution of pressures over the width for tests without a lateral constriction. The two figures on the left show peak pressures, the two figures on the right show pressure-impulses. Furthermore, the two figures on the top compare individual pressure sensor recordings to the ensemble averaged pressure time series, while the two figures on the bottom show the cross flume distribution. In Figure 8, note that the y-axis scales differ. Figure 8a describes the relation between the pressure peaks measured at the individual pressure sensors with the pressure peaks measured at the ensemble averaged time series. Thus, it is observed that the peak pressures measured by the individual pressure sensors are not observed simultaneously along the whole structure. This leads to a corresponding overestimation of peak forces at the structure if the peak pressure at one location is assumed to take place over the whole width. Figure 8b shows the same comparison for pressure-impulses, and a significantly smaller variability is observed. Based on these observations, it is found that the pressure-impulse measured at one location can be assumed to take place over the whole structure width with a high degree of confidence, while the same cannot be done for pressure peaks. Nevertheless, the spatial distribution of loads obtained in this study may not be directly assumed to take place in other wave impact situations. Still, these results highlight the importance of studying in more detail the spatial distribution of loads during the design of hydraulic structures subjected to wave impacts. The larger variability in the p and P in Figures 8a and 8b (e.g. rBS test for p and rAL for P) is caused by the larger entrapped air pockets, which break down in smaller bubbles during the wave impact and cause a larger loading variability. The cross flume distribution of peak pressures and pressure-impulses are presented in Figure 8c and Figure 8d. Those figures include also a second order polynomial fit for the shorter overhang (blue line), for the longer overhang (red line) and for all tests combined (black line). Figure 8c shows that, besides a variability between the different tests, larger pressure peaks were measured at the sides compared with the centre. Figure 8d shows the same comparison for pressure-impulses, with a similar behaviour but significantly smaller variability.

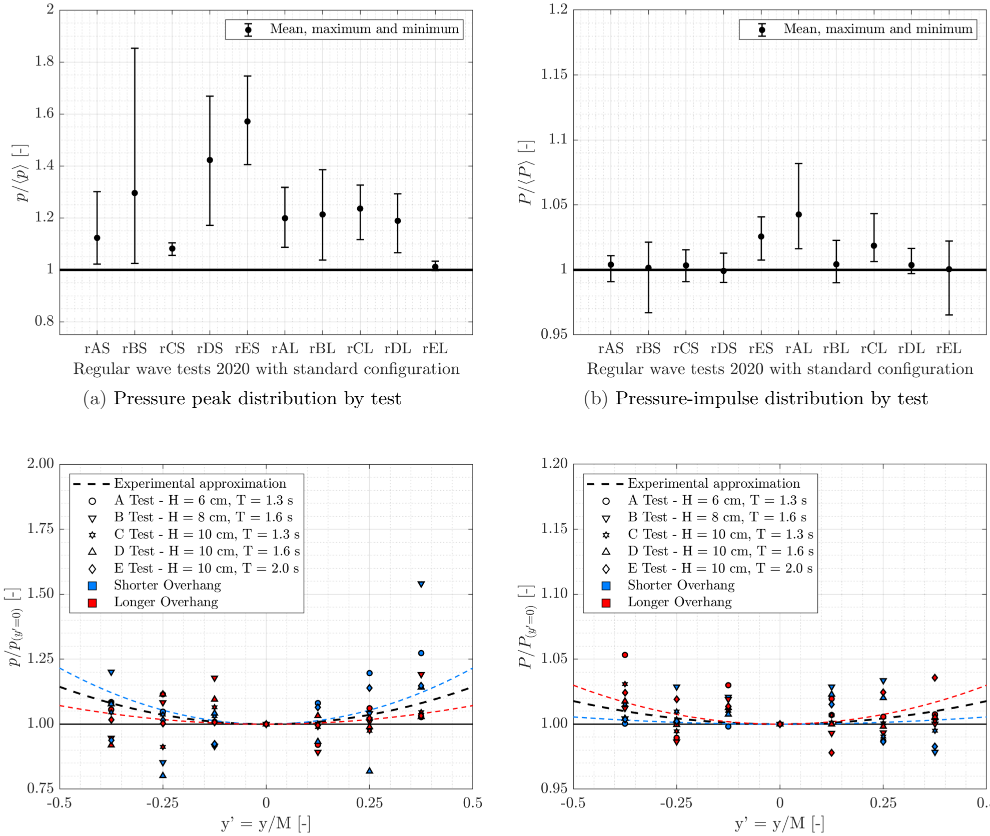

(a) Pressure peak distribution by test

(b) Pressure-impulse distribution by test

(c) Cross-flume pressure peak distribution

(d) Cross-flume pressure-impulse distribution

Figure 8: Spatial distribution of pressures peaks and pressure-impulses. Note that axis scales differ.

4.2 Regular wave tests with lateral constriction and ventilation gaps

Flood gates often consist of a series of gates that are bordered by pylons or similar lateral constrictions (e.g. Eastern Scheldt, Afsluitdijk, Haringvliet, Fudai or Pont-vannes du Millac). Consequently, those lateral constrictions represent an additional and often-occurring complication in the design of such flood gates. Also, ventilation gaps are present in front of vertical flood gates (e.g. Afsluitdijk), leading to the reduction of wave impact loads. Thus, these two variations of the standard configurations are studied in this section, given their importance for the design of such flood gates. Furthermore, these results also aim to highlight the applicability of the proposed loading prediction expressions to more realistic structural configurations.

Spatial variation over the width with lateral constriction

This section presents the tests with a lateral constriction of 22% of the structure width M. This resembles the presence of a support wall in a flood gate complex as shown in Figure 9. During the 10 tests with a lateral constriction (5 with shorter overhang and 5 with longer overhang), 6 pressure sensors were placed at the top of the vertical wall along the remaining structure width (see Figure 4d). These tests had the goal of studying the spatial distribution of wave impact loadings affected by such three-dimensional structural features.

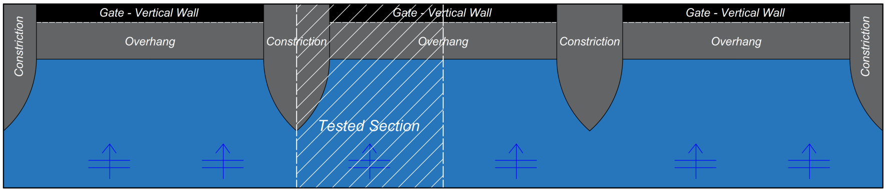

Figure 9: Top view of a schematic flood gate complex with constriction elements.

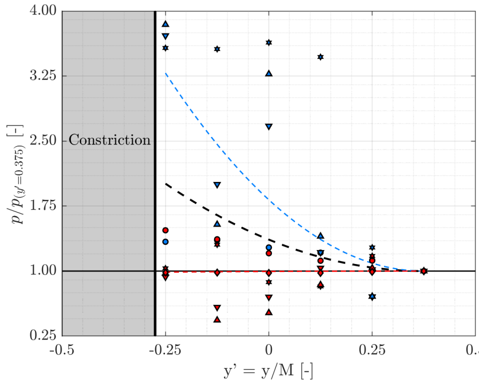

(a) Cross-flume pressure peaks

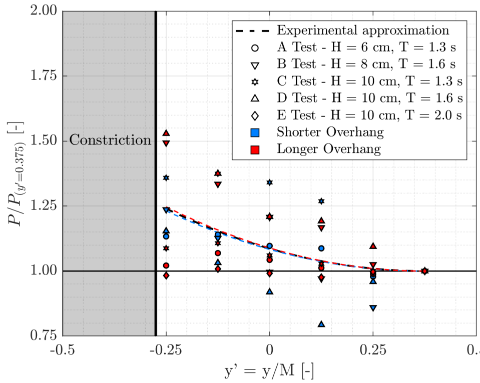

(b) Cross-flume pressure-impulses

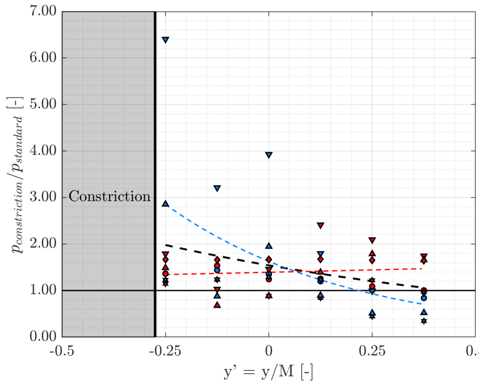

(c) Cross-flume pressure peaks

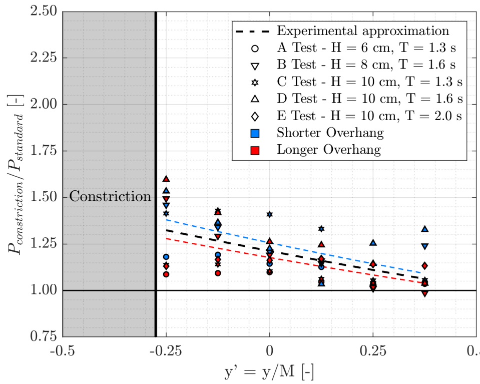

(d) Cross-flume pressure-impulses

Figure 10: Constriction effect on the spatial distribution of pressures peaks and pressure-impulses.

The results of the tests with a lateral constriction are summarized in Figure 10. The two figures on the left show peak pressures, the two figures on the right show pressure-impulses. Furthermore, the two figures on the top compare individual pressure sensor measurements to the ones at $y' = 0.375$, while the two figures on the bottom compare the results from the tests with a constriction to the tests without a constriction (i.e. the regular wave tests with a standard configuration). All four figures include a second order polynomial fit for the shorter overhang (blue line), for the longer overhang (red line) and for all tests combined (black line). The fit in Figure 10a shows that pressure peaks for the shorter overhang are significantly amplified at the constriction edge. On the contrary, the pressure peaks for the longer overhang remain uniform across the structure. The fit in Figure 10b shows a clear pattern of amplified pressure-impulses at the constriction edge for both the shorter and the longer overhang. Figure 10c shows that for the shorter overhang the presence of a constriction leads to a large amplification of the pressure peaks at the constriction edge. On the contrary, for the longer overhang, the presence of a constriction leads to a uniform amplification of the pressure peaks along the width of the structure. Figure 10d shows a clear pattern of amplified pressure-impulses at the constriction edge caused by the presence of a constriction for both the shorter and the longer overhang. In summary, the presence of a lateral constriction modifies significantly the spatial distribution of wave loads, amplifying the pressure peaks and pressure-impulses closer to the constriction edge. Besides, the pressure-impulse results show less variability and more predictability compared with the pressure peaks.

Load reducing ventilation gaps

This section describes the effect of ventilation gaps in the reduction of wave impact loads. Figure 11 describes the detailed geometry of the ventilation gaps tested in this study. For the shorter overhang, tests with $G = 1$ cm were carried out, while for the longer overhang, tests with $G = 1$ cm and $G = 2$ cm were carried out. In all tests tests $B = 1$ cm, $B' = 48$ cm and $G' = W - 1$ cm. These ventilation gap dimensions are constant along the whole structure width (i.e $M = 80$ cm). The 30 tests in this experimental set included, besides the three different ventilation gap variations, two different water levels and five different incident wave conditions. This study aims to assess the use of ventilation gaps to reduce wave impact loadings. Thus, the wave impact loads measured in the tests with ventilation gaps are compared to the identical tests (i.e. regular wave tests with standard configuration) carried out in the same test campaign.

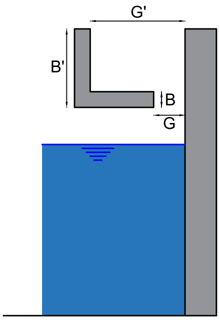

Figure 11: Ventilation gap configuration parameters: inner ventilation gap width G; outer ventilation gap width G'; inner vertical gap boundary B; outer vertical gap boundary B'.

Figure 12 presents all the results for the tests with ventilation gaps, describing the load reduction induced by the presence of a ventilation gap. Figure 12a shows force peaks, while Figure 12b shows force-impulses. In these figures, the test names that include a "58" refer to tests carried at $d = 0.58$ m, while the test names that include a "60" refer to tests carried at $d = 0.60$ m. Figure 12a shows that for the shorter overhang (blue markers), in all cases the presence of a ventilation gap reduced the force peaks. In contrast, for the tests with longer overhangs (red markers), the force peaks in some cases increased with the presence of a ventilation gap. This is explained by the fact that, in those cases, the tests without a ventilation gap lead to very long and low force curves related to the presence of large air entrapments. Thus, in those cases, the presence of a ventilation gap leads to shorter and higher force curves related to the removal of entrapped air. Figures 12b show that in all tests carried out for the shorter and the longer overhangs, the force-impulses were smaller in the tests with ventilation gaps. In summary, the results obtained in this study show that ventilation gaps are effective in reducing standing wave impact loads.

4.3 Irregular wave tests

Up to now, this study presented the analysis of regular waves but, in reality, hydraulic structures are loaded by irregular wave fields. Hence, this section describes the results from the irregular wave tests. The 52 irregular wave tests were carried out for four water levels, five incident wave conditions and two overhang lengths.

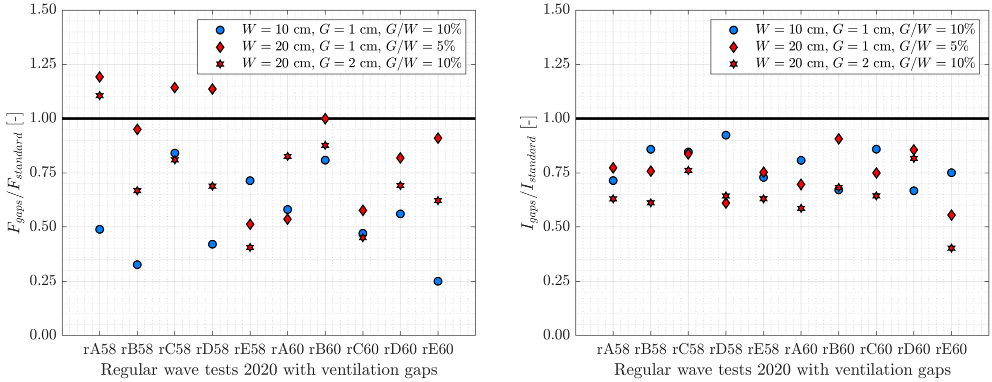

(a) Force peak reduction by test

(b) Force-impulse reduction by test

Figure 12: Effect of ventilation gaps in force peaks and force-impulses.

Furthermore, 50 tests were carried out with 1000 waves, while two extra long tests were carried out with 5000 waves. The spectral incident wave parameters (H_{m0}, T_p) and the incident and reflected wave time series were calculated by the method of Zelt and Skjelbreia (1992) with an array of three wave gauges (see Section 3.3). The time-domain incident wave parameters ($H_{1/3}$, T_m) were obtained from the incident wave time series employing a zero-downcrossing analysis. Further on in this study, the time-domain incident wave parameters are used, instead of the spectral incident wave parameters. For each incident wave propagating towards the structure identified in the zero-downcrossing analysis, the corresponding wave load acting on the structure was identified from the synchronized pressure measurements. For each of these wave loads acting on the structure, the pressure/force peaks and the pressure/force-impulses were obtained in an automatic way for each test.

Figure 13 and Figure 14 summarize the results from all the 52 irregular wave tests. Figure 13 presents the exceedance probability plots for the total force-impulse I (Figure 13a) and for the total force peak F (Figure 13b). Figure 14 illustrates the the relations between force-impulses (I), force peaks (F) and impact durations (t_d). In these figures, a clear difference is observed between force-impulses and force peaks but also between the tests with shorter overhangs and the tests with longer overhangs. The largest force peaks correspond to the smallest impact durations (see Figure 14a), as is also seen for breaking wave impacts (Cuomo et al., 2010). Differently, the largest force-impulses correspond to middle-low impact durations of 30-100 ms (see Figure 14b), in line with the results from Chen et al. (2019). Furthermore, Figures 14a and 14b show that the tests with the longer overhang lead to longer impact durations compared with the tests with shorter overhangs. As discussed in the previous sections, this can be explained by the fact that a longer overhang is directly related to larger air entrapments and thus directly related to longer impact durations (Ramkema, 1978; de Almeida and Hofland, 2020*b*). Furthermore, it is observed that force peaks for both shorter and longer overhangs present similar high values, while significantly higher force-impulses have been measured in the tests with longer overhangs compared with the tests with shorter overhangs. All these conclusions can also be observed in Figure 14c. This figure shows that for equal force peaks, larger force-impulses are measured in the tests with longer overhangs (corresponding to longer impact durations) compared with the tests with shorter overhangs. Also, the extra long tests (5000 waves) present very similar results compared with the standard tests with 1000 waves.

Figure 15 shows the wave impact time series corresponding to the largest force-impulse in each test for the experiments carried out with $R_c = 0$. This condition of zero freeboard corresponds to the largest wave impact velocities at the moment of the wave impact and consequently the largest wave impact loads. Figure 15 shows the diversity of impact magnitudes and characteristics among the different irregular wave test conditions. It can be seen that the irregular wave tests show a less distinct difference between the loading time series of shorter and longer overhangs, as was observed during the regular wave tests (Figures 5 and 6). For example, individual longer impact durations can be found in tests with shorter overhangs (Figure 15c) and individual shorter impact durations can be found in tests with longer overhangs (Figure 15j). Thus, this shows that the dynamic interactions of the incident waves with the structural configurations are even more dynamic and variable in tests with irregular wave conditions.

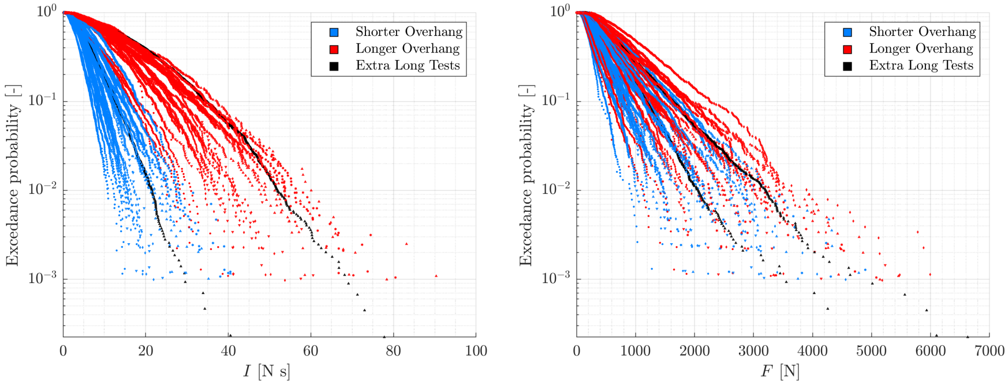

(a) Exceedance force-impulses I (b) Exceedance force peaks F

Figure 13: Exceedance probability per wave impact for force-impulses and force peaks.

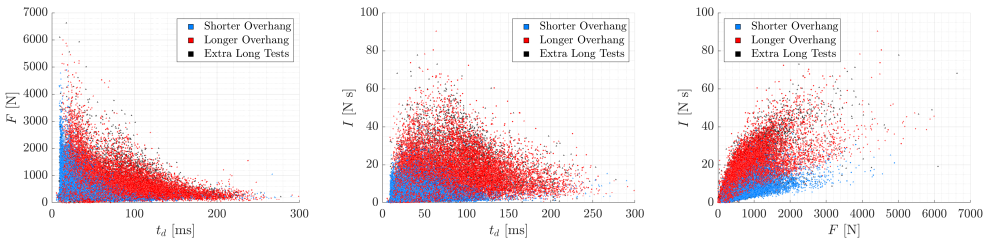

(a) F vs t_d (b) I vs t_d (c) I vs F

Figure 14: Impact duration in relation to force-impulse and force peaks.

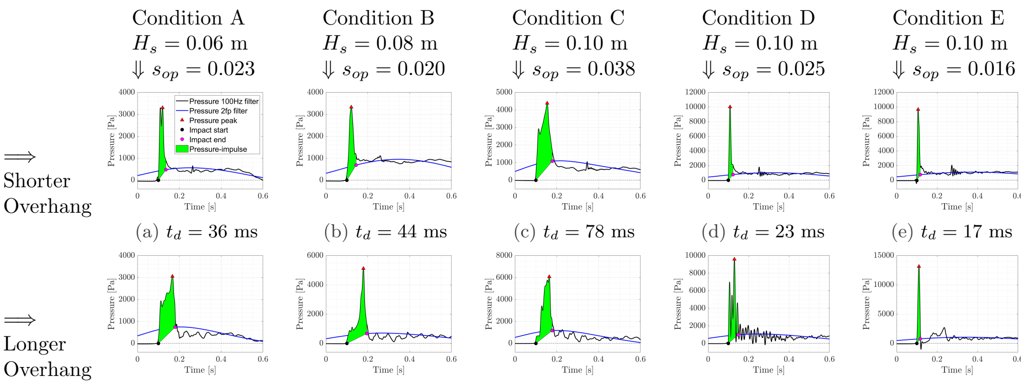

(a) $t_d = 36$ ms (b) $t_d = 44$ ms (c) $t_d = 78$ ms (d) $t_d = 23$ ms (e) $t_d = 17$ ms

(f) $t_d = 81$ ms (g) $t_d = 95$ ms (h) $t_d = 78$ ms (i) $t_d = 48$ ms (j) $t_d = 17$ ms

Figure 15: Wave impact with the maximum force-impulse I for each irregular wave test with $R_c = 0$ m.

To carry out load estimations, it is necessary to predict the effective bounce-back factor β based on wave and structure parameters. To that end, the Gamma Parameter ($\Gamma = U^2L/gW^2$) is introduced to describe the effective air entrapment characteristics. Figure 16 shows the relation between β and Γ for all irregular and regular wave tests. The Gamma Parameter Γ includes the effect of the wave impact velocity U (i.e. for a larger impact velocity the air has less time to flow away from below the overhang and can be more easily entrapped), and the relation between wave length L and overhang length W (i.e. for a larger relative wave length a more uniform wave surface can impact parallel to the whole overhang length creating a longer air entrapment). In the irregular waves tests, β was obtained from $I_{1\%}$. More precisely, $I_{1\%}$ is the force-impulse exceeded by 1% of the incident waves. Furthermore, $\bar{I}_{1\%}$ was calculated according to Equation 3, being $U_{1\%}$ the impact velocity determined according to Equation 8 with wave period T_m and wave height $H_{1\%}$ (obtained from Equation 9). This leads to β being calculated as $\beta = \bar{I}_{1\%}/C_I$. Also, for calculating Γ from the irregular wave tests $U_{1\%}$ and L_m were used. This figure shows an upper limit of β around 2, which does not grow further for larger values of Γ. This upper limit of β around 2 is also in agreement with the theoretical limit predicted by Wood et al. (2000), in which ($1 < \beta < 2$). Figure 16 also shows the range of data collected in this study, showing that regular wave tests had lower values of Γ compared to the irregular wave tests. For this reason, the experimental approximation shown in the figure ($R^2 = 0.83$, $RMSE = 0.12$) only includes the irregular wave tests, although the regular wave test results are also in agreement. An outlier value of $\beta = 0.63$ from the irregular wave tests can be seen and is not included in the approximation. It corresponds to the test with the longer overhang ($W = 0.2$ m), the smallest incident wave condition (Condition A) and the highest water level with a negative freeboard ($d = 0.63$ m, $R_c = -0.03$ m). In this condition the incident waves were not able to reach and impact the overhang at the vertical wall, leading to this low value of β. This is in line with the results from the regular wave tests, in which the smallest incident waves did not produce wave impacts for the tests with the highest water level with a negative freeboard ($d = 0.63$ m, $R_c = -0.03$ m), see Figures 5d and 6d. In summary, Figure 16 and Equation 10 can be used for calculating effective bounce-back factor β using the Gamma Parameter Γ for carrying out loading estimations, as it will be introduced hereafter.

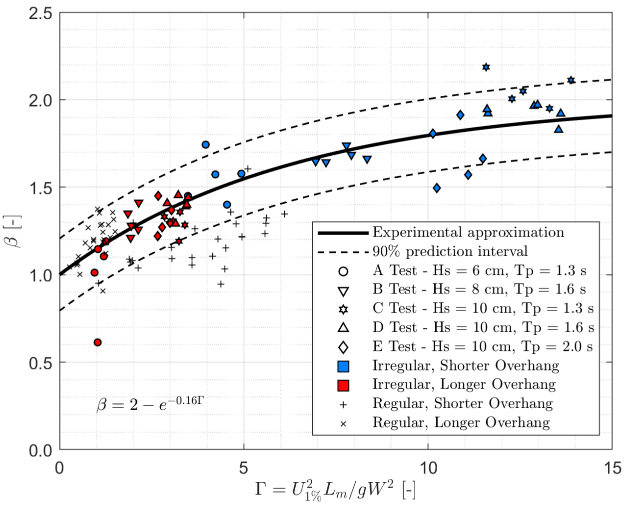

Figure 16: Summary of experimental laboratory results for the effective bounce-back factor

$$\beta = 2 - e^{-0.16\Gamma} \tag{10}$$

Figure 17 compares the measured force-impulses in irregular wave tests (markers), with the loading predictions (lines). The loading predictions in this figure were calculated using Figure 16 and Equation 10 for obtaining β, Equation 9 (for obtaining H), Equation 8 (for obtaining U), Equation 4 (for obtaining $\bar{I}$) and Equation 3 (for obtaining I). In Figure 17, the figures on the top row show the tests with the shorter overhang, while the figures in the bottom row show the tests with the longer overhang. Furthermore, the two figures on the left show the comparison for $R_c = 0.04$ m, while the two figures on the right show the comparison for $R_c = 0.00$ m. The results shown in Figure 17 illustrates that the loading prediction expressions presented in this study can be used for preliminary loading estimations for standing wave impacts on relatively short overhangs. The largest deviations between the measured and predicted loads are found for the most energetic wave conditions, and is considered to be closely related to the variations in the air entrapment dimensions. Following these results, the previously described loading prediction expressions are found to be sufficiently accurate for a variety of incident wave characteristics, standard and extra long tests, different overhang lengths and different water levels.

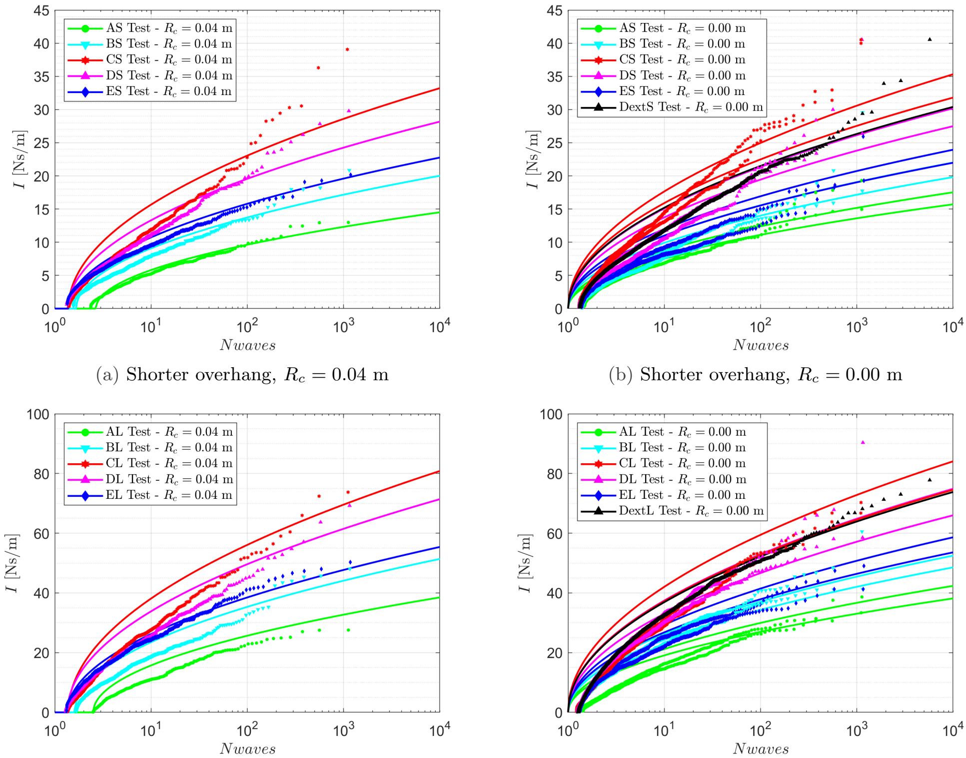

(a) Shorter overhang, $R_c = 0.04$ m

(b) Shorter overhang, $R_c = 0.00$ m

(c) Longer overhang, $R_c = 0.04$ m

(d) Longer overhang, $R_c = 0.00$ m

Figure 17: Predicted (lines) and measured (markers) force-impulse exceedance curves per incident wave.

5 Discussion

This section discusses the results from this study, including the regular wave tests with the standard configuration, the spatial distribution of wave impact loads over the structure width, the effect of load reducing ventilation gaps and the irregular wave tests.

From the regular wave tests with standard configuration, a large number of findings were presented in Section 4.1. Furthermore, extended validation of the pressure impulse theory was found (see Figure 7). Nevertheless, the relatively constant effective bounce-back factors β from the regular wave tests were not directly confirmed by the irregular wave tests. This is explained by the fact that the regular wave tests consisted of significantly less extreme wave impacts (i.e. lower Γ) compared with the irregular wave results (see Figure 16). Thus, two conclusions can be drawn regarding the regular wave test results. First, that the results of regular waves alone were not sufficient for describing loading prediction expressions for preliminary design. To this end, irregular wave tests were used, as addressed in Section 4.3. Second, besides the previously mentioned aspects, the extended validation this study presents based on regular and irregular waves offer sufficient confidence that the pressure-impulse theory can be used for describing the impulsive loading generated by standing wave impacts.

Two remarks may be added regarding the pressure measurements shown in Figures 5 and 6. First, vibrations on the pressure measurements are observed in many tests, mainly in the tests with longer overhangs (see Figures 6a, 6b, 6e, 6i and 6j), but also in the tests with shorter overhangs (see Figures 5c and 5g). These vibrations took place mainly during the wave impacts but also after the wave impacts. All pressure vibrations recorded during the wave impacts showed a different vibration frequency. This indicates that these vibrations are related to the dimensions of the entrapped air, which varies between the different tests and to a smaller extend between every single wave impact. The post-impact vibrations also showed the same pattern, of unique vibrations frequencies in each test, besides one exception for the longest wave impacts found in the tests with the longer overhang. For the longest wave impacts with the longer overhang, with impact durations larger than 100 ms (see Figures 6c, 6f and 6g), a vibration pattern of 22 Hz is visible after the wave impacts. This vibration pattern originates in the flume bottom, which responds in a dynamic way to the longest impact durations. This illustrates the importance of considering the dynamic response of all elements of the test setup in wave impact laboratory experiments. Second, in the tests with $R_c \leq 0$ m, (e.g. Figures 5c and 6c) the pressure recording is below zero before the wave impact, while in the tests with $R_c > 0$ m, (e.g. Figures 5a, and 6a) the pressure recording is approximately at zero before the wave impact. In the tests with $R_c > 0$ m, the pressure sensor is in contact with the air at the start of the test, the same condition as before the wave impact. On the contrary, in the tests with $R_c \leq 0$ m the pressure sensor is in contact with water at the start of the test, while before the wave impact the pressure sensor is in contact with air. This deviation from zero in the tests with $R_c \leq 0$ includes the hydrostatic pressure difference for the pressure sensor measurements at $z = 0.59$ m shown in Figures 5 and 6. The temperature effect of the pressure sensors is found to be reduced in the case of the Kulite HKM-375M-SG and do not influence any conclusion from this study. Nevertheless, the performance of the instrumentation used in wave impact studies (e.g. the temperature effect of pressure sensors), should always be examined.

In the tests with a lateral constriction, a particular load pattern was found for test rES (test condition rE with the shorter overhang) caused by a cross-flume wave resonance pattern. This can be observed in Figure 18 (where all 10 constriction test results are included) in comparison with Figure 10 (where only 9 constriction test results are included, excluding the mentioned rES condition). Note that the y-axis scales differ between the two figures (i.e. Figure 10 and Figure 18). This cross-flume wave resonance pattern was not only observed in the analysis of the test results but also clearly visible during the laboratory tests. This wave resonance pattern is not expected to take place in an irregular wave field because the frequency of the irregular incident waves is not constant. Thus, this test condition was not considered in the analysis of the spatial distribution over the width presented earlier in this study in Section 4.2.

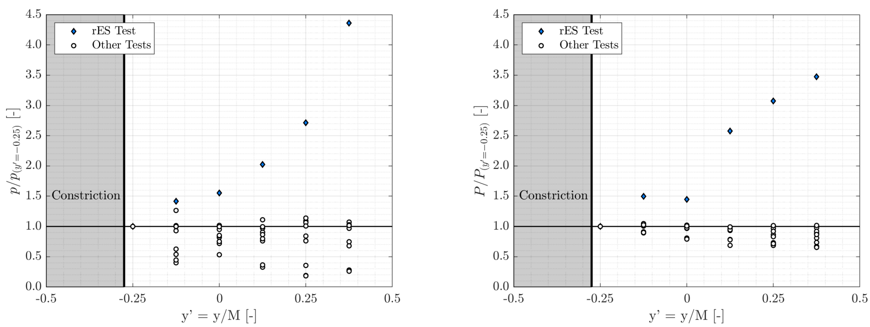

(a) Cross-flume pressure peaks

(b) Cross-flume pressure-impulses

Figure 18: Constriction effect on the spatial distribution of pressures peaks and pressure-impulses.

In the experiments with load reducing ventilation gaps, two ventilation gap widths were tested (i.e. $G = 1$ cm and $G = 2$ cm, see Section 4.2 and Figure 11). In addition, the other ventilation gap dimensions were constant in all tests (i.e. $B = 1$ cm, $B' = 48$ cm and $G' = W - 1$ cm). Thus, these geometric characteristics should be taken into account when assessing the effect of load reducing ventilation gaps. Other configurations, such as the ones presented in Figure 19 (i.e. with equal G but with variations in G', B or B') may lead to different results regarding the effect of ventilation gaps for reducing standing wave impact loads. In summary, for assessing the effect of loading ventilation gaps, the precise configuration of such gaps should be described with sufficient precision (i.e. not only the inner ventilation gap width G) in order to have a higher degree of confidence in the corresponding load reduction.

In the irregular wave tests, the effective bounce-back factor β was calculated from $I_{1\%}$. This exceedance level was used for describing the effective bounce-back factor β for extreme wave impacts given its expected reduced statistical variation, and it allowed the derivation of preliminary load prediction expressions. In addition, this

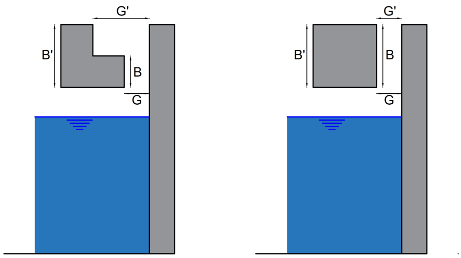

(a) (b)

Figure 19: Alternative ventilation gaps configurations.

study carried out 50 tests of 1000 waves, and two tests of 5000 waves. Nevertheless, for a more complete definition of the extreme distribution of wave impact loads, additional longer tests may be considered. This would provide a better description of the wave impact magnitudes with a very small exceedance probability. Also, this study includes laboratory experiments with a reduced scale, from which the loading prediction expressions are calibrated (i.e. β). Thus, the study on the scaling of such loading prediction expressions to prototype structures should be considered. This should include in particular the effect and scaling of entrapped air, following the work from Mitsuyasu (1966) and Ramkema (1978). Furthermore, in the load prediction expressions described in Section 4.3 the mean wave period T_m is used. Figure 20 discusses this assumption based on experimental results. Figure 20a presents the results for the tests with shorter overhangs, while Figure 20b presents the results for the tests with longer overhangs. These two figures show that for the largest wave impact velocities in each test, a relation of T/T_m close to 1 is observed. Further, the distribution of wave periods T and its relation with T_m were in agreement with Goda (2010). Based on these observations, it is concluded that the use of the mean wave period T_m for preliminary load predictions is sufficiently accurate at this stage.

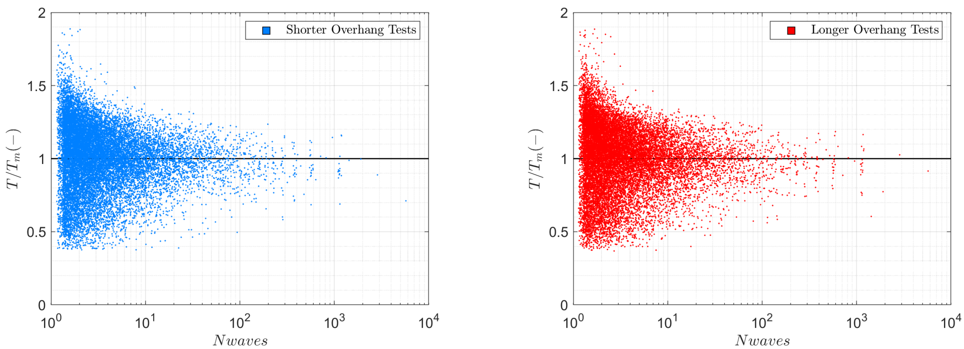

(a) Shorter Overhang (b) Longer Overhang

Figure 20: Return period of U vs T/T_m.

6 Conclusions

This section summarizes the main conclusions on wave loading on vertical structures in consequence of standing wave impacts on an adjacent relatively short overhang, with an emphasis on describing this loading using the pressure-impulse theory. This paper addressed two complementary objectives. Firstly, it extends the knowledge on standing wave impacts addressing the following aspects: changes in hydraulic loading conditions (regular/irregular waves and varying freeboards) and changes in the structure geometry (lateral constriction and loading reducing ventilation gaps). Secondly, it presents loading prediction expressions for preliminary loading estimations built up by the previously developed pressure-impulse theory that is empirically calibrated using the presently acquired experimental data.

The standard regular wave tests describe the influence of the overhang length, incident conditions and water levels on the wave impact loading characteristics and magnitudes, including the spatial distribution. First, the tests with the shorter overhangs presented shorter, higher and less variable wave impact loading signals compared to the tests with longer overhangs. Second, the different incident wave conditions lead to different loading characteristics and magnitudes. Identical loading behaviour was found for repeated tests with equal incident wave conditions. Third, the change in water levels affected the wave impact loading magnitudes as predicted, with higher loads measured in tests with smaller freeboards. On tests with the water level higher than the overhang level (i.e. negative freeboard), a significantly more variable behaviour was observed. Also, during the tests with the shorter overhang, lower water levels were strongly related to shorter impact durations. In the tests with the longer overhang, lower water levels were only partially related to shorter impact durations. Fourth, it was found that the pressure peaks measured at one location does not take place instantly along the whole structure width. Thus, pressure peaks at one single location were found to be higher than the pressure peaks of the averaged pressure signal. On the contrary, the pressure-impulse at one single location was found to be very similar to the pressure-impulses of the averaged pressure signal.

The constriction tests showed the effect of such a lateral constriction on the spatial distribution of the wave impact loading. The presence of a lateral constriction modifies significantly the spatial distribution of wave loads, amplifying the pressure peaks and pressure-impulses closer to the constriction edge. The ventilation gap tests showed the effect of such ventilation gaps on the reduction of wave impact loadings. First, force peaks were lower in most of the tests with the presence of a ventilation gap, in comparison to tests without ventilation gaps. An increase in force peaks was only found in some tests with longer overhangs, explained by the fact that without a ventilation gap these tests showed long and lower force curves related to the presence of larger air entrapments. Thus, in those cases, the presence of a ventilation gap leads to shorter and higher force curves related to the removal of entrapped air. Second, force-impulses were always lower for all test conditions with the presence of a ventilation gap, in comparison to tests without ventilation gaps. This data highlights thus the effect of ventilation gaps on reducing wave impact loadings.

The irregular wave tests contributed to extending previous conclusions towards design applications. This study includes both standard and extra long irregular wave tests, from which a few remarks should be made. First, and differently from regular wave tests, irregular wave tests showed a large range of different loading curves in all overhang lengths and water levels. This highlighted that the dynamic interactions of the incident waves with the structural configurations are even more dynamic and variable in irregular wave conditions. Second, the largest force peaks corresponded to the smallest impact durations, while the largest force-impulses corresponded to middle-low impact durations of 30-100 ms. Third, the irregular wave tests allowed to describe loading prediction expressions for preliminary loading estimations. To that end, the Gamma Parameter ($\Gamma = U^2L/gW^2$) is introduced to describe the effective air entrapment characteristics. Furthermore, the relation between the effective bounce-back factor ($1 < \beta < 2$) with the Gamma Parameter Γ was presented ($\beta = 2 - e^{-0.16\Gamma}$). These expressions presented in this study were shown to be suitable for carrying out load estimations for standing wave impacts on vertical hydraulic structures with relatively short overhangs.

This study constitutes a step forward in the study of confined wave impacts. In particular, the load prediction expressions based on the Gamma Parameter Γ overcomes a significant knowledge gap and provide a validated design tool for this type of wave impact. Nevertheless, this study also presents two main limitations to its applicability in design. Firstly, this study includes schematic representations of a vertical hydraulic structure with relatively short overhangs in a flat bottom subjected only to normally incident waves. Thus, for its use in design, the conclusions of this study should be combined with the detailed analysis of the structure geometry, the incident wave characteristics and the local bathymetry particularities. Secondly, this study is based on laboratory experiments with a reduced scale. Thus, for its use in design, the scaling of loads and wave impact processes (e.g. air entrapment and impact duration) should be considered. Additional research on standing wave impacts on vertical hydraulic structures with overhangs may continue in the future and may include experimental, analytical and numerical methods. This would allow to further reduce the uncertainties and increase the reliability in the design of vertical hydraulic structures with overhangs. This is particularly relevant for thin steel structures such as flood gates which are especially susceptible to a dynamic behaviour under such impulsive wave impact loads.

4

Notations

Name	Symbol	Unit
Total wave amplitude at wall	A_w	m
Inner vertical gap boundary	B	m
Outer vertical gap boundary	B'	m
Theoretical dimensionless force-impulse	C_I	-
Wave reflection coefficient	c_r	-
Still water depth	d	m
Force	F	N
Gravitational acceleration	g	m/s^2
Inner ventilation gap width	G	m
Outer ventilation gap width	G'	m
Overhang height	h	m
Dimensionless overhang height	$\bar{h}$	-
Wave height	H	m
Time domain significant wave height	$H_{1/3}$	m
Frequency domain significant wave height	H_{m0}	m
Significant wave height	H_s	m
Force-impulse	I	N s
Dimensionless force-impulse	$\bar{I}$	-
Wave length	L	m
Wave length based on T_m	L_m	m
Wave length based on T_p	L_p	m
Deep water wave length	L_0	m
Structure width	M	m
Pressure	p	Pa
Pressure-impulse	P	Pa s
Dimensionless pressure-impulse	$\bar{P}$	-
Exceedance probability	pr	-
R-Square coefficient of determination	R^2	-
Freeboard	R_c	m
Root mean squared error	$RMSE$	-
Wave steepness	s	-
Deep water wave steepness	s_0	-
Wave period	T	s
Mean wave period	T_m	s
Peak wave period	T_p	s
Wave impact duration	t_d	s
Impact velocity	U	m/s
Overhang length	W	m
Dimensionless overhang length	$\bar{W}$	-
Effective bounce-back effect	β	-
Gamma Parameter	Γ	-
Wave surface position	η	m
Wave surface velocity	$\dot{\eta}$	m/s
Peregrine Number	Λ	-
Angular wave frequency	ω	rad/s
Fluid density	ρ	kg/m^3

Acknowledgements

This study is part of the DynaHicS (Dynamics of Hydraulic Structures) Project, supported by NWO (Nederlandse Organisatie voor Wetenschappelijk Onderzoek) grant ALWTW.2016.041. The authors would like to thank Sander de Vree for his support during the experiments carried out at Delft University of Technology.

4

Author contributions (CRediT)

EdA: conceptualization, methodology, design and execution of laboratory experiments, validation, investigation, software, writing-review and editing, formal analysis, data curation, writing-original draft preparation and visualization. BH: conceptualization, methodology, validation, investigation, software, writing-review and editing, resources, supervision, project administration and funding acquisition.

References

Bagnold, R.A. (1939). Wave-pressure research. *The institution of Civil Engineers*, **12**, 202 – 226.

Bogaert, H. (2018). *An experimental investigation of sloshing impact physics in membrane LNG tanks on foating structures*. Ph.D. thesis, Delft University of Technology,.

Castellino, M., Romano, A., Lara, J.L., Losada, I.J. and De Girolamo, P. (2021). Confined-crest impact: Forces dimensional analysis and extension of the goda's formulae to recurved parapets. *Coastal Engin.*, **163**, 103814.

Castellino, M., Sammarco, P., Romano, A., Martinelli, L., Ruol, P., Franco, L. and Girolamo, P.D. (2018). Large impulsive forces on recurved parapets under non-breaking waves. a numerical study. *Coastal Engin.*, **136**, 1 – 15.

Chen, X., Hofland, B., Altomare, C., Suzuki, T. and Uijttewaal, W. (2015). Forces on a vertical wall on a dike crest due to overtopping flow. *Coastal Engin.*, **95**, 94 – 104.

Chen, X., Hofland, B., Molenaar, W., Capel, A. and van Gent, M. (2019). Use of impulses to determine the reaction force of a hydraulic structure with an overhang due to wave impact. *Coastal Engin.*, **147**, 75 – 88.

Chen, X., Hofland, B. and Uijttewaal, W. (2016). Maximum overtopping forces on a dike-mounted wall with a shallow foreshore. *Coastal Engin.*, **116**, 89 – 102.

Cooker, M.J. and Peregrine, D.H. (1990). A model for breaking wave impact pressures. In: *Proc. Coastal Engin. Conference 1990*. Delft, The Netherlands.

Cooker, M.J. and Peregrine, D.H. (1995). Pressure-impulse theory for liquid impact problems. *Journal of Fluid Mechanics*, **297**, 193 – 214.

Cuomo, G., Allsop, W., Bruce, T. and Pearson, J. (2010). Breaking wave loads at vertical seawalls and breakwaters. *Coastal Engin.*, **57**(4), 424 – 439.

Cuomo, G., Tirindelli, M. and Allsop, W. (2007). Wave-in-deck loads on exposed jetties. *Coastal Engin.*, **54**(9), 657 – 679.

de Almeida, E. and Hofland, B. (2020*a*). Validation of pressure-impulse theory for standing wave impact loading on vertical hydraulic structures with short overhangs. *Coastal Engin.*, **159**, 103702.

de Almeida, E. and Hofland, B. (2020*b*). Experimental observations on impact velocity and entrapped air for standing wave impacts on vertical hydraulic structures with overhangs. *J. Mar. Sci. Eng.*, **8**(11), 857.

Dermentzoglou, D., Castellino, M., De Girolamo, P., Partovi, M., Schreppers, G.J. and Antonini, A. (2021). Crownwall failure analysis through finite element method. *Journal of Marine Science and Engineering*, **9**(1).

Dias, F. and Ghidaglia, J.M. (2018). Slamming: Recent progress in the evaluation of impact pressures. *Annual Review of Fluid Mechanics*, **50**(1), 243–273.

Goda, Y. (1974). A new method of wave pressure calculation for the design of composite breakwater. In: *Proc. Coastal Engin. Conference 1974*. Copenhagen, Denmark.

Goda, Y. (2010). *Random seas and design of maritime structures*. World Scientific, Singapore, 3rd edition.

Hayatdavoodi, M., Seiffert, B. and Ertekin, R.C. (2014). Experiments and computations of solitary-wave forces on a coastal-bridge deck. part ii: Deck with girders. *Coastal Engin.*, **88**, 210 – 228.

Hedges, T. (1995). Regions of validity of analytical wave theories. In: *Proc. ICE Water Maritime and Energy 1995*. London, United Kingdom.

Hofland, B. (2015). Modeltesten golfkrachten spuisluizen afsluitdijk. Meetrapport 1220263, Deltares, Delft, The Netherlands.

Kisacik, D., Troch, P., Bogaert, P.V. and Caspeele, R. (2014). Investigation of uplift impact forces on a vertical wall with an overhanging horizontal cantilever slab. *Coastal Engin.*, **90**, 12 – 22.

Longuet-Higgins, M. (1952). On the statistical distribution of the heights of sea waves. *Journal of Marine Research*, **11**(3), 245 – 266.

Martinelli, L., Ruol, P., Volpato, M., Favaretto, C., Castellino, M., Girolamo, P.D., Franco, L., Romano, A. and Sammarco, P. (2018). Experimental investigation on non-breaking wave forces and overtopping at the recurved parapets of vertical breakwaters. *Coastal Engin.*, **141**, 52 – 67.

McConnell, K., Allsop, W. and Cruickshank, I. (2004). *Piers, jetties and related structures exposed to waves: Guidelines for hydraulic loadings*. Thomas Telford Publishing, London, United Kingdom.

Minikin, R.R. (1950). *Winds, waves and maritime structures*. Griffin, London, United Kingdom.

Mitsuyasu, H. (1966). Shock pressure of breaking wave. In: *Proc. Coastal Engin. Conference 1996*. Orlando, United States.

Oumeraci, H., Kortenhaus, A., Allsop, W., de Groot, M., Crouch, R., Vrijling, H. and Voortman, H. (2001). *Proverbs: Probabilistic design tools for vertical breakwaters*. Balkema, Lisse.

Ramkema, C. (1978). A model law for wave impacts on coastal structures. In: *Proc. Coastal Engin. Conference 1978*. Hamburg, Germany.

Renzi, E., Wei, Y. and Dias, F. (2018). The pressure impulse of wave slamming on an oscillating wave energy converter. *Journal of Fluids and Structures*, **82**, 258 – 271.

Seiffert, B., Hayatdavoodi, M. and Ertekin, R.C. (2014). Experiments and computations of solitary-wave forces on a coastal-bridge deck. part i: Flat plate. *Coastal Engin.*, **88**, 194 – 209.

Sonneville, B., Hofland, B., Mowinckel, A. and Paulsen, B. (2015). Wave impact loads on offshore gravity based structure. In: *Proc. OMAE Conference 2015*. St. John's, Canada.

Takahashi, S., Tanimoto, K. and Shimosako, K. (1994). A proposal of impulsive pressure coefficient for design of composite breakwaters. In: *Proc. International Conference of Hydro-Technical Engineering for Port and Harbour Construction 1994*. Yokosuka, Japan.

Tieleman, O., Hofland, B., Tsouvalas, A., de Almeida, E. and Jonkman, S. (2021). A fluid–structure interaction model for assessing the safety of flood gate vibrations due to wave impacts. *Coastal Engineering*, **170**, 104007.

Tieleman, O.C., Tsouvalas, A., Hofland, B. and Jonkman, S.N. (2019). A three dimensional semi-analytical model for the prediction of gate vibrations. *Marine Structures*, **65**, 134 – 153.

WL (1977). Wave impacts on the gate in the eastern scheldt caisson (in dutch: Golfklappen op de schuif in de oosterschelde-caisson). Verslag M 1335 deel I, WL Delft Hydraulics (presently Deltares), Delft, The Netherlands.

WL (1978). Wave impacts against concrete perforated gates (in dutch: Golfklappen tegen betonnen rooster-schuiven). Verslag M 1381 deel II, WL Delft Hydraulics (presently Deltares), Delft, The Netherlands.

WL (1979). Wave impacts: A literature review and scale effects in model studies (in dutch: Golfklappen: een literaturroverzicht en schaaleffekten in modelonderzoek). Verslag M 1335 deel III, WL Delft Hydraulics (presently Deltares), Delft, The Netherlands.

Wood, D.J. and Peregrine, D.H. (1996). Wave impact beneath a horizontal surface. In: *Proc. Coastal Engin. Conference 1996*. Orland, United States.

Wood, D.J., Peregrine, D.H. and Bruce, T. (2000). Study of wave impact against a wall with pressure-impulse theory. i: trapped air. *Journal of Waterway, Port, Coastal and Ocean Engineering*, **126**(4), 182 – 190.

Zelt, J. and Skjelbreia, J. (1992). Estimating incident and reflected wave fields using an arbitrary number of wave gauges. In: *Proc. Coastal Engin. Conference 1992*. Venice, Italy.

A Appendix - Tables

Table A1: Summary of the configurations tested for each hydrodynamic condition. Incident wave characteristics shown in this table are the target wave conditions. "x1", "x2", and "x3" repesent the number of repetitions for the $W = 0.1$ m (S) and $W = 0.2$ m (L) overhangs.

Regular Wave Tests - Standard (50 waves/test) and Gaps/Constriction (25 waves/test)						
d [m]	R_c [m]	Condition rA H 0.06 m, T 1.3 s, L_0 2.64 m, s_0 0.023	Condition rB H 0.08 m, T 1.6 s, L_0 3.99 m, s_0 0.020	Condition rC H 0.10 m, T 1.3 s, L_0 2.64 m, s_0 0.038	Condition rD H 0.10 m, T 1.6 s, L_0 3.99 m, s_0 0.025	Condition rE H 0.10 m, T 2.0 s, L_0 6.24 m, s_0 0.016
0.56	0.04	Standard: S (x1) + L (x1)	Standard: S (x1) + L (x1)	Standard: S (x1) + L (x1)	Standard: S (x1) + L (x1)	Standard: S (x1) + L (x1)
0.58	0.02	Standard: S (x1) + L (x1) Gaps: S (x1) + L (x2)	Standard: S (x1) + L (x1) Gaps: S (x1) + L (x2)	Standard: S (x1) + L (x1) Gaps: S (x1) + L (x2)	Standard: S (x1) + L (x1) Gaps: S (x1) + L (x2)	Standard: S (x1) + L (x1) Gaps: S (x1) + L (x2)
0.60	0.00	Standard: S (x3) + L (x3) Gaps: S (x1) + L (x2) Constriction: S (x1) + L (x1)	Standard: S (x2) + L (x2) Gaps: S (x1) + L (x2) Constriction: S (x1) + L (x1)	Standard: S (x2) + L (x2) Gaps: S (x1) + L (x2) Constriction: S (x1) + L (x1)	Standard: S (x2) + L (x2) Gaps: S (x1) + L (x2) Constriction: S (x1) + L (x1)	Standard: S (x3) + L (x3) Gaps: S (x1) + L (x2) Constriction: S (x1) + L (x1)
0.63	-0.03	Standard: S (x1) + L (x1)	Standard: S (x1) + L (x1)	Standard: S (x1) + L (x1)	Standard: S (x1) + L (x1)	Standard: S (x1) + L (x1)

Irregular Wave Tests - Standard (1000 waves/test) and Extra Long (5000 waves/test)						
d [m]	R_c [m]	Condition A H_s 0.06 m, T_p 1.3 s, L_{0p} 2.64 m, s_{0p} 0.023	Condition B H_s 0.08 m, T_p 1.6 s, L_{0p} 3.99 m, s_{0p} 0.020	Condition C H_s 0.10 m, T_p 1.3 s, L_{0p} 2.64 m, s_{0p} 0.038	Condition D H_s 0.10 m, T_p 1.6 s, L_{0p} 3.99 m, s_{0p} 0.025	Condition E H_s 0.10 m, T_p 2.0 s, L_{0p} 6.24 m, s_{0p} 0.016
0.56	0.04	Standard: S (x1) + L (x1)	Standard: S (x1) + L (x1)	Standard: S (x1) + L (x1)	Standard: S (x1) + L (x1)	Standard: S (x1) + L (x1)
0.58	0.02	Standard: S (x1) + L (x1)	Standard: S (x1) + L (x1)	Standard: S (x1) + L (x1)	Standard: S (x1) + L (x1)	Standard: S (x1) + L (x1)
0.60	0.00	Standard: S (x2) + L (x2)	Standard: S (x2) + L (x2)	Standard: S (x2) + L (x2)	Standard: S (x2) + L (x2) Extra Long: S (x1) + L (x1)	Standard: S (x2) + L (x2)
0.63	-0.03	Standard: S (x1) + L (x1)	Standard: S (x1) + L (x1)	Standard: S (x1) + L (x1)	Standard: S (x1) + L (x1)	Standard: S (x1) + L (x1)

Table A2: Measured impact characteristics for all 54 regular wave tests with standard configuration.

Shorter Overhang - $W = 0.1$m																					
d [m]	R_c [m]	rAS				rBS				rCS				rDS				rES			
		I [Ns]	β [m]	t_d [ms]	Λ [-]	I [Ns]	β [m]	t_d [ms]	Λ [-]	I [Ns]	β [m]	t_d [ms]	Λ [-]	I [Ns]	β [m]	t_d [ms]	Λ [-]	I [Ns]	β [m]	t_d [ms]	Λ [-]
0.56	0.04	3.22	0.95	12	0.02	5.20	1.29	28	0.07	9.64	1.36	26	0.12	5.69	1.06	11	0.04	5.97	1.26	16	0.05
0.58	0.02	4.87	1.07	42	0.12	5.70	1.16	15	0.04	10.29	1.32	17	0.08	7.98	1.29	17	0.07	6.12	1.20	22	0.07
0.60	0.00	4.95 4.89 4.97	1.04 1.09 1.08	37 38 40	0.11 0.11 0.11	5.84 5.36	1.10 1.09	52 59	0.17 0.18	10.88 10.00	1.35 1.29	36 33	0.18 0.16	8.19 7.62	1.23 1.22	42 46	0.17 0.18	5.33 5.50 6.16	1.03 1.11 1.15	10 16 14	0.03 0.05 0.05
0.63	-0.03	0.00	-	-	-	6.25	1.31	89	0.26	11.78	1.60	67	0.30	7.54	1.21	56	0.22	4.77	0.94	90	0.28

Longer Overhang - $W = 0.2$m																					
d [m]	R_c [m]	rAL				rBL				rCL				rDL				rEL			
		I [Ns]	β [m]	t_d [ms]	Λ [-]	I [Ns]	β [m]	t_d [ms]	Λ [-]	I [Ns]	β [m]	t_d [ms]	Λ [-]	I [Ns]	β [m]	t_d [ms]	Λ [-]	I [Ns]	β [m]	t_d [ms]	Λ [-]
0.56	0.04	11.43	1.04	38	0.04	13.47	1.00	118	0.15	27.70	1.20	79	0.18	21.07	1.20	133	0.22	22.00	1.37	34	0.05
0.58	0.02	15.32	1.07	79	0.11	19.02	1.15	41	0.07	33.43	1.32	116	0.28	25.73	1.21	42	0.09	20.19	1.19	41	0.07
0.60	0.00	16.51 15.19 15.79	1.10 1.06 1.06	110 114 116	0.16 0.16 0.17	20.72 20.11	1.19 1.27	69 91	0.11 0.14	34.03 30.82	1.36 1.28	101 98	0.24 0.23	27.55 23.94	1.25 1.18	57 68	0.12 0.13	21.55 21.90 20.20	1.29 1.35 1.12	37 40 54	0.06 0.06 0.09
0.63	-0.03	0.00	-	-	-	17.58	1.18	158	0.23	20.56	0.91	37	0.08	23.98	1.24	90	0.17	20.87	1.28	95	0.15

5

DESIGN APPROACH FOR CONFINED WAVE IMPACT LOADS

This chapter describes tools, methods and techniques to be used in the design of hydraulic structures subject to confined wave impacts. Firstly, it presents the contributions to the design of such structures, as developed in the previous chapters. In particular, it summarizes the load prediction model to estimate the impulses from a confined wave impact, based on the pressure-impulse theory and validated with extensive laboratory experimental data. A design application example is presented to illustrate the use of this load prediction model for a realistic coastal hydraulic structure configuration. This chapter also includes design approaches to be considered for varying geometries such as ventilating gaps, lateral constrictions and very long overhangs. To this end, the use of physical modelling and numerical models is discussed. Secondly, this chapter evaluates the effect of the entrapped air on both laboratory and real prototype scales. Thus, this chapter addresses the suitability of the validated load prediction model for estimating real prototype scale confined wave impact loads. These load estimations can be used for preliminary design and can be complemented by numerical simulations. Finally, these estimated confined wave impact loads can be used as input for structural response and reliability models.

5.1. INTRODUCTION

This chapter synthesises the knowledge developed in the previous chapters and other literature sources on confined wave impacts on vertical hydraulic structures with overhangs. It presents the steps and equations that designers can use to estimate confined wave impact loads and also methods to optimize their designs. Section 5.2 presents the currently available expressions and considerations for the design of vertical hydraulic structures subjected to confined wave impacts. Section 5.3 addresses the effect of entrapped air in wave impact loads, the scaling between model and prototype loads and the impact durations of wave impacts in model and prototype scales. Section 5.4 presents a design application example on how to estimate confined wave impact loads and recommendations on how to reduce confined wave impact loads. Section 5.5 discusses the main aspects and conclusions from this chapter. As such, the content of this chapter is intended to be used by designers in engineering practice.

5.2. EXISTING DESIGN INSTRUMENTS

This section summarizes the different design tools and expressions to be used in the design of vertical hydraulic structures subjected to confined wave impacts, mainly based on Chapters 2, 3 and 4. The application of these tools and expressions for design is described in more detail in Section 5.4, including the proposed design procedure and a practical application example. As a reference, Figure 5.1 describes the main parameters and dimensions considered in confined wave impact configurations.

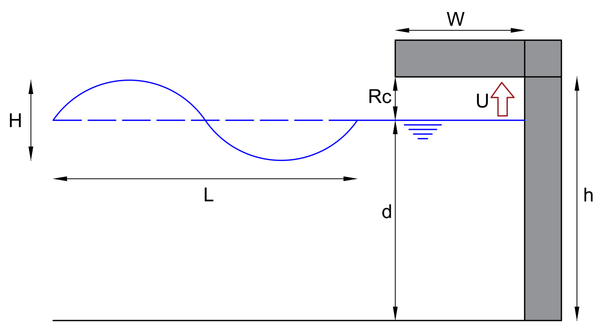

Figure 5.1: Parameters and dimensions: incident wave height H [m]; incident wave length L [m]; still water depth d [m]; overhang height h [m], overhang width W [m]; freeboard R_c [m]; impact velocity U [m/s].

5.2.1. ANALYTICAL AND EMPIRICAL EXPRESSIONS

This section presents the experimentally validated analytical and empirical expressions to be used for predicting wave impact pressure- and force-impulses. Figure 5.2 summarizes the prediction method developed in this research. The prediction of pressure- and force-impulses are described in this section. Based on the predicted pressure- and force-impulses, the derivation of pressure and force peaks are addressed in Section 5.3.4.

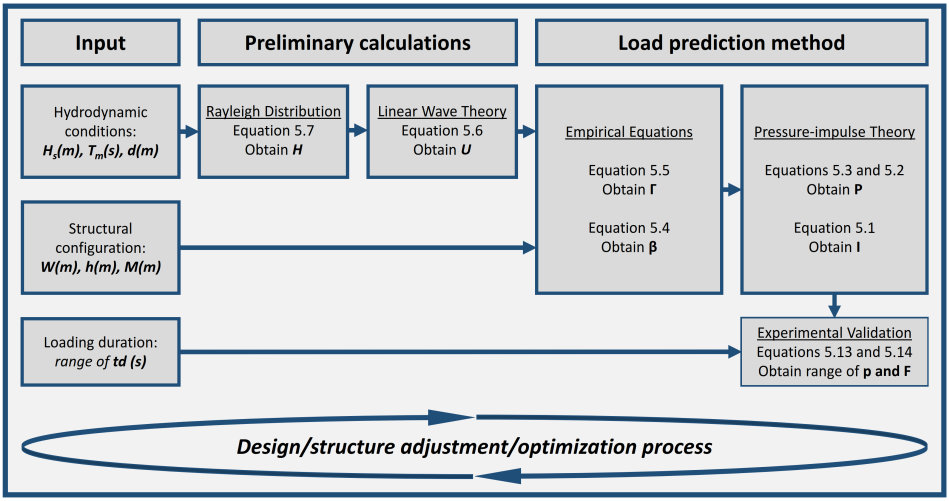

Figure 5.2: Load prediction method

5

IMPULSE ESTIMATION

The pressure-impulse theory was validated in Chapter 2 for describing confined wave impact loads acting on vertical hydraulic structures with overhangs. In addition, Chapter 4 presented load prediction expressions based on this theory and extensive laboratory experiments. Hereafter the most important expressions for carrying out preliminary design load estimations are summarized. For the detailed theoretical descriptions of the model and full validation process, see Chapter 2 and Chapter 4. The total force-impulse (I) acting on a vertical wall (overhang height h, see Figure 5.1) caused by a confined wave impact can be estimated according to Equation 5.1 per meter of width for various dimensionless overhang heights ($\bar{h} = h/W$). Similarly, the Equations 5.2 and 5.3 present the expressions for obtaining the maximum (i.e. P_{max}, at the top of the wall) and minimum (i.e. P_{min}, at the bottom of the wall) pressure-impulse P. The description of the pressure-impulse profile over the vertical wall is presented in Chapter 2.

$$I = C_I \beta \rho U W^2 \quad \text{being} \quad C_I = 2\bar{h}^{0.18} - 1.14 \quad \text{for} \quad 1 \leq \bar{h} \leq 10 \tag{5.1}$$

$$P_{max} = C_{P,max} \beta \rho U W \quad \text{being} \quad C_{P,max} = 0.18\bar{h}^{-1.9} + 1 \quad \text{for} \quad 1 \leq \bar{h} \leq 10 \tag{5.2}$$

$$P_{min} = C_{P,min} \beta \rho U W \quad \text{being} \quad C_{P,min} = 0.75\bar{h}^{-0.97} \quad \text{for} \quad 1 \leq \bar{h} \leq 10 \tag{5.3}$$

where β [-] represents the effective bounce-back factor, ρ [kg/m^3] represents the fluid density, U [m/s] represents the wave surface impact velocity, W [m] represents the overhang length and $\bar{h}$ [-] represents the dimensionless overhang height.

Furthermore, the effective bounce-back factor β is given by Equation 5.4 (with an RMSE of 0.12), as presented in Chapter 4. This factor β is effectively the experimental calibration parameter for using the pressure-impulse theory in design calculations. Parameter β can be calculated based on Parameter Γ, which describes the effective air entrapment characteristics (see more detail in Chapter 4). Parameter Γ was derived based on the wave heights and impact velocities exceeded by 1% of the waves (i.e. $H_{1\%}$ and $U_{1\%}$). Nevertheless, the parameter Γ can be used for any required exceedance probability when predicting confined wave impact loads. The parameter Γ can be obtained according to Equation 5.5, being g the gravitational acceleration.

$$\beta = 2 - e^{-0.16\Gamma} \tag{5.4}$$

$$\Gamma = U^2 L_m / g W^2 \tag{5.5}$$

VELOCITY ESTIMATION

The wave surface impact velocity is a key magnitude for carrying out load estimations for confined wave impacts on vertical hydraulic structures with overhangs. A method to calculate the wave surface impact velocity was developed and assessed in Chapter 2, Chapter 3 and Chapter 4 based on linear wave theory. Particularly, the conclusions from laboratory experiment results from Chapter 3 showed that the impact velocity described by this method is suitable and accurate to be used for such load estimations. According to this method, the wave impact velocity U can be calculated based on the incident wave height H and the overhang freeboard R_c for $|R_c| < H$, see Equation 5.6.

5

$$U = \omega \sqrt{H^2 - R_c^2} \tag{5.6}$$

where ω [rad/s] represents the angular wave frequency ($\omega = 2\pi/T$).

Equation 5.6 shows that the maximum wave impact velocities are expected to take place when the water level is at the same height as the overhang ($h = d$). In other words, the largest wave impact velocities would occur when the freeboard is equal to zero ($R_c = 0$). Nevertheless, other studies from Huang et al. (2022) highlight that the largest impact loads occur for very small positive freeboards ($h > d$), instead of zero freeboards ($h = d$). These observations suggest the presence of possible surface dumping effects for zero freeboard and make the predictions based on Equation 5.6 to be conservative.

WAVE HEIGHT ESTIMATION

For irregular wave fields, the incident wave height of the single waves (H) should be obtained from the wave field parameters (i.e. significant wave height H_s) and given a certain exceedance probability (i.e. pr). The Rayleigh distribution can be used to describe the wave height distribution for a set of given incident wave parameters (Longuet-Higgins, 1952). This method is suitable for the relative water depths considered in this research ($d > L/10$). For shallower water conditions ($d < L/20$), this would be less accurate and the method from Battjes and Groenendijk (2000) should be considered. Equation 5.7 allows obtaining the incident wave heights associated with a given exceedance probability pr (or similarly with a given return period). This wave height can be used to describe the wave impact velocity of each wave according to Equation 5.6.

$$H = H_s \sqrt{-\frac{\log(pr)}{2}} \tag{5.7}$$

VENTILATION GAPS

As presented in Chapter 4, ventilation gaps were found to be effective in reducing confined wave impact loads acting on vertical hydraulic structures with overhangs. Relative ventilation gap widths (i.e. G/W) between 5% and 10% lead to the reduction of force-impulses acting on the vertical wall between 10% and 50%. Nevertheless, this study highlighted the importance of considering the precise ventilation gap dimensions (inner ventilation gap width G, outer ventilation gap width G', inner vertical gap boundary B and outer vertical gap boundary B') when assessing the effect of load reducing ventilation gaps. For example, configurations with equal G but with variations in G', B or B' may lead to different wave impact load reductions. In summary, for assessing the effect of load reducing ventilation gaps, the precise configuration of such gaps should be described with sufficient precision (i.e. not only the inner ventilation gap width G) to have a higher degree of confidence in the corresponding load reduction. In addition, the load reductions for the same relatively gap width (G/W) were larger for larger ventilation gaps ($G = 2$cm) in comparison with smaller ventilation gaps ($G = 1$cm). This suggests the presence of secondary processes for smaller ventilation gaps. Besides the experimental methods used in this research, the effect of ventilation gaps can also be assessed by the use of numerical methods and computational fluid dynamics (Hofland et al., 2019). In conclusion, ventilation gaps can be regarded as an effective load reduction measure for confined wave impacts. To this end, numerical and physical methods should be used in order to determine the precise load reduction factor.

5

LATERAL CONSTRICTIONS

Flood gates often consist of a series of gates that are bordered by pylons or similar lateral constrictions (e.g. Eastern Scheldt, Afsluitdijk, Haringvliet, Fudai or Pont-Vannes du Millac). Consequently, those lateral constrictions represent an additional and often-occurring complication in the design of such flood gates. Tests were carried out in Chapter 4 with a lateral constriction that resembles the presence of a support wall in a flood gate complex. The lateral constriction considered in these tests had a width of 22% of the total structure width. These experimental results showed that the presence of a lateral constriction amplifies the wave impact loads at the constriction edge, leading to pressure-impulse amplification at the constriction edge between 10% and 50%.

5.2.2. LABORATORY EXPERIMENTS

Physical modelling has been widely used as a research and design tool in hydraulic engineering over the past century. And this relevance and applicability of physical modelling in the field of hydraulic engineering are expected to continue in the future. Thus, this section summarizes the most important learnings from the laboratory experiments carried out during this research. These learnings can be used for future research on wave impact loads and/or for the design of hydraulic structures.

This research carried out a large number of laboratory tests in the wave flume. Those experiments provided process knowledge on confined wave impacts on hydraulic structures and were used to validate load prediction expressions. The focus of this research was the description of the wave loads on a schematized structure, so a significantly rigid structure was built (with 10 mm thick aluminium plates) in order to minimize the influence of the structure response on the measured loads. Also, the instrumentation, including load cells and pressure sensors, was carefully selected to be able to accurately capture the loading on the structure. The experience from these experiments was applied during the laboratory tests with a flexible structure below the overhang (i.e. representing a closed flood gate, see Tieleman (2022)). Those laboratory experiments evaluated the response of a thinner and more flexible vertical structure to confined wave impacts, see Figure 5.3. The results from these tests were then used to validate a structural response model and a close agreement between predicted and measured response was found.

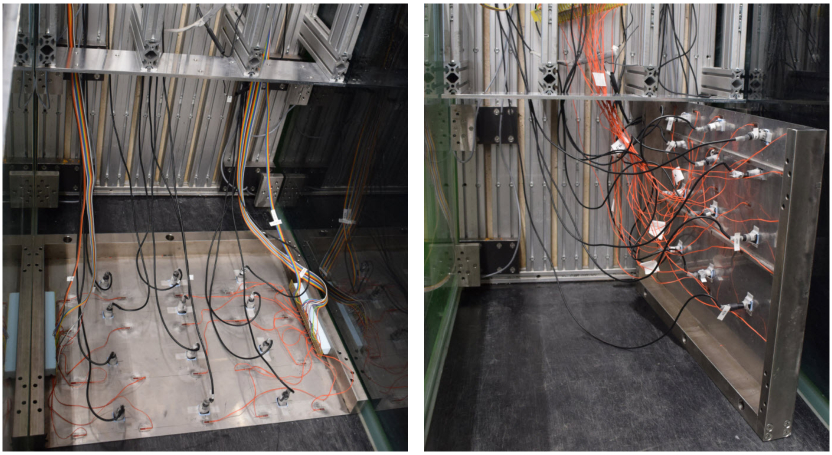

(a) Plain gate

(b) Reinforced gate

Figure 5.3: Laboratory tests with flexible gate, during preparations (Tieleman, 2022).

These laboratory experiences showed the potential of experimental techniques to study the confined wave impact loading and the response of a given structure to those loads. Thus, this technique should be considered in the design of hydraulic structures prone to facing confined wave impacts. In this case, the following aspects should be considered based on the learnings from this research. Firstly, the test setup should be built without influencing the load and response measurements. To this end, a solid base for the structure should be constructed. For example, the 1-tonne concrete block used in this research proved to properly work as a solid support for the structural setup. Furthermore, all elements surrounding the test setup (e.g. flume bottom, flume wall, setup features, etc.) should be checked for possible influences in the experimental observations. Secondly, the instrumentation should also not influence the experimental measurements. To this end, pressure sensors used in laboratory experiments should not have temperature effects (e.g. "temperature shock", see Hofland et al. (2010)) affecting the measured load characteristics. Those sensors should also provide a sampling frequency able to capture such impulsive wave loads (e.g. 20kHz used in this research). This requirement for high measurement frequencies also applies to other measurement devices such as force transducers, accelerometers, strain gauges, etc. Thirdly, variations on the setup to measure additional processes should be carefully assessed before being implemented. For example, transparent setups made of highly-resistant polycarbonate could allow the visualization of processes such as air entrapment and entrainment evolution across the structure. Nevertheless, this alternative was not used in this research given the effect that such a more flexible construction would have on the measured impulsive loads. Thus, the design of the test setup should consider the implications that such choices would have on the reliability of the measured processes. Fourthly, the split between quasi-static and impulsive loads can be carried out based on pressure and force measurements. To this end, the method described in Chapter 2 can be used. Lastly, the measured pressure- and force-impulses can be accurately scaled from model to prototype based on Froude scaling. On the other hand, this cannot be done for pressure peaks, force peaks and impact durations. This will be further discussed in Section 5.3.

In addition, a LED PIV (Particle Image Velocimetry) system was developed in-house during this research, as described in Bakker et al. (2021). This LED PIV system allowed us to measure the evolution of the velocity field in high spatial and temporal resolution. Figure 5.4 shows the velocity field measurements during a given wave impact. Those velocity field measurements were used further to estimate the pressure-impulse generated by such wave impacts. To this end, the wave impact pressure-impulse was estimated based on the velocity field difference during this given wave impact, by integrating the velocity difference field from the free surface (i.e. $P = 0$) to the wall as $\nabla P = -\rho\Delta\vec{u}$ (see pressure-impulse theory in Chapter 2 and (Bakker et al., 2021) for more details). Figure 5.5a describes the velocity difference field during the wave impact, and the two integration paths used to obtain the pressure-impulse at the vertical wall. Finally, Figure 5.5b shows a close agreement between the pressure-impulse obtained by this LED PIV system and the pressure-impulse measured by pressure sensors at the vertical wall.

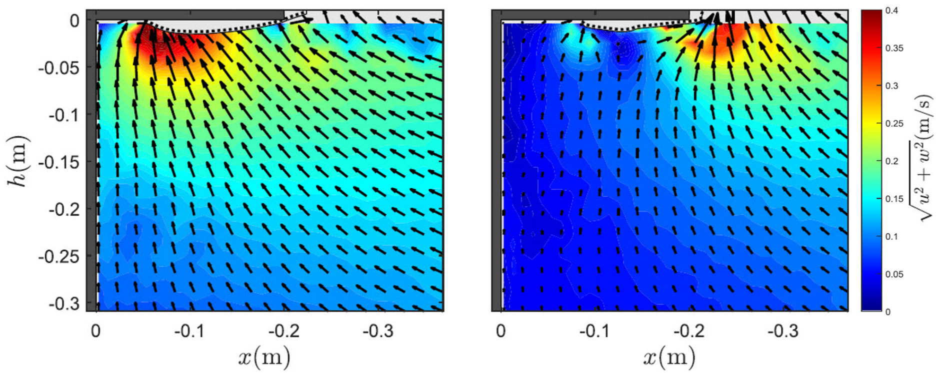

(a) Velocity field before confined wave impact

(b) Velocity field after confined wave impact

Figure 5.4: LED PIV velocity field measurements before and after a wave impact (Bakker et al., 2021).

For future research on confined wave impacts, carrying out larger scale experimental tests (i.e. at Deltares Delta Flume) would provide valuable results regarding the effect of entrained and entrapped air, which would certainly justify the associated significant costs of using those facilities. The use of wave flumes located inside vacuum chambers is also another promising development that will provide significant contributions to the study of the effect of entrapped and entrained air in wave impacts.

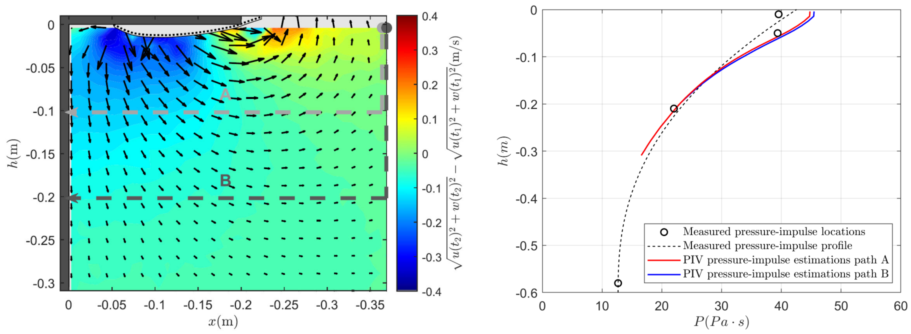

(a) Velocity difference field

(b) Comparison of PIV-estimated pressure-impulse

Figure 5.5: Pressure-impulse estimation based on PIV velocity measurements (Bakker et al., 2021).

5.2.3. COMPUTATIONAL FLUID DYNAMICS

For situations outside the range of structures studied in the main body of this thesis, computational fluid dynamics simulations can be used. This technique can be used to study various processes related to the occurrence of confined wave impacts. One example is that this research has only focused on relatively short overhangs, with ratios of wave length (L in regular wave tests, L_m in irregular wave tests) to overhang length (W) between 10 and 40 and with ratios of overhang height (h) to overhang length (W) between 3 and 6. Nevertheless, vertical hydraulic structures can include longer overhangs, and in some situations even feature very long overhangs (i.e. overhang lengths longer than one-fourth of the incident wave length). Examples of such structures are culverts and other enclosed areas of various coastal hydraulic structures that can lead to confined wave impacts. In such cases, the confined wave impact mechanisms may be significantly different compared to the case of much shorter overhangs.

Numerical simulations with OpenFOAM have been carried out during this research for vertical hydraulic structures with very long overhangs (i.e. $W > L/4$), see Figure 5.6. These simulations were done using OpenFOAM (v3.0+), in combination with waves generated by waves2foam (r2101) within a larger domain of OceanWaves3D (28cf612). These numerical simulations had the aim to visualise the confined wave impact process for such very long overhangs and the very large air entrapment that takes place in those configurations. These simulations also highlighted that the confined wave impact takes place over a small fraction of the whole overhang, which is related to the incident wave length. Based on these numerical simulations, the confined wave impact at the edge of a very long overhang takes place over a length of about $L/8$. Numerical tools such as OpenFOAM or ComFLOW (see van der Eijk and Wellens (2020)) can be used in future research and design practice. This can be done to gain insight into wave impacts on complex structure geometries and eventually also be used for the estimation of confined wave impact loads. Nevertheless, the simulations carried out with OpenFOAM shown in Figure 5.6 did not include the compressibility of air. This was addressed by Batlle Martin et al. (2021), who carried out OpenFOAM simulations with compressible air. Including the compressibility of air is crucial to accurately describe the impact duration and pressure/force peaks. Thus, numerical simulations like the ones carried out by van der Eijk and Wellens (2020) and Batlle Martin et al. (2021) including the compressibility of air should be used in future studies on confined wave impacts.

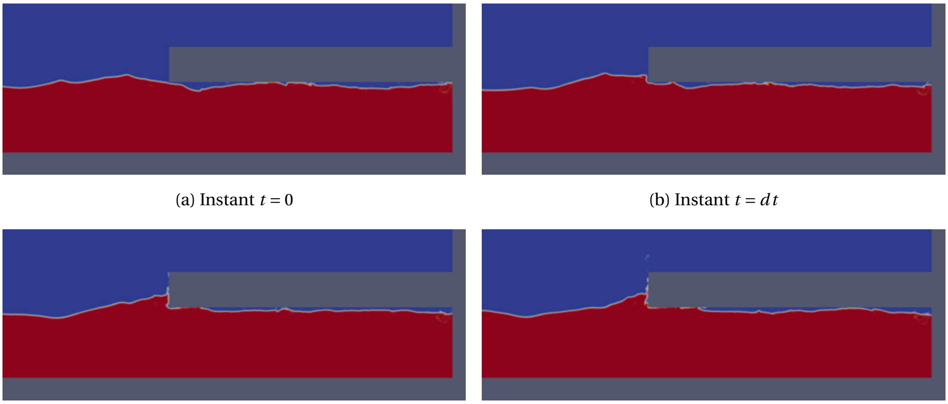

(a) Instant $t = 0$

(b) Instant $t = dt$

(c) Instant $t = 2dt$

(d) Instant $t = 3dt$

Figure 5.6: Overview of OpenFOAM simulations for very long overhangs.

5.2.4. STRUCTURAL RESPONSE MODELS

The load prediction expressions previously presented in this section can be used in the design of hydraulic structures. Chen et al. (2019) introduced the advantages of using the pressure-impulses and force-impulses in the structural design, instead of using the pressure peaks and force peaks. Furthermore, these load prediction expressions can be coupled with semi-analytical structural response models and probabilistic design tools. This has been done in (Tieleman et al., 2021). This work establishes a computationally efficient model to predict flood gate vibrations due to wave impacts including fluid-structure interaction. The load prediction expressions based on pressure-impulse theory are employed here to predict the impulsive wave impact loads, which are superposed on the quasi-steady wave loads. The computational efficiency of the developed model allows for a large number of simulations. This makes it possible for the first time to perform probabilistic evaluations for this type of problem, resulting in the explicit quantification of the failure probability of flood gates subjected to confined wave impacts.

Furthermore, Chen et al. (2019) distinguishes three types of loads based on the previous work from Humar (2002). A quasi-static load is defined when the load duration is longer than four times the structure's natural period ($t_d > 4T_n$). In this case, the structure reaches its maximum deflection well before the load is over. This leads to reaction forces equivalent to the maximum forces. A dynamic load is defined when the load duration is between one-fourth and four times the structure's natural period ($T_n/4 < t_d < 4T_n$). In this case, the structure reaches its maximum deflection close to the moment when the load is over. This leads to reaction forces even larger than the maximum forces. An impulsive load is defined when the load duration is smaller than one-fourth of the structure's natural period ($t_d < T_n/4$). In this case, the load is over well before the structure reaches its maximum deflection. This leads to reaction forces smaller than the maximum forces, and the structural response can be fully described given the impulse and the structure's natural frequency. Thus, the wave impact loads should be considered in the design of hydraulic structures in combination with the structural characteristics. This is particularly important for dynamic loads. In that case, the shape of the wave impact loading over time is crucial to describe the structural response (Tieleman, 2022).

5.3. AIR ENTRAPMENT AND SCALING

This section studies the effect of air entrapment on the design of hydraulic structures subjected to confined wave impacts. This study is justified by the lack of validated models able to describe the impact durations and pressure and force peaks generated by a confined wave impact. The aim of this section is to introduce design considerations on how to potentially incorporate the effect of entrapped air in design, related to the scaling of loads and the description of the impact duration.

5.3.1. EXPERIMENTAL OBSERVATIONS

The air entrapment in confined wave impacts has been studied in Chapter 3 based on laboratory experiments. These results showed, among other observations, a large variation in air entrapment for the different test conditions. This variability of air is described hereafter in both absolute values of entrapped air area (A_A), but also in relation to the overhang length (W) as the air entrapment factor $\alpha = A_A/W^2$. The tests with the shorter overhang showed a range of entrapped air area in the range (50 mm^2 < A_A < 350 mm^2) and an air entrapment factor in the range (0.005 < α < 0.035). The tests with the longer overhang showed a range of entrapped air area in the range (250 mm^2 < A_A < 1300 mm^2) and an air entrapment factor in the range (0.006 < α < 0.033). Those results highlight that a relatively constant entrapped air factor range was found for both overhang lengths, besides the large air entrapment variability between the individual tests.

This variability in entrapped air characteristics led to significant variability in the loads acting on the structure (i.e. pressure and force peaks, pressure- and force-impulses, impact durations, load vibrations, etc.). Furthermore, longer impact durations were found to be closely related to larger entrapped air dimensions. Nevertheless, how to incorporate the effect of air entrapment in design has not been studied yet. This will be addressed in more detail further in this chapter. Furthermore, the presence of entrained air (i.e. smaller air bubbles) can have a significant effect, not only on the wave impact loads but also on the structural response. Among others, the presence of entrained air reduces the speed of sound in water from 1500 m/s to 150 m/s (Gibson, 1970). And results from structural model calculations indicate that such air entrapment can lead to reduced stresses on the structures subjected to confined wave impacts (Kleiberg et al., 2022). Thus, similarly to air entrapment, the presence of entrained air in wave impacts is a key factor for understanding the impulsive wave loads acting on a given hydraulic structure, and the corresponding structural response.

5.3.2. ANALYTICAL MODELS

This section describes previous analytical studies on air entrapment in wave impacts, in particular the work from Bagnold (1939), Mitsuyasu (1966) and Ramkema (1978). This section aims to increase the understanding on the air entrapment dynamics and present design considerations on how to account for entrapped air in the design of vertical hydraulic structures with overhangs. Those analytical models consider a schematic description of the air entrapment that takes place on a confined wave impact.

BAGNOLD MODEL

The piston model was presented by Bagnold (1939) to describe the behaviour of the entrapped air pocket caused by breaking waves on a vertical wall. Thus, this model aimed to describe the response of the entrapped air pocket schematically, as presented in Figure 5.7. Equation 5.8 presents the relation between the maximum peak pressures and the air entrapment dimensions, assuming an adiabatic compression of the air pocket.

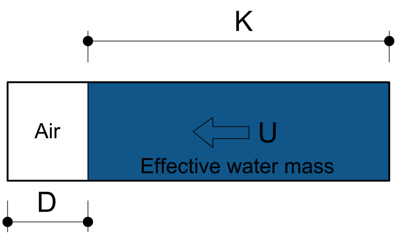

Figure 5.7: Schematic description of the Piston Model at the moment of impact (Bagnold, 1939).

$$\frac{p_{max}}{p_0} = 1 + 2.7\frac{\rho K U^2}{p_0 D} \tag{5.8}$$

where p_{max} [Pa] represents the maximum pressure in the air layer, p_0 [Pa] represents the atmospheric pressure, K [m] represents the length of the moving water mass, D [m] represents the initial length of the air pocket and ρ [kg/m^3] represents the water density.

The dynamics of the system are described in Equations 5.9-5.11. Being x the length of the air pocket, the pressure of the enclosed air is described by Equation 5.9. Furthermore, the motion of the water mass is determined by Equation 5.10. Combining those two equations, Equation 5.11 allows us to describe the dynamics of the system. Although this model has been initially described within the study of breaking wave impact loads, it is also suitable for describing the behaviour of entrapped air in other wave impact types. Among others, this model was used for describing the loads generated by the same type of confined impacts that are treated in this thesis by Ramkema (1978).

$$p = p_0\left(\frac{D}{x}\right)^{\gamma} \tag{5.9}$$

$$\rho K\frac{d^2x}{dt^2} = p - p_0 \tag{5.10}$$

$$\frac{d^2x}{dt^2} = \frac{p_0}{\rho K}\left(\left(\frac{D}{x}\right)^{\gamma} - 1\right) \tag{5.11}$$

MITSUYASU SOLUTION

Mitsuyasu (1966) solved the model initially presented by Bagnold, with the exact solutions for the pressure peaks, as given in Equation 5.12, besides other contributions and additional approximate solutions. Figure 5.8 presents both the approximate model solution from Bagnold (Equation 5.8) and the exact solution from Mitsuyasu (Equation 5.12).

$$\frac{2}{\gamma-1}\left(\frac{p_{max}}{p_0}\right)^{1-1/\gamma}+2\left(\frac{p_{max}}{p_0}\right)^{-1/\gamma}-\frac{2\gamma}{\gamma-1}=\frac{\rho K U^2}{p_0 D}=S \tag{5.12}$$

where γ [-] represents the heat capacity ratio (i.e. the ratio between the specific heat at constant pressure and that at constant volume), being $\gamma \approx 1.4$ for air in an adiabatic compression as it is used by Mitsuyasu (1966). The work from Abrahamsen and Faltinsen (2011) experimentally measured $\gamma = 1.38$ in wave slamming impacts so for high intensity and large scale wave impacts air compression is indeed expected to be adiabatic. Works from Cuomo et al. (2010a) and Bogaert (2018) on the scaling of wave impact loads (based on previous contributions from Takahashi et al. (1985)) also consider Equation 5.12 using a heat capacity ratio of $\gamma = 1.4$ for an adiabatic air compression.

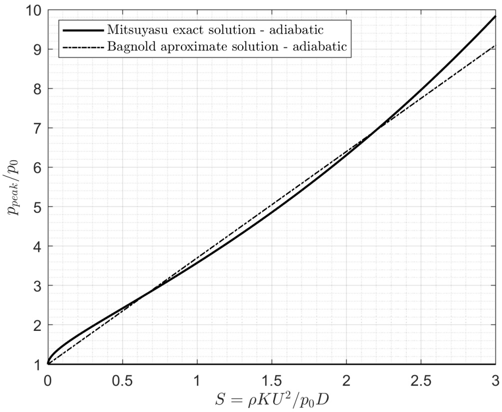

Figure 5.8: Adiabatic model solutions from Bagnold (Equation 5.8) and Mitsuyasu (Equation 5.12).

RAMKEMA SOLUTION

The work from Ramkema (1978) also addresses the behaviour of air in wave impacts and was carried out while studying confined wave impacts for the design of the Eastern Scheld Storm Surge Barrier. This study aimed to present scaling rules for the confined wave impact loads based on the model presented by Bagnold. Thus, considering the same basic definitions and equations, the solution from Ramkema describes the scaling model to translate model load values to prototype real scale loads in nature.

According to Ramkema (1978), the scaling of the air and water dimensions (D and K) are linear (i.e. $n_D = n_K = n_l$). The water mass velocity (U) scales according to Froude (i.e. $n_U = \sqrt{n_l}$), while the atmospheric pressure (p_0) is constant (i.e. $n_{p_0} = 1$). Furthermore, Ramkema (1978) considers the water mass length (K) to be half of the overhang length (W) and the maximum air thickness to be 1/10 of the overhang length (W).

In summary, previous authors (Bagnold, 1939; Mitsuyasu, 1966; Cuomo et al., 2010a; Ramkema, 1978; Bogaert, 2018) have all used the Bagnold's Piston Model without effectively defining the air (D) and water (K) dimensions. Instead, this model has been used based on different assumptions. Thus, given the currently available information, this model can only be used with a higher degree of confidence for qualitative assessments.

5.3.3. SCALING RULES

Figure 5.9 summarizes the previously presented tools for the scaling of impulsive wave impact loads between model and prototype. Figure 5.9a includes the three model solutions from Mitsuyasu (1966), Bagnold (1939) and Ramkema (1978) that can be used to scale confined wave impact loads. Furthermore, Figure 5.9b illustrates the differences in the scaling of impulsive wave impact loads carried out according to Mitsuyasu (1966) and Froude, where pressures are linearly scaled (i.e. $n_p = n_l$). To this end, a scaling example is presented, given a geometric scale 1:15 (i.e. $n_l = 15$) between model and prototype. Figure 5.9b shows that scaling impulsive loads obtained from model measurements (see the blue point) to prototype dimensions based on Froude (see the magenta point) would lead to a large overestimation of loads compared to the scaling based on Mitsuyasu (see the red point). The results presented in Figure 5.9b are consistent with previous research on the scaling of wave impact loads. Cuomo et al. (2010a) describes how pulsating or quasi-static loads can be accurately scaled by Froude. Also pressure- and force-impulses can be accurately scaled by Froude. Nevertheless, pressure peaks, force peaks and impact durations are found to be strongly affected by the air effects and not correctly scaled with Froude. In this case, a significant overestimating of the pressures and forces takes place when considering Froude scaling between model and prototype scales (Allsop et al., 1996). The work from Cuomo et al. (2010a) also highlights that several authors (e.g. Bullock et al. (2001)) have attempted to use other scaling methods based on Cauchy, Weber and other scaling laws with limited practical applications.

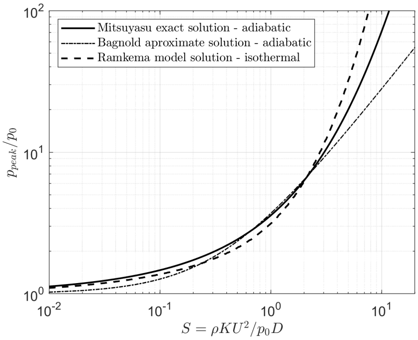

(a) Models from Bagnold, Mitsuyasu and Ramkema

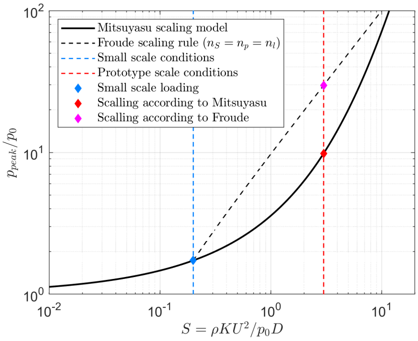

(b) Load scaling with Mitsuyasu and Froude

Figure 5.9: Comparison of model solutions from Bagnold, Mitsuyasu, Ramkema and Froude.

5

5.3.4. PEAK PRESSURES AND FORCES

The dynamics of the air compression system can be described by the piston model presented in Equations 5.9, 5.10 and 5.11. The results of the normalized pressure time-series are shown in Figure 5.10 for an adiabatic compression and calculated by means of an explicit numerical integration. This figure distinguishes the different pressure signals for different wave impact scales: smaller scale ($S = 0.03$), medium scale ($S = 0.30$) and larger scale ($S = 1.40$). This model could be used in the future to estimate the impact durations in both model and prototype. Nevertheless, this method is not yet validated to describe impact durations for design estimations. The description of impact durations currently is still significantly based on existing literature and experimental measurements. When these impact durations are known, the peak pressures and peak forces can be obtained from pressure-impulses and force-impulses assuming a triangular load distribution based on Chen et al. (2019), see Equations 5.13 and 5.14.

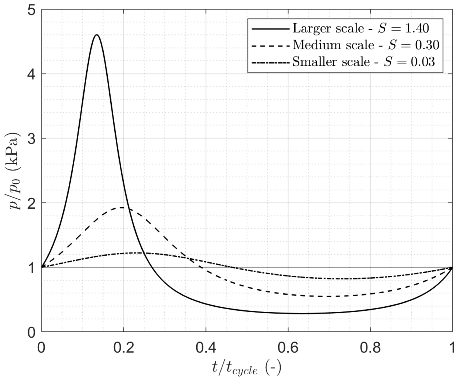

Figure 5.10: Comparison of pressure peaks for different scales for an adiabatic compression.

$$p = \frac{2P}{t_d} \tag{5.13}$$

$$F = \frac{2I}{t_d} \tag{5.14}$$

5.4. DESIGN APPLICATION

This section addresses the design of coastal hydraulic structures subjected to confined wave impacts. In particular, it presents the application of the previously developed load prediction methods to design. Section 5.4.1 describes a design application example, while Section 5.4.2 discusses design adaptations to limit confined wave impact loads.

5.4.1. APPLICATION EXAMPLE

In this section, an example is given for the potential use of the developed load prediction methods for design applications. The confined wave impact load prediction approach developed in this research is summarized in Figure 5.2. In addition, the main parameters and dimensions to be considered in this load prediction method are described in

Figure 5.1. This load prediction method can be used to estimate confined wave impact loads, while considering its assumptions and range of application. Firstly, the laboratory tests in this research considered a horizontal bottom without any slope inclination and with non-breaking incident waves. Secondly, the structure is composed of a fully vertical wall and a fully horizontal overhang, without any 3D feature. In the standard tests (i.e. excluding the tests with a ventilation gap and the tests with a lateral constriction) no other element affected the wave dynamics before, during or after the wave impacts. Thirdly, the laboratory experiments were carried out in a small scale facility. As previously discussed, this affects the applicability of this model to prototype scales. In summary, the pressure- and force-impulses can be accurately scaled with Froude. Nevertheless, the peak pressures, peak forces and impact durations cannot be accurately scaled with Froude. The scaling of peak pressures and peak forces with Froude would lead to a significant overestimation of the loads (Cuomo et al., 2010a).

Furthermore, it should be highlighted that this load prediction method has been experimentally validated for conditions of deep water in relation to the wave length ($d > L/10$). But it has also been validated for conditions of deep water in relation to the wave height ($d > 4H$), without the presence of wave breaking. Based on those conditions the Rayleigh distribution can be used. Nevertheless, the method from Battjes and Groenendijk (2000) should be used to describe the wave height distribution in shallow water conditions ($d < L/20$). For conditions in which previously broken waves act on the structure, the method from Goda (2010) may be considered. Circumstances in which breaking waves act directly on the structure are outside the scope of this study. In this case, the work from Kisacik et al. (2014) may be considered. In addition, the use of numerical and physical modelling should be always considered in order to investigate non-standard configurations subjected to confined wave impact loads.

Figure 5.11 shows a coastal hydraulic structure subjected to confined wave impacts. This configuration is used as a case study for predicting such confined impulsive wave loads, applying the prediction method previously presented in this research. Table 5.1 describes the main load prediction calculations following the steps presented in Figure 5.2. This application example aimed to describe the loads acting on the structure with an exceedance probability of 0.1% within a give wave state (i.e. $H_{0.1\%}$, $U_{0.1\%}$, $I_{0.1\%}$, $F_{0.1\%}$). This exceedance level is chosen given its wide use in practice (Goda, 2010). For example, the expected value of the maximum load for a typical storm duration of 1000 waves can be estimated with a Rayleigh-distributed wave height of $H_{0.1\%} = 1.86 H_s$. As discussed in Section 5.2.1, a similar calculation with this prediction method can be carried out for other exceedance probabilities (e.g. 0.01%). The outcome of this preliminary calculation is the impulsive loading caused by such a confined wave impact, described by the total force-impulse (I) acting on the vertical wall. Assuming that those wave impacts would have impact durations in the range of 20 to 100 ms, these force-impulses can be then translated to a range of expected peak forces based on Equation 5.14. The results presented in Table 5.1 are calculated for one metre structure width (i.e. $M = 1$ m).

Such loading prediction calculations can be used for the preliminary design of hydraulic structures, but it is recommended to use them accompanied by detailed assessments of the expected entrapped air dimensions. This could be done with numerical and/or physical models. Such studies on air entrapment would allow us to determine

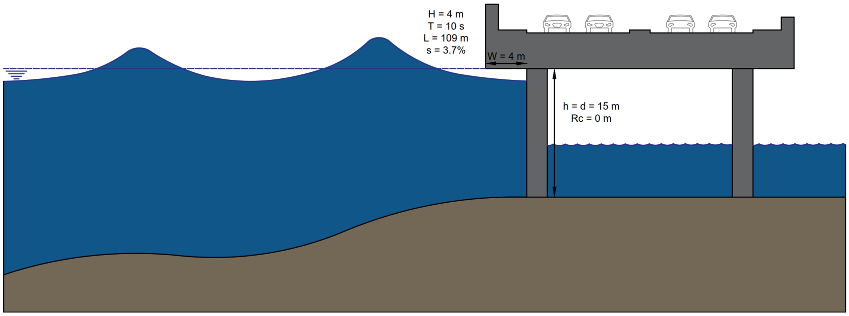

Figure 5.11: Example application configuration

Table 5.1: Example of load prediction for a confined wave impact (for one metre width), based on Figure 5.2.

Input Parameters								
H_s [m]	T_m [s]	W [m]	h [m]	d [m]	M [m]	ρ [kg/m^3]	g [m/s^2]	t_d [ms]
2.15	10.0	4.0	15.0	15.0	1.0	1025	9.81	20 to 100
Intermediate Calculations								
$\bar{W}$ [-]	$\bar{h}$ [-]	R_c [m]	L_m [m]	ω_m [rad/s]	$H_{0.1\%}$ [m]	$U_{0.1\%}$ [m/s]	Γ [-]	β [-]
1.0	3.75	0.0	109	0.6	4.0 (Eq. 5.7)	2.5 (Eq. 5.6)	4.4 (Eq. 5.5)	1.5 (Eq. 5.4)

Load prediction estimation	
Force-impulse $I_{0.1\%}$ [kNs]	Force peak $F_{0.1\%}$ [kN]
117 (Equation 5.1)	2 347 to 11 736 (Equation 5.14)

the most appropriate and accurate impact durations and scaling rules to be considered. This would then be used in the corresponding structural model, taking into account the sensitivity of the structure to such impulsive loads (i.e. the relation between T_n and t_d).

For design application purposes, Figures 5.12 and 5.13 allow us to carry out the load predictions estimations previously described in this section. In addition, these figures highlight the sensitivity of the load prediction model to the different input parameters. Figures 5.12 and 5.13 also allow us to present a series of conclusions regarding the load prediction method developed in this research. Figure 5.12 focuses on the estimation of the force-impulse (I) based on the various input parameter combinations. Figure 5.12a shows the model sensitivity to the wave height, with larger impulses for higher incident waves. Figure 5.12b shows the model sensitivity to the overhang length, with larger impulses for longer overhangs. Figure 5.12c shows the model sensitivity to the freeboard, with maximum impulses for the conditions of zero freeboard. Figure 5.12d shows the model sensitivity to the wave steepness, with larger impulses for steeper incident waves. Figure 5.13 highlights the influence of the impact duration while deriving the force peaks (F) with Equation 5.14 based on the force-impulses (I) estimations. This figure highlights that shorter impact durations lead to higher force (and pressure) peaks. Figure 5.13a describes the derivation of the total force as a function of the impact duration for varying wave heights, while Figure 5.13b describes the derivation of the total force as a function of the impact duration for varying overhang lengths.

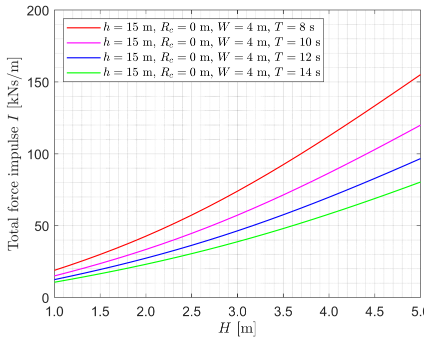

(a) Wave height (H) sensitivity

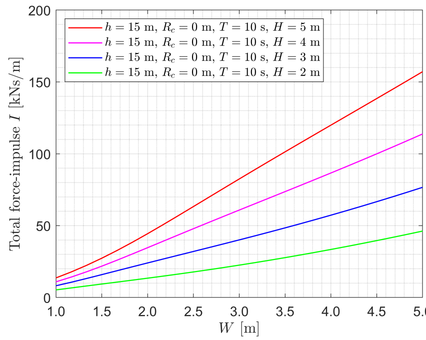

(b) Overhang length (W) sensitivity

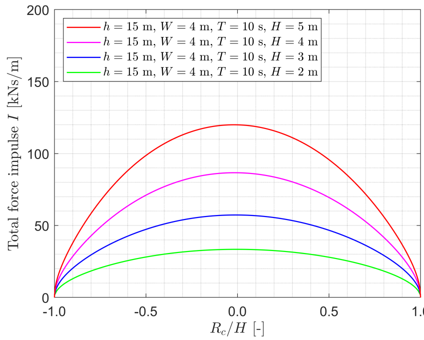

(c) Freeboard (R_c/H) sensitivity

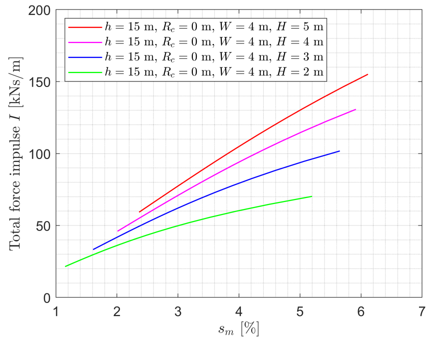

(d) Wave steepness ($s = H/L$) sensitivity

Figure 5.12: Sensitivity of the force-impulse (I) prediction model.

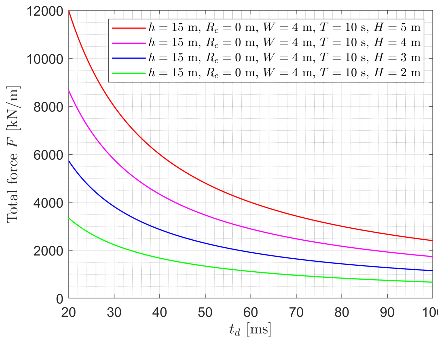

(a) Influence of impact duration (d_t) and H

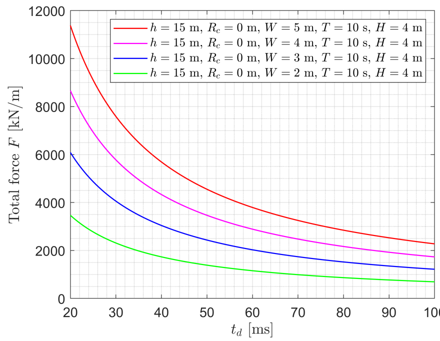

(b) Influence of impact duration (d_t) and W

Figure 5.13: Influence of the impact duration to the total force (F)

5.4.2. DESIGN ADAPTATIONS

To reduce the confined wave impact loads acting on the hydraulic structure, different approaches can be considered in the design. The most fundamental and important consideration in the design of hydraulic structures is to avoid as much as possible the occurrence of wave impacts, as previously highlighted in the study of breaking wave impacts on vertical breakwaters (Takahashi, 2002). Thus, the design of vertical hydraulic structures should avoid the presence of structural elements, such as horizontal overhangs, that could cause confined wave impacts. If it becomes infeasible to avoid the presence of such overhangs, different measures should be considered, see Figure 5.14. Firstly, the overhang features should be as small as possible, in order to reduce the wave impact loads acting on the structure (see Figure 5.14a). Secondly, the overhang should be placed where the maximum freeboard is observed, either positive or negative, reducing the wave impact velocity (see Figure 5.14b). Thirdly, the incident wave heights could be reduced by means of other protective structures, leading to less energetic confined wave impacts (see Figure 5.14c). Fourthly, ventilation gaps could be included in the design, in order to further reduce the wave impact loads (see Figure 5.14d). Fifthly, overhangs with angles ϕ to the vertical wall smaller than 90° could also reduce the confined wave impact loads (see Figure 5.14e). Sixthly, locally placed dissipative elements below the overhang could also reduce the confined wave impact loads (see Figure 5.14f). All those measures, and also others, should be considered to avoid or at least limit the confined wave impact loads acting on the hydraulic structure. To evaluate the effectiveness of those load-reducing measures, a combination of analytical, numerical and experimental methods should be considered. In this design optimization process, the associated costs and constructability aspects should also be considered.

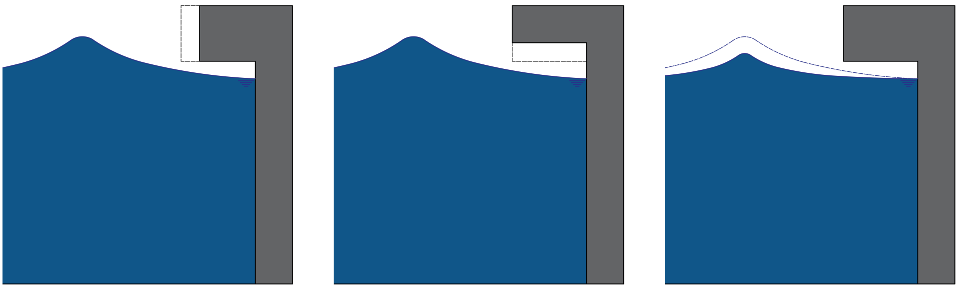

(a) Overhang length (W) (b) Freeboard (R_c) (c) Wave height (H)

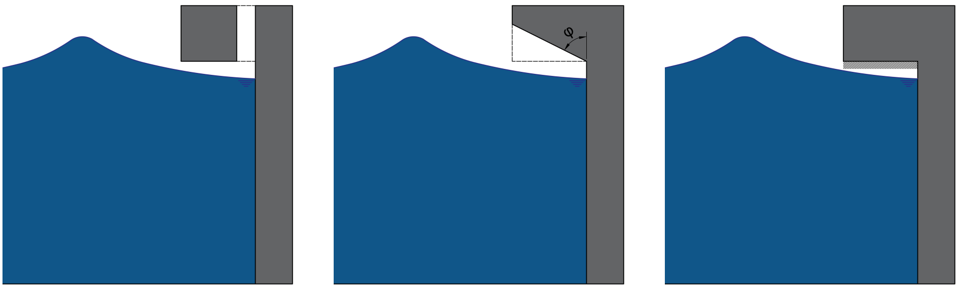

(d) Ventilation gaps (e) Overhang angle ϕ (f) Dissipative elements

Figure 5.14: Design alternatives to reduce confined wave impact loads

Furthermore, Figure 1.2 presented a list of vertical hydraulic structures with overhangs, which could be subjected to confined wave impacts. Such examples in various locations worldwide highlight the applicability of the load prediction expressions previously described in this work for the design of future hydraulic structures. Nevertheless, Figure 1.2 also highlights that those hydraulic structures may present extremely diverse characteristics and requirements. Thus, future research on design guidelines would need to explore the common features but also particularities of such hydraulic structures. This future work would benefit from a standard international database of hydraulic structures, comparable to the *International Levee Performance Database* (Ozer et al., 2020) or the *Dataset in the Planning and Conceptual Design of Storm Surge Barriers* (Kluijver et al., 2019). Such a structured database of worldwide hydraulic structures could also include experimental and monitoring data. This would contribute to more efficient and reliable research and design of such hydraulic structures, including the ability to identify the most effective and suitable load reduction measure.

5.5. CONCLUSION

This chapter addressed two objectives. Firstly, it summarized previous contributions on confined wave impacts with a focus on their application to design. This includes the experimentally validated load prediction expressions based on the pressure-impulse theory. Secondly, it discussed the effect of air entrapment in the design of such structures, in particular its effect on the impact duration, pressure and force peaks and the scaling between model and prototype dimensions. Furthermore, it presented a design application example and a series of load reduction measures to be considered in the design. Such load prediction model results can be then incorporated into semi-analytical structural response models, and consequently in efficient probabilistic calculations.

Additional research on the design of hydraulic structures with overhangs subjected to confined wave impacts should continue in the future. This is particularly relevant for thin steel structures such as flood gates which are especially susceptible to a dynamic behaviour under impulsive wave impact loads. In particular, future studies should address the effect of entrapped and entrained air on wave impacts, given its influence on both loads and responses. This study of the effect of air on wave impacts would provide key improvements to the scaling rules between model and prototype dimensions, and allow for the validation of CFD models with compressible air. To that end, additional experimental tests should be carried out, including the use larger scale facilities or experiments at facilities with lowered atmospheric pressures. Furthermore, the use of numerical models (i.e. computational fluid dynamics) such as OpenFOAM and ComFLOW that include the compressibility of air would also provide valuable contributions.

6

Conclusions and Recommendations

This chapter summarizes the main conclusions and recommendations from this research on confined wave impacts. Firstly, this research validated the pressure-impulse theory for describing confined wave impact loads based on laboratory experiments, see Chapter 2. Secondly, it studied in detail the description of the wave surface impact velocity and the small scale air entrapment characteristics, see Chapter 3. Thirdly, it extended the validation of the pressure-impulse theory based on extensive laboratory experiments with variations in hydraulic loading conditions (regular/irregular waves and varying freeboards) and changes in the structure geometry (overhang length, lateral constriction and ventilation gaps), see Chapter 4. Finally, it described the use of the validated load prediction expressions to be used in the design, in addition to considerations regarding the scaling of loads to prototype dimensions, see Chapter 4 and Chapter 5.

6.1. CONCLUSIONS

This dissertation had the goal *to develop a load prediction method and design considerations for vertical hydraulic structures with horizontal overhangs subjected to confined wave impacts*. Confined wave impacts acting on vertical hydraulic structures with overhangs have not been widely studied in the past, despite their significant relevance for existing and future hydraulic structures. This knowledge gap has been addressed in four chapters. Among other contributions, this research validates a load prediction method to estimate confined wave impact pressure- and force-impulses acting on hydraulic structures with overhangs. Hereafter, the main conclusions from this work are presented.

VALIDATION OF PRESSURE-IMPULSE THEORY

The first aim of this work was to validate the pressure-impulse theory for describing the confined wave impact loads on vertical hydraulic structures with relatively short overhangs. The pressure-impulse theory was previously developed in the work by Cooker and Peregrine (1990, 1995) and Wood and Peregrine (1996) but it was not yet validated for its use as a design tool for wave impact loads on vertical hydraulic structures with overhangs. This knowledge gap was addressed based on laboratory experiments. Thus, this study highlighted and validated the suitability of the pressure-impulse theory to describe the loads caused by confined wave impacts on hydraulic structures with overhang configurations. This validated theory represents a significant contribution to the design of this type of structure, providing a first tool for preliminary load estimations. Nevertheless, the pressure-impulse theory has been validated in this research for a specific set of structural configurations (i.e. horizontal bottom, vertical wall and horizontal overhang) and hydrodynamic conditions (i.e. low steepness, non-breaking incident waves). The validation of this theory for other more complex geometries including 2D and 3D process interactions (e.g. sloped bottom, non-horizontal overhangs, ventilation gaps, breaking waves, etc.) should be further investigated in the future.

This study also showed that the force-impulse is characterized by being a more stable magnitude compared with the force peaks. The average mean variability (i.e. the standard deviation divided by the mean) for the force-impulses was 5.7%, while the average mean variability for the force peaks was 11.4%. This lower variability highlights one advantage of considering pressure- and force-impulses in the design of hydraulic structures. The fact that pressure- and force-impulses can be accurately scaled between model and prototype scales using the Froude law represents another advantage. This work also introduced a method to obtain the pressure- and force-impulses from laboratory measurements, using one single set of constant criteria (i.e. low-pass filtering methods, impact start/end thresholds, pressure to force integration and pressure/force to impulse integration). This method was later on used for analysing the total of 146 laboratory tests in this research and can be applied to other types of wave impacts such as the ones caused by breaking waves or overtopping waves.

WAVE SURFACE IMPACT VELOCITY AND AIR ENTRAPMENT

The second aim of this work was to describe the wave impact velocity and quantify the air entrapment. This work addressed this aim based on laboratory experiments. This study highlighted the complex wave hydrodynamics before and during the wave impacts, influenced by the incident wave conditions and the structural characteristics. The

6

experimental results in this study showed that the impact velocity described by the linear wave theory is suitable to be used for confined wave load estimations. The suitability of the linear wave theory was supported not only by its agreement with the experimental data but also by its agreement with higher order wave theories considered in this study. Nevertheless, this agreement was found for the relatively deep water conditions considered in this study. For conditions outside this range of validation, the suitability of this method to predict the wave impact velocity should be reassessed.

This study also showed a large variation in air entrapment for multiple tests with the same structural configuration. The results from the laboratory tests showed a range of dimensionless entrapped air area of $0.005 < \alpha = A_A/W^2 < 0.035$ for both the tests with a shorter and a longer overhang. This variability in entrapped air characteristics leads to significant variability in peak pressures and forces, impact durations and pressure oscillations, among others. Furthermore, longer impact durations and larger wave loads were found to be closely related to larger entrapped air dimensions.

VARYING INCIDENT WAVE FIELDS AND CONFIGURATIONS

The third aim of this work was to extend the validation of the pressure-impulse theory to more realistic situations including varying incident wave fields (e.g. regular/irregular incident waves) and considering a wider range of structural configurations. This work addressed this aim based on the analysis of extensive laboratory experimental data. These laboratory experiments included 146 wave flume tests with variations in the hydraulic loading conditions (regular/irregular waves and varying freeboards) and changes in the structure geometry (overhang length, lateral constriction and loading reducing ventilation gaps). Based on the results of these laboratory experiments, the Parameter Gamma (Γ, representing the effective air entrapment characteristics) was introduced and related to the Parameter Beta (β, representing the effective bounce-back factor). Based on those two parameters, the confined wave impact pressure- and force-impulses acting on a given hydraulic structure with an overhang could then be estimated.

The constriction tests showed that a lateral constriction of 22% of the total structure width amplifies the wave impact loads at the constriction edge. This amplification of pressure-impulses per metre of structure width at the constriction edge varies between 10% and 50% for the different individual tests in comparison to the test without the presence of a constriction. This shows that the incident wave is funnelled by the lateral constriction, and the confined wave impact load is not directly reduced but forced instead to be distributed over a smaller section of the structure. The tests with ventilation gaps showed that those structural features are effective in reducing confined wave impact loads. These experimental results showed that the presence of relative ventilation gaps between 5% and 10% (i.e. G/W which describes the percentage of the ventilation gap in relation to the whole overhang length W) leads to the reduction of force-impulses acting on the vertical wall between 10% and 50%. Nevertheless, those load reduction factors are strongly sensitive to variations in the structural characteristics and geometries. Thus, for the design of ventilation gaps on structures subjected to confined wave impacts, the detailed geometrical characteristics should be taken into account. Based on these detailed characteristics and geometries, the ventilation gaps load reduction factors can be studied by means of numerical and physical methods.

Design approach for confined wave impact loads

The fourth and final aim of this work was to contribute to the design of hydraulic structures subjected to confined wave impacts. This work addressed this aim by combining and synthesising all previous research steps. This work shows that the load prediction expressions based on the pressure-impulse theory and validated with laboratory experiments can be used for preliminary design estimations. To this end, the practical use of the load prediction expressions is shown with an application example, followed by a series of alternatives to be considered in order to reduce confined wave impact loads. This research also highlights that the pressure- and force-impulses can be accurately scaled with Froude, while the scaling of pressure and force peaks would lead to significant overestimations. Furthermore, the use of the Rayleigh distribution for describing the individual incident wave heights (and the corresponding wave impact velocity based on linear wave theory) allows us to describe the full range of impulses acting on the given hydraulic structure. Such load prediction expressions can then be used for the design of hydraulic structures in combination with the use of structural and reliability models.

For the design of such hydraulic structures, the load characteristics should be assessed in combination with the structural characteristics. This would allow us to determine the loading type based on the load duration(t_d) and the natural period of the structure (T_n): quasi-static loads ($t_d > 4T_n$), dynamic loads ($T_n/4 < t_d < 4T_n$) and impulsive loads ($t_d < T_n/4$). Furthermore, the advantages of considering pressure- and force-impulses in the design of hydraulic structures are described: a reduced variability, a better predictability, the suitability of Froude scaling laws to accurately scale pressure- and force-impulses between model and prototype scales and the fact that the structural response in the impulsive regime can be fully described by the impulse. Furthermore, this work described the importance of considering the effect of entrapped and entrained air for accurately describing both the wave impact loads and the corresponding structural responses. Lastly, it highlights the advantages of combining the use of analytical, experimental and numerical tools for the research and design of such structures.

6.2. Recommendations

A number of recommendations are presented hereafter for future studies on impulsive wave loads on hydraulic structures. In particular, various recommendations are presented for studies on confined wave impacts on vertical hydraulic structures with overhangs. Those future studies are expected to include a wider range of wave impact types and structural configurations, using various complementary research tools and coupling wave load prediction methods with structural response models. The aim of these future studies is to contribute to revised and modernized techniques, tools and guidelines for the design and renovation of hydraulic structures subjected to wave impacts.

Wave impact types and structural configurations

Future studies on wave impacts should extend the range of wave impact types and structural configurations. This would extend the current knowledge on conditions in which combined wave impacts take place. In other words, future studies should systematically consider the complex impulsive wave loading on hydraulic structures in which breaking, standing and overtopping impact types take place at the same time. This would allow us to extend the validation of the pressure-impulse theory presented in this study, towards other areas and ranges of applicability. This can also include the study of conditions in which more complex geometries (i.e. structural dimensions and foreshore bathymetry) would lead to variation in the wave loading characteristics. Furthermore, structures with very long overhangs (i.e. overhang lengths longer than one-fourth of the incident wave length) should be also considered, given their relevance for the design practice (e.g. long water discharge tunnels in front of flood gates). This study on very long overhangs should include numerical and physical methods and focus on two particular aspects. Firstly, on the wave transmission underneath such a long overhang. This is particularly important to determine the impact length in those conditions, currently estimated as one-eight the wave length. Secondly, studying the large air entrapments that occur in those conditions, and their effect on the confined wave impact loads. Those studies would provide a better understanding on confined wave impact loads and contribute to the design of more reliable hydraulic structures subjected to wave impacts.

RESEARCH TOOLS AND EXPERIMENTS

This study used experimental, analytical and numerical tools with an important focus on laboratory experiments carried out in a small scale wave flume. Future studies on this field may also consider these same research tools, but also include large-scale experiments (e.g. using among others the Delta Flume at Deltares in Delft) and prototype scale field measurements. Furthermore, tests on existing wave flumes located inside vacuum chambers should be considered. These tests would provide key advances in the study of entrapped air in (confined) wave impacts and thus lead to significant contributions to the scaling of loads to prototype scales. In particular, the use of flumes in vacuum chambers would allow modifying the atmospheric pressure, making it possible to correctly scale loads between model and prototype. Furthermore, carrying out experiments in such flumes inside vacuum chambers, without the presence of air, would lead to a better understanding of the actual effect of air in wave impact loads. In addition, those flumes could also be used to study the fluid-structure interaction following such impulsive wave impacts, as the presence of entrapped and entrained air also affects the structural response. Furthermore, future studies may study the effect of surface dumping effects that can affect the wave impact loads for circumstances of approximately zero freeboards, and for configurations with the presence of relatively small ventilation gaps. In general, future research on wave impacts would provide increased confidence in the application of the presented methods to prototype structures and would benefit from the combination of various research techniques, tools and facilities.

COUPLED LOAD-RESPONSE MODELS

Future design tools should include the combination of wave load prediction models with efficient structural response models. This would allow designing hydraulic structures with a higher degree of confidence, considering a wide range of conditions and incorporating the use of probabilistic design methods. Furthermore, the combination and coupling of such models (i.e. wave load prediction models and structural response models) can be a significant development for design optimization of hydraulic structures. In summary, coupled load and response models could be used to directly estimate the effect of various design modifications not only on the loads acting on the structures but also on the structural response. This would allow us to directly visualize the effect of such design modifications and optimizations on the stresses expected on the structure, contributing to the design of more reliable and efficient hydraulic structures.

Design guidelines

The load prediction method and the design approach introduced in this research can be used in the design practice. Further research to extend the validation of these methods and approaches will contribute to the consolidation of these methods and approaches in the design practice. Such future studies will also contribute to implementing these methods and approaches in revised design guidelines. Consequently, the development of revised design guidelines including extensive research and validation studies will allow us to design increasingly reliable hydraulic structures subjected to wave impacts.

References

B.C. Abrahamsen and O.M. Faltinsen. The effect of air leakage and heat exchange on the decay of entrapped air pocket slamming oscillations. *Physics of Fluids*, 23(10), 2011.

N.W.H. Allsop, A.M. Vann, M.W. Howarth, R.J. Jones, and J.P. Davis. Measurments of wave impacts at full scale: Results of fieldwork on concrete armour units. In *Proceedings ICE Breakwaters Conference 1995*, London, United Kingdom, 1995.

N.W.H Allsop, J.E. McKenna, D. Vicinanza, and T.T.J. Wittaker. New design formulae for wave loadings on vertical breakwaters and seawalls. In *Proceedings Coastal Engineering Conference 1996*, Orlando, United States, 1996.

C. Altomare, T. Verwaest, T. Suzuki, and K. Trouw. Characterization of wave impacts on curve faced storm return walls within a stilling wave basin concept. In *Proceedings Coastal Engineering Conference 2014*, Seoul, South Korea, 2014.

R. A. Bagnold. Interim report on wave-pressure research. *The institution of Civil Engineers, London, United Kingdom*, 12:202 – 226, 1939.

W. Bakker, B. Hofland, E. de Almeida, G. Oldenziel, and E.F.J. Overmars. Pulsed led line light for large-scale piv—development and use in wave load measurements. *Measurement Science and Technology*, 32(11):115205, 2021.

M. Batlle Martin, G. Pinon, J. Reveillon, and O. Kimmoun. Computations of soliton impact onto a vertical wall: Comparing incompressible and compressible assumption with experimental validation. *Coastal Engineering*, 164:103817, 2021.

J. A. Battjes and H.W. Groenendijk. Wave height distributions on shallow foreshores. In *Proceedings Coastal Engineering Conference 2000*, Sydney, Australia, 2000.

H. Bogaert. *An experimental investigation of sloshing impact physics in membrane LNG tanks on foating structures.* PhD thesis, Delft University of Technology,, 2018.

H. Bredmose, D.H. Peregrine, and G.N. Bullock. Violent breaking wave impacts. part 2: modelling the effect of air. *Journal of Fluid Mechanics*, 641:389 – 430, 2009.

G.N. Bullock, A.R. Crawford, P.J. Hewson, M.J.A. Walkden, and P.A.D. Bird. The influence of air and scale on wave impact pressures. *Coastal Engineering*, 42(4):291–312, 2001.

M. Castellino, P. Sammarco, A. Romano, L. Martinelli, P. Ruol, L. Franco, and P. De Girolamo. Large impulsive forces on recurved parapets under non-breaking waves. a numerical study. *Coastal Engineering*, 136:1 – 15, 2018.

M. Castellino, A. Romano, J.L. Lara, I.J. Losada, and P. De Girolamo. Confined-crest impact: Forces dimensional analysis and extension of the goda's formulae to recurved parapets. *Coastal Engineering*, 163:103814, 2021.

X. Chen, B. Hofland, C. Altomare, T. Suzuki, and W. Uijttewaal. Forces on a vertical wall on a dike crest due to overtopping flow. *Coastal Engineering*, 95:94 – 104, 2015.

X. Chen, B. Hofland, and W. Uijttewaal. Maximum overtopping forces on a dike-mounted wall with a shallow foreshore. *Coastal Engineering*, 116:89 – 102, 2016.

X. Chen, B. Hofland, W. Molenaar, A. Capel, and M. van Gent. Use of impulses to determine the reaction force of a hydraulic structure with an overhang due to wave impact. *Coastal Engineering*, 147:75 – 88, 2019.

M. J. Cooker and D. H. Peregrine. A model for breaking wave impact pressures. In *Proceedings Coastal Engineering Conference 1990*, Delft, The Netherlands, 1990.

M. J. Cooker and D. H. Peregrine. Pressure-impulse theory for liquid impact problems. *Journal of Fluid Mechanics*, 297:193 – 214, 1995.

G. Cuomo, M. Tirindelli, and W. Allsop. Wave-in-deck loads on exposed jetties. *Coastal Engineering*, 54(9):657 – 679, 2007.

G. Cuomo, K. Shimosako, and S. Takahashi. Wave-in-deck loads on coastal bridges and the role of air. *Coastal Engineering*, 56(8):793–809, 2009.

G. Cuomo, N.W.H. Allsop, and S. Takahashi. Scaling wave impact pressures on vertical walls. *Coastal Engineering*, 57(6):604–609, 2010a.

G. Cuomo, W. Allsop, T. Bruce, and J. Pearson. Breaking wave loads at vertical seawalls and breakwaters. *Coastal Engineering*, 57(4):424 – 439, 2010b.

E. de Almeida and B. Hofland. Validation of pressure-impulse theory for standing wave impact loading on vertical hydraulic structures with short overhangs. *Coastal Engineering*, 159:103702, 2020a.

E. de Almeida and B. Hofland. Experimental observations on impact velocity and entrapped air for standing wave impacts on vertical hydraulic structures with overhangs. *J. Mar. Sci. Eng.*, 8(11):857, 2020b.

E. de Almeida and B. Hofland. Standing wave impacts on vertical hydraulic structures with overhangs for varying wave fields and configurations. *Journal of Coastal and Hydraulic Structures*, 1:1–24, 2021.

E. de Almeida, B. Hofland, and S.N. Jonkman. Wave impact pressure-impulse on vertical structures with overhangs. In *Proceedings Coastal Structures Conference 2019*, Hannover, Germany, 2019.

D. Dermentzoglou, M. Castellino, P. De Girolamo, M. Partovi, G.J. Schreppers, and A. Antonini. Crownwall failure analysis through finite element method. *Journal of Marine Science and Engineering*, 9(1), 2021.

F. Dias and J.M. Ghidaglia. Slamming: Recent progress in the evaluation of impact pressures. *Annual Review of Fluid Mechanics*, 50(1):243–273, 2018.

Eurotop. Manual on wave overtopping of sea defences and related structures. an overtopping manual largely based on european research, but for worldwide application. Second edition, Van der Meer, J.W., Allsop, N.W.H., Bruce, T., De Rouck, J., Kortenhaus, A., Pullen, T., Schüttrumpf, H., Troch, P. and Zanuttigh, B., www.overtopping-manual.com, 2018.

F.W. Gibson. Measurement of the Effect of Air Bubbles on the Speed of Sound in Water. *Journal of the Acoustical Society of America*, 48:1195–1197, 1970.

Y. Goda. Finite periodic stationary gravity waves in a perfect liquid. *Jornal of Coastal Engineering in Japan*, 10:1–11, 1967.

Y. Goda. A new method of wave pressure calculation for the design of composite breakwater. In *Proceedings Coastal Engineering Conference 1974*, Copenhagen, Denmark, 1974.

Y. Goda. *Random seas and design of maritime structures*. W. Scientific, Singapore, 2010.

M. Hattori and N. Tsujioka. Dynamic response of vertical eslastic walls to breaking wave impact. In *Proceedings Coastal Engineering Conference 1996*, Orlando, United States, 1996.

M. Hayatdavoodi, B. Seiffert, and R.C. Ertekin. Experiments and computations of solitary-wave forces on a coastal-bridge deck. part ii: Deck with girders. *Coastal Engineering*, 88:210 – 228, 2014.

T.S. Hedges. Regions of validity of analytical wave theories. In *Proceedings ICE Water Maritime and Energy 1995*, London, United Kingdom, 1995.

J.G. Herterich, R. Cox, and F. Dias. How does wave impact generate large boulders? modelling hydraulic fracture of cliffs and shore platforms. *Mar. Geology*, 399:34 – 46, 2018.

B. Hofland. Modeltesten golfkrachten spuisluizen afsluitdijk. Meetrapport 1220263, Deltares, Delft, The Netherlands, 2015.

B. Hofland, M. L. Kaminski, and G. Wolters. Large scale wave impacts on a vertical wall. In *Proceedings Coastal Engineering Conference 2010*, Shanghai, China, 2010.

B. Hofland, M. Passos, and E. de Almeida. Effect of venting holes to relieve wave impact pressures on flood gates with overhangs. In *Proceedings Coastal Structures Conference 2019*, Hannover, Germany, 2019.

J. Huang, G. Chen, and R.J. Lowe. Experimental study on the probability of different wave impact types on a vertical wall with horizontal slab by separation of quasi-static wave impacts. *Journal of Marine Science and Engineering*, 10(5), 2022.

J.L Humar. *Dynamic of structures*. A.A. Balkema Publishers, Rotterdam, The Neterlands, 2002.

S. N. Jonkman, R. E. Jorissen, T. Schweckendiek, and J. P. van den Bos. *Flood defences lecture notes*. Delft University of Technology, Delft, The Netherlands, 2018.

D. Kisacik, P. Troch, P. van Bogaert, and R. Caspeele. Investigation of uplift impact forces on a vertical wall with an overhanging horizontal cantilever slab. *Coastal Engineering*, 90:12 – 22, 2014.

T.N.J. Kleiberg, O.C. Tieleman, M. Versluis, B.Hofland, W. Kortlever, and E. Ten Oever. A novel design method for wave-induced fatigue of flood gates. *Journal of Coastal and Hydraulic Structures*, 2:(submitted), 2022.

M. Kluijver, C. Dols, S.N. Jonkman, and L.F. Mooyaart. Dataset in support of Advances in the Planning and Conceptual Design of Storm Surge Barriers. 2019.

P. A. Kolkman and T. H. G. Jongeling. *Dynamic behaviour of hydraulic structures*. WL Delft Hydraulics (presently Deltares), Delft, The Neterlands, 1996.

A. Kortenhaus and H. Oumeraci. Classification of wave loads on monolithic coastal structures. In *Proceedings Coastal Engineering Conference 1998*, Yokohama, Japan, 1998.

M.S. Longuet-Higgins. On the statistical distribution of the heights of sea waves. *Journal of Marine Research*, 11(3):245 – 266, 1952.

L. Martinelli, P. Ruol, M. Volpato, C. Favaretto, M. Castellino, P. De Girolamo, L. Franco, A. Romano, and P. Sammarco. Experimental investigation on non-breaking wave forces and overtopping at the recurved parapets of vertical breakwaters. *Coastal Engineering*, 141:52 – 67, 2018.

K. McConnell, W. Allsop, and I. Cruickshank. *Piers, jetties and related structures exposed to waves: Guidelines for hydraulic loadings*. Thomas Telford Publishing, London, United Kingdom, 2004.

N.E. Meinen, R.D.J.M. Steenbergen, B. Hofland, and S.N. Jonkman. Applicability of the Goda–Takahashi Wave Load Formula for Vertical Slender Hydraulic Structures. *J. Mar. Sci. Eng.*, 8(11):868, 2020.

M. Miche. Mouvement ondulatoire de la mer en profondeur constante ou decroissante. *Annales des Ponts et Chaussées*, 121:285 – 318, 1944.

R.R. Minikin. *Winds, waves and maritime structures*. London, United Kingdom, 1950.

H. Mitsuyasu. Shock pressure of breaking wave. In *Proceedings Coastal Engineering Conference 1996*, Orlando, United States, 1966.

W.F. Molenaar and M.Z. Voorendt. *Manual hydraulic structures*. Delft University of Technology, Delft, The Neterlands, 2017.

W.F. Molenaar, M.Z. Voorendt, J.K Vrijling, S. van Baars, K.G Bezuyen, W. Colenbrander, H.K.T Kuijper, and C. Spaargaren. *Hydraulic Structures lecture notes*. Delft University of Technology, Delft, The Neterlands, 2018.

H. Oumeraci, A. Kortenhaus, W. Allsop, M. de Groot, R. Crouch, H. Vrijling, and H. Voortman. *Proverbs: Probabilistic design tools for vertical breakwaters*. Balkema, Lisse, 2001.

I.E. Ozer, M. van Damme, and S.N. Jonkman. Towards an international levee performance database (ilpd) and its use for macro-scale analysis of levee breaches and failures. *Water*, 12(1), 2020.

D. H. Peregrine. Water-wave impact on walls. *Fluid Mechanics*, 35:23 – 43, 2003.

D. H. Peregrine and L. Thais. The effect of entrained air in violent wave impacts. *Journal of Fluid Mechanics*, 325:377 – 397, 1996.

C. Ramkema. A model law for wave impacts on coastal structures. In *Proceedings Coastal Engineering Conference 1978*, Hamburg, Germany, 1978.

E. Renzi, Y. Wei, and F. Dias. The pressure impulse of wave slamming on an oscillating wave energy converter. *Journal of Fluids and Structures*, 82:258 – 271, 2018.

G. Richert. Experimental investigation of shock pressures against breakwaters. In *Proceedings Coastal Engineering Conference 1968*, London, United Kingdom, 1968.

M. Sainflou. Essai sur les digues maritimes verticales. *Annales des Ponts et Chaussées*, 98 (Tome II Fascicule 4):5 – 48, 1928.

B. Seiffert, M. Hayatdavoodi, and R.C. Ertekin. Experiments and computations of solitary-wave forces on a coastal-bridge deck. part i: Flat plate. *Coastal Engineering*, 88:194 – 209, 2014.

R. Slomp. Flood risk management in the netherlands. Rws, The Netherlands, 2012.

C. Small and J.E. Cohen. Continental physiography, climate and the global distribution of human population. *Current Anthropology*, 45(2):269 – 277, 2004.

B. Sonneville, B. Hofland, A. Mowinckel, and B.T. Paulsen. Wave impact loads on offshore gravity based structure. In *Proceedings OMAE Conference 2015*, St. John's, Canada, 2015.

T. Suzuki, O. García-Feal, J.M. Domínguez, and C. Altomare. Simulation of 3d overtopping flow–object–structure interaction with a calibration-based wave generation method with dualsphysics and swash. *Computational Particle Mechanics*, 9(5):1003 – 1015, 2022.

S. Takahashi. *Design of vertical breakwaters*. Port and Airport Research Institute,, Yokosuka, Japan, 2002.

S. Takahashi, K. Tanimoto, and S. Miyanaga. Uplift wave forces due to compression of enclosed air layer and their similitude law. *Coastal Engineering in Japan*, 28(1):191–206, 1985.

S. Takahashi, K. Tanimoto, and K. Shimosako. A proposal of impulsive pressure coefficient for design of composite breakwaters. In *Proceedings International Conference of Hydro-Technical Engineering for Port and Harbour Construction 1994*, Yokosuka, Japan, 1994.

O. C. Tieleman, B. Hofland, and S. N. Jonkman. Bending vibrations of the afsluitdijk gates subjected to wave impact. In *Proceedings PIANC Congress 2018*, Panama City, Panama, 2018.

O.C. Tieleman. *Wave-induced vibrations of flood gates*. PhD thesis, Delft University of Technology,, 2022.

O.C. Tieleman, A. Tsouvalas, B. Hofland, and S.N. Jonkman. A three dimensional semi-analytical model for the prediction of gate vibrations. *Jornal of Marine Structures*, 65: 134 – 153, 2019.

O.C. Tieleman, B. Hofland, A. Tsouvalas, E. de Almeida, and S.N. Jonkman. A fluid–structure interaction model for assessing the safety of flood gate vibrations due to wave impacts. *Coastal Engineering*, 170:104007, 2021.

H. Tuin, H. Voortman, B. Hofland, and E. de Almeida. Evaluation and validation of the spectral linear wave theory and 'traditional' formulae for pulsating wave loads for uni-modal and bimodal seas: Comparison to Goda and measurements. *Journal of Coastal and Hydraulic Structures*, 2:1–28, 2022.

UN. The ocean conference factsheet. United nations, New York, United States, 2017.

M. van der Eijk and P.R. Wellens. A compressible two-phase flow model for pressure oscillations in air entrapments following green water impact events on ships. *International Shipbuilding Progress*, 66(4):315–343, 2020.

K. van Doorslaer, A. Romano, J. de Rouck, and A. Kortenhaus. Impacts on a storm wall caused by non-breaking waves overtopping a smooth dike slope. *Coastal Engineering*, 120:93–111, 2017.

WL. Wave impacts on the gate in the eastern scheldt caisson (in dutch: Golfklappen op de schuif in de oosterschelde-caisson). Verslag M 1335 deel I, WL Delft Hydraulics (presently Deltares), Delft, The Netherlands, 1977.

WL. Wave impacts against concrete perforated gates (in dutch: Golfklappen tegen betonnen roosterschuiven). Verslag M 1381 deel II, WL Delft Hydraulics (presently Deltares), Delft, The Netherlands, 1978.

WL. Wave impacts: A piston model with compressible water (in dutch: Golfklappen: een zuigermodel met samendrukbaar water). Verslag M 1335 deel II, WL Delft Hydraulics (presently Deltares), Delft, The Netherlands, 1979a.

WL. Wave impacts: A literature review and scale effects in model studies (in dutch: Golfklappen: een literaturroverzicht en schaaleffekten in modelonderzoek). Verslag M 1335 deel III, WL Delft Hydraulics (presently Deltares), Delft, The Netherlands, 1979b.

D. J. Wood, D. H. Peregrine, and T. Bruce. Study of wave impact against a wall with pressure-impulse theory. i: trapped air. *Journal of Waterway, Port, Coastal and Ocean Engineering*, 126(4):182 – 190, 2000.

D.J. Wood and D.H. Peregrine. Wave impact beneath a horizontal surface. In *Proceedings Coastal Engineering Conference 1996*, Orland, United States, 1996.

J.A. Zelt and J.E. Skjelbreia. Estimating incident and reflected wave fields using an arbitrary number of wave gauges. In *Proceedings Coastal Engineering Conference 1992*, Venice, Italy, 1992.

Acknowledgements

This dissertation represents the end of my journey as a doctoral researcher at the Delft University of Technology, and I would like to thank everybody that made this journey possible. This research has been carried out within the DynaHicS Project, thus my gratitude to the organizations that made this project possible: NWO, Delft University of Technology, Rijkswaterstaat, Deltares, Witteveen+Bos and PT Structural. I would like to thank all the members of those organizations that joined DynaHicS, and also Cor Ramkema, for their interest and contribution to this research. I would also like to thank Marcel van Gent, Peter Troch, Nils Goseberg, Wim Kortlever and Wim Uittewaal for being part of my external committee and providing a valuable review of this research.

Furthermore, I would like to thank Bas Hofland, Bas Jonkman and Alessandro Antonini for being part of my committee and guiding me through this research. I would like to especially thank Bas Hofland for giving me the opportunity of joining this project, and for the continuous guidance during the last few years. After seven years of work, including my master thesis and doctoral research, I cannot thank Bas enough for his time, dedication and support. This research would also not be possible without Orson Tieleman, with whom I shared this research and good moments. I would also like to acknowledge the help provided by the laboratory staff. Thanks Sander de Vree for being always available to help me to carry out the experiments. I would also like to thank my office colleagues Orson, Ece, Erik, Stefan and Job for their company and enjoyable working days during the first half of my research, which I missed so much during the second half. And also thanks to all the other colleagues that made the PhD experience so enjoyable before the lockdowns, I definitely missed our regular Thursday meetings at PSOR.

Concluding this research would also not have been possible without so many friends that made it possible, especially during corona times. Thanks to you two for always being around and making everything more enjoyable, either in Holland, Belgium or while training for Roland Garros. Thanks to you two for your presence during these years, as bouldering and pasta were fun but it was your company that kept me going. Thanks to the person who besides the distance has been there for more than twenty years, during endless mountain bike rides or by phone. Thanks to you three for bringing Greece to my heart and being there in the difficult moments, but for the good moments while sharing pimientos and calamari. Thanks to you two for showing what the real meaning of amigo is. Thanks to you for making Doerak a good tradition, although Utrecht is also perfect. Thanks to the four of you for making me feel at home on the other side of the world. Thanks to the ones who gave me corona, not because of that, but for being always around. Thanks to my two native flatmates for sharing with me the difficult start of corona, and also to my non-native flatmates for sharing with me the difficult long months of corona. Also thanks to the one who joined the best 3-people lockdown party on a rainy winter day. Thanks also to who received me in their place to have the best ramen for dinner, and to who allowed my nephew to discover Hollland chilling in a bike car. Many other important people were not named above, and to them also thanks for the many good moments in the previous years.

In addition, I would like to remember some of the people who decisively influenced my journey so far in hydraulic engineering. I would start by remembering the two gentlemen who received me at TU Delft for the first time in March 2012. Also who received me at TU Delft later on in March 2014, or the three people that made it possible for me to visit the laboratories at Deltares for the first time in August 2014. My dream to study hydraulic engineering was initiated by the person who showed me the Langosteira port under construction in 2008. This dream grew during my bachelor's project supervised by the person who encouraged me to come to Delft in 2012. I finally joined the CoMEM Master and TU Delft in 2015 motivated by who was always a great source of inspiration. And after overcoming 70 courses during my bachelor and masters, nothing would be the same without your lessons during the best one, neither without those really enjoyable hours attending your course, my very favourite one. I would like to show my deepest appreciation to all of you for your decisive contribution to my journey. I would not be the same without you and all the professors, supervisors, and colleagues I met in the previous years. Among them, my team and my jefe in Schaan are lifelong sources of great inspiration. As my desk colleague and the person who inspired me the most to one day do a doctorate said every afternoon: it was a pleasure! This list could include many more histories that show that I could not have done anything alone. To all of you, thanks!

To conclude, my endless thanks to whom were with me since that late night in Nova Friburgo. All I have done started with the unconditional support from the three of them, muito obrigado por tudo! Finally, no words can describe how grateful I am for ending this chapter of my life with the most beautiful and supportive company. I cannot wait for enjoying our next chapters to come, mersi khoshgelam!

Curriculum Vitæ

Ermano de Almeida Sousa

23-09-1988	Born in Nova Friburgo, Brazil.

Education

2006–2012	B.Sc. in Civil Engineering Technical University of Madrid Technical University of Lisbon
2012–2014	M.Sc. in Civil Engineering Technical University of Catalonia RWTH Aachen University
2015–2017	M.Sc. in Hydraulic Engineering Delft University of Technology University of Southampton Norwegian University of Science and Technology
2017–2023	Ph.D in Hydraulic Engineering Delft University of Technology

Work Experience

2011–2012	TomTom*
2012–2013	Wasser*
2013–2013	Ports de Balears*
2014–2015	Hilti
2015–2016	NTNU*
2016–2017	Deltares*
2017–2021	TU Delft
2022–2022	TNO
2022–current	Arcadis

* Internships

List of Publications

This dissertation

1. **E. de Almeida**, B. Hofland, *Validation of pressure-impulse theory for standing wave impact loading on vertical hydraulic structures with short overhangs*, Coastal Engineering **159**, 103702, 2020.

2. **E. de Almeida**, B. Hofland, *Experimental observations on impact velocity and entrapped air for standing wave impacts on vertical hydraulic structures with overhangs*, Journal of Marine Science and Engineering **8**(11), 857, 2020.

3. **E. de Almeida**, B. Hofland, *Standing wave impacts on vertical hydraulic structures with overhangs for varying wave fields and configurations*, Journal of Coastal and Hydraulic Structures **1**, 10, 2021.

4. W. Bakker, B. Hofland, **E. de Almeida**, G. Oldenziel, E.F.J Overmars, *Pulsed LED line light for large-scale PIV—development and use in wave load measurements*, Measurement Science and Technology **32**, 115205, 2021.

5. O.C Tieleman, B. Hofland, A. Tsouvalas, **E. de Almeida**, S.N. Jonkman, *A fluid-structure interaction model for assessing the safety of flood gate vibrations due to wave impacts*, Coastal Engineering **170**, 104007, 2021.

6. H. Tuin, B. Hofland, **E. de Almeida**, H. Voortman, *Spectral linear wave theory for wave loads on walls for bimodal seas: comparison to Goda and measurements*, Journal of Coastal and Hydraulic Structures **2**, 21, 2022.

7. **E. de Almeida**, B. Hofland, S.N. Jonkman, *Wave impact pressure-impulse on vertical structures with overhangs*, Proc. Coastal Structures Conference 2019, Hannover, Germany, Bundesanstalt für Wasserbau, 2019.

8. B. Hofland, M. Passos, **E. de Almeida**, *Effect of venting holes to relieve wave impact pressures on flood gates with overhangs*, Proc. Coastal Structures Conference 2019, Hannover, Germany, Bundesanstalt für Wasserbau, 2019.

OTHER PUBLICATIONS

1. **E. de Almeida**, M.R.A. van Gent, B. Hofland, *Damage characterization of rock slopes*, Journal of Marine Science and Engineering **7**(10), (2019).

2. M.R.A. van Gent, **E. de Almeida**, B. Hofland, *Statistical analysis of the stability of rock slopes*, Journal of Marine Science and Engineering **7**(60), (2019).

3. **E. de Almeida**, M.R.A. van Gent, B. Hofland, *Damage characterization of rock armoured slopes*, Proc. Coastlab 2018, Santander, Spain, 2018.

4. M.R.A. van Gent, **E. de Almeida**, B. Hofland, *Statistical analysis of the stability of rock armoured slopes*, Proc. Coastlab 2018, Santander, Spain, 2018.

5. B. Hofland, P. Rosa-Santos, F. Taveira-Pinto **E. de Almeida**, R. Lemos, A. Mendonça, C.J. Fortes *Measuring damage in physical model tests of rubble mounds*, Proc. ICE Breakwaters 2017, Liverpool, United Kingdom, 2017.